Universidade do Minho
Escola de Engenharia

Mohammadreza Aali

Viscoelastic Fluids in Profile Extrusion: Relevance and Characterization

October 2022

Viscoelastic Fluids in Profile Extrusion: Relevance and Characterization
Mohammadreza Aali
UMinho | 2022

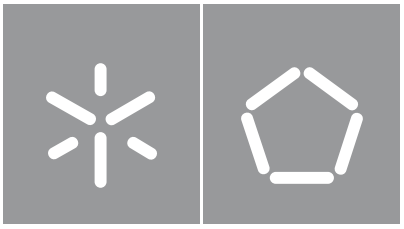

Universidade do Minho
Escola de Engenharia

Mohammadreza Aali

Viscoelastic Fluids in Profile Extrusion: Relevance and Characterization

Doctoral Thesis for PhD degree in Engineering
and Science of Polymers and Composites

Work accomplished under the supervision of
Professor Olga Machado de Sousa Carneiro
Professor João Miguel de Amorim Novais da Costa Nóbrega

October 2022

Acknowledgments

My Ph.D. project has been begun with traveling to Portugal, such I would like to name it a **JOURNEY**. That was a long and delightful journey with a lot of challenges. Anyway, I reached the end of this journey, and I would like to deliver my acknowledgments to those without whose support, encouragement, and assistance I would not have been able to finish this project.

First, I would like to express my deepest gratitude to my supervisors and friends, Professor Olga Sousa Carneiro, and Professor João Miguel Nóbrega, for their always encouragement, advice, and support. Definitely, this work would be impossible to complete without them. Their insightful feedback pushed me to sharpen my thinking and brought my work to a higher level, and this is my great pleasure to get the opportunity to work with them.

A special thanks to my colleagues and friends, as well as the technical administrative staff of the Polymer Engineering Department for their support and friendships throughout the years, which have left me with great memories.

I would like to offer my heartfelt and endless appreciation to my father Asghar Ali, my mother Fakhri Shoghiaghghaleh, and my sisters for their love, wise guidance, sympathetic ears, and their delivered hope. You are always available to me.

I would also want to thank everyone who has ever doubted me or attempted to disappoint me; if they weren't there, I may have given up on my tasks.

I gratefully acknowlagde funding FEDER funds through the COMPETE 2020 Program and National Funds through FCT - Portuguese Foundation for Science and Technology under the projects UIDB/05256/2020/, UIDP/05256/2020, CPCA/A2/6202/2020, CPCA_A2_6231_2020, NORTE-08-5369-FSE-000034, under program IMPULSE – Polímeros e Compósitos: Drivers da Inovação Tecnológica e da Competitividade Industrial.

I also acknowledge the support of the computational clusters Search-ON2 (NORTE-07-0162-FEDER-000086) and Minho Advanced Computing Center (MACC).

To my parents and all my family,

For their unconditional support and endless encouragement and loves

Statement of integrity

I hereby declare having conducted this academic work with integrity. I confirm that I have not used plagiarism or any form of undue use of information or falsification of results along the process leading to its elaboration. I further declare that I have fully acknowledged the Code of Ethical Conduct of the University of Minho. University of Minho, 27th October 2022.

Name: Mohammadreza Aali

Signature: AALI MOHAMMADREZA Digitally signed by AALI MOHAMMADREZA Date: 2022.10.27 13:10:16 +01'00'

Resumo

A extrusão de perfis termoplásticos é uma técnica de fabrico contínua essencialmente empregue na produção de produtos de seção transversal constante. O projeto de cabeças de extrusão requer uma modelação realista do escoamento que ocorre no seu canal de fluxo e, portanto, necessita de uma caracterização reológica rigorosa do polímero fundido. A presente tese de doutoramento foca-se em dois assuntos, nomeadamente: (i) os efeitos da viscoelasticidade no escoamento confinado que ocorre no canal de fluxo da cabeça de extrusão, e (ii) os efeitos de erros (dimensões das amostras e temperatura) que ocorrem comummente em de testes de reometria extensional uniaxial realizados com a plataforma Sentmanat (SER), com fluidos inelásticos e fluidos viscoelásticos. Os estudos computacionais foram realizados recorrendo à biblioteca computacional OpenFOAM.

Relativamente ao primeiro assunto, inicialmente é implementado um sistema de cálculo computacional, e os resultados obtidos com modelos inelástico e viscoelástico são comparados. Para permitir uma comparação adequada dos modelos, primeiramente os comportamentos linear e não linear do material são caracterizados experimentalmente, e os dados obtidos ajustados com um modelo viscoelástico de Giesekus. Em seguida, este modelo é usado para gerar a curva de fluxo (viscosidade de corte versus taxa de corte), e os dados gerados são ajustados, com um código desenvolvido para o efeito, a um modelo inelástico de Bird Carreau. Subsequentemente, os modelos constitutivos viscoelástico e inelástico equivalente são empregues na modelação do escoamento numa cabeça de extrusão de perfil, para aferir o efeito do modelo utilizado na queda de pressão e na distribuição do escoamento previstas. Os resultados obtidos demonstram que a viscoelasticidade desempenha um papel significativo tanto na distribuição do fluxo quanto na queda de pressão, pelo que, idealmente, deveria ser considerada no projeto de cabeças de extrusão de perfil.

Relativamente ao segundo assunto estudado, é desenvolvido um modelo computacional que replica os testes de reometria extensional uniaxial efetuados com a plataforma Sentmanat (SER). Numa primeira fase, o trabalho realizado com um modelo inelástico permitiu definir os requisitos computacionais adequados. Esta fase permitiu também concluir que os resultados obtidos com a estratégia de captura de superfície baseada num método Volume-de-Fluido (VOF) geométrico, são melhores que aqueles obtidos com a alternativa algébrica. Tendo em consideração os resultados obtidos com o modelo inelástico, foi desenvolvido um novo código para modelar o escoamento viscoelástico multifásico, usando o método VOF geométrico, para permitir capturar a interface ar-polímero de modo mais preciso. Para além disso, o utilitário do OpenFOAM usado para calcular forças e binários foi adaptado para fluidos viscoelásticos. O sistema computacional desenvolvido é então usado para avaliar o efeito dos erros comuns acima mencionados. Para quantificar o efeito dos erros induzidos, são comparadas as viscosidades extensionais resultantes da modelação numérica com os valores teóricos. Os resultados obtidos mostram que o efeito de erros relativos à temperatura de ensaio é mais significativo do que o correspondente às dimensões da amostra, principalmente quando se utilizam modelos constitutivos viscoelásticos.

Palavras-chave: extrusão de perfis, modelagem computacional, modelos constitutivos viscoelásticos, Sentmanat Extensional Rheometer (SER), termoplásticos.

Abstract

Thermoplastics profile extrusion is a continuous manufacturing technique that is mostly employed to produce constant cross-section polymeric products. Proper extrusion die design involves realistic modeling of the flow occurring inside the die flow channel and, therefore, accurate polymer melt characterization. The present thesis focuses on two subjects, namely: (i) the effects of viscoelasticity in the confined flow that takes place inside the extrusion die flow channel, and (ii) the effects of common experimental error sources (sample dimensions and test temperature) on the accuracy of the uniaxial extensional rheometry tests performed with the Sentmanat Extensional Rheometer (SER), both for inelastic and viscoelastic fluid models. The computational studies were carried out with the OpenFOAM computational library.

Concerning the first subject, a computational framework is developed, and the results obtained from the inelastic and viscoelastic fluids model are compared. To allow a proper model comparison, first, the material linear and nonlinear behavior are characterized experimentally, and the collected data is fitted with the Giseskus viscoelastic model. Afterwards, the fitted Giesekus model is used to generate the material flow curve (shear viscosity versus shear rate), and the data is fitted, with an in-house code, to a Bird Carreau (inelastic) model. Subsequently, the viscoelastic and corresponding inelastic models are employed in a computational study, aiming at comparing the effect of viscoelasticity on the calculated pressure drop and flow distribution. The results obtained demonstrate that viscoelasticity plays a relevant role in both the flow distribution and pressure drop obtained, and, consequently, it should be taken into account when designing profile extrusion dies.

Regarding the second subject, a computational setup is devised to model uniaxial extensional rheometry tests performed with the SER device. The work carried out initially with an inelastic model allowed defining of the appropriate computational setup requirements (the computational domain geometry, mesh refinement level, and initial and boundary conditions). This part of the study allowed concluding that the results obtained from a surface-capturing approach based on the geometric Volume-of-Fluid (VOF) method were better than the ones provided with the algebraic counterpart. Having in mind the results obtained with the inelastic model, a new multiphase viscoelastic flow solver was implemented using the geometric VOF, to allow capturing a sharper polymer-air interface. Also, the OpenFOAM utility devised to calculate forces and torques, was adapted to viscoelastic fluids models. The computational framework was then used to assess the effect of the common errors mentioned above. To quantify the effect of the induced errors, the extensional viscosities resulting from the numerical computational studies and the ones achieved with the theoretical counterpart were compared. The results obtained show that the effect of the test temperature errors is more significant than the one corresponding to the sample dimensions, especially when viscoelastic constitutive models are employed.

Keywords: Computational modeling, profile extrusion, Sentmanat Extensional Rheometer (SER), thermoplastics, viscoelastic constitutive models.

Table of Contents

List of Figures

List of Tables

List of Abbreviations and Symbols

Abbreviations

2D-SG	2D Version of Sample Geometry
CG	Complex Geometry
ES	Elemental Section
ESs	Elemental Sections
FEM	Finite Element Method
FENE-CR	Finite Extendable Non-linear Elastic–Chilcott and Rallison
FSR	Filament-Stretching Rheometer
FVM	Finite Volume Method
G1	First Geometry Used in Uniaxial Extensional Rheometry test
G2	Second Geometry Used in Uniaxial Extensional Rheometry test
GNF	Generalized-Newtonian Fluid
HER	Horizontal Extensional Rheometry
IEP	Inverse Extrusion Problem
K-BKZ	Kaye–Bernstein-Kearsley-Zapas
LVE	Linear Viscoelastic Property
MTR	Münstedt Tensile Rheometer
PC	Polycarbonate
PTT	Phan-Thien-Tanner
PVC	Polyvinyl Chloride
RME	Rheometrics Melt Extensometer
Ref	Reference Case Study
SAOS	Small-amplitude Oscillatory Shear
SER	Sentmanat Extensional Rheometer
SG	Simple Geometry
VOF	Volume-of-Fluid
symH	Vertical Symmetry Plane
symV	Horizontal Symmetry Plane

Symbols

A	Cross-sectional Area of the Sample
A_0	Initial Cross-sectional Area of the Sample
E	Elastic Fluid
F	Force
$\underline{F}_P$	Normal Pressure Force Vector
$\underline{F}_v$	Viscous Force Vector
G	Relaxation Modulus
G'	Storage Modulus
G''	Loss Modulus
G_k	Relaxation Modulus of the k_{th} Mode
H	Height of Domain
I	Inelastic Fluid
$\underline{\underline{I}}$	Identity Tensor
L	Sample Length
L	Polymer Sample Initial length
L/t	Length over Thickness
L_T	Total Length of Domain
$\underline{M}_d$	Distance Vector to the Origin of the Domain
N	Number of Modes
$P1$	Pressure Evolution Location in Flow Channel
P	Pressure
R	Drum Radius
R_1	Outer Radius
T	Torque
T_0	Sample Initial Thickness
U	Average Outlet Velocity
$U+$	Higher Average Outlet Velocity
$U-$	Lower Average Outlet Velocity
U_x	Velocity in the x direction
U_z	Velocity in the z direction
W	Domain Width
W_s	Sample Width
W_0	Sample Initial Width
dp/dz	Pressure Gradient
i	Each Boundary Face
k_{th}	Element of the Stress Tensor
n	Power-law Index
$\underline{s}_f$	Face Area Vector
t	Time
t_s	Sample Thickness
y	y direction

z	z direction
Ⓔ	Entrance of Parallel Zone
Ⓞ	Flow Channel Outlet
$\uparrow W$	Case Study with Higher Width of Sample
$\downarrow W$	Case Study with Lower Width of Sample
$\uparrow T$	Case Study with Higher Thickness of Sample
$\downarrow T$	Case Study with Lower Thickness of Sample
α	Mobility Factor of Material
α_k	Mobility Factor of the k_{th} Mode
α	Function Value
β	Convergence Angle
$\beta+$	Higher Convergence Angle
$\beta-$	Lower Convergence Angle
γ	Shear Strain
$\underline{\underline{\dot{\gamma}}}$	Rate of Deformation Tensor
$\dot{\gamma}$	Shear Rate
$\dot{\varepsilon}_H$	Hencky Strain Rate
η	Shear Viscosity
η_k	Extensional Viscosity of the k_{th} Mode
η_{0_k}	Zero-shear Viscosity of the k_{th} Mode
η_∞	Infinite Shear Rate Viscosity
η_E	Extensional Viscosity for a Viscoelastic Fluid
λ	Relaxation Time
λ_k	Relaxation Time of the k_{th} Mode
λ	Characteristic Time (Bird-Carreau model)
μ	Dynamic Shear Viscosity of Newtonian Fluids
μ_A	Dynamic Shear Viscosity of Air
μ_E	Newtonian Extensional Viscosity
μ_p	Dynamic Shear Viscosity of Polycarbonate
ρ_A	Density of Air
ρ_p	Density of Polycarbonate
$\underline{\underline{\tau}}_{dev}$	Deviatoric Stress Tensor for an Inelastic Fluid
$\underline{\underline{\tau_k}}$	Stress Tensor of the k_{th} Mode
$\overset{\nabla}{\underline{\underline{\tau_k}}}$	Upper-convective Shear Stress Tensor of the k_{th} Mode
$\underline{\underline{\tau}}_{MF,i}$	Combination of the Polymeric and Solvent Multiphase Stress Tensor In each Cell
$\underline{\underline{\tau_T}}$	Total Stress Tensor
τ_{yz}	Shear Stress
τ_{zz}	Normal Stress

$\lvert\tau_{yz}\rvert$	Absolute Shear Stress
$\lvert\tau_{zz}\rvert$	Absolute Normal Stress
σ	Stress for Newtonian Fluids
ω	Angular Frequency
Ω	Drum Angular Velocity

CHAPTER 1

INTRODUCTION

1.1. Introduction

Nowadays, polymeric material-based products have significant impacts in several fields, such as health, mobility, civil construction, energy, leisure, commodities, etc. The extrusion process, particularly profile extrusion, is one of the available processing techniques used in the production of a wide range of polymer-based products. Extrusion is a steady-state process that transforms a polymer raw material into a constant cross-section product [1]. Some examples of extruded products include tubes, pipes, films, sheets, and profiles. The latter is particularly important since it covers a wide range of complex shaped profiles, for a wide variety of applications. Home cladding, electrical wire gutters, window frames, and medical catheters are just a few of the products manufactured by profile extrusion [2]. A typical profile extrusion line consists of one extruder or more (in case of co-extrusion), an extrusion die, a calibration/cooling system (encompassing one or several calibrators in series and, eventually, a cooling bath), a caterpillar haul-off, and a cutting unit or a winder [3], as depicted in Figure 1.1.

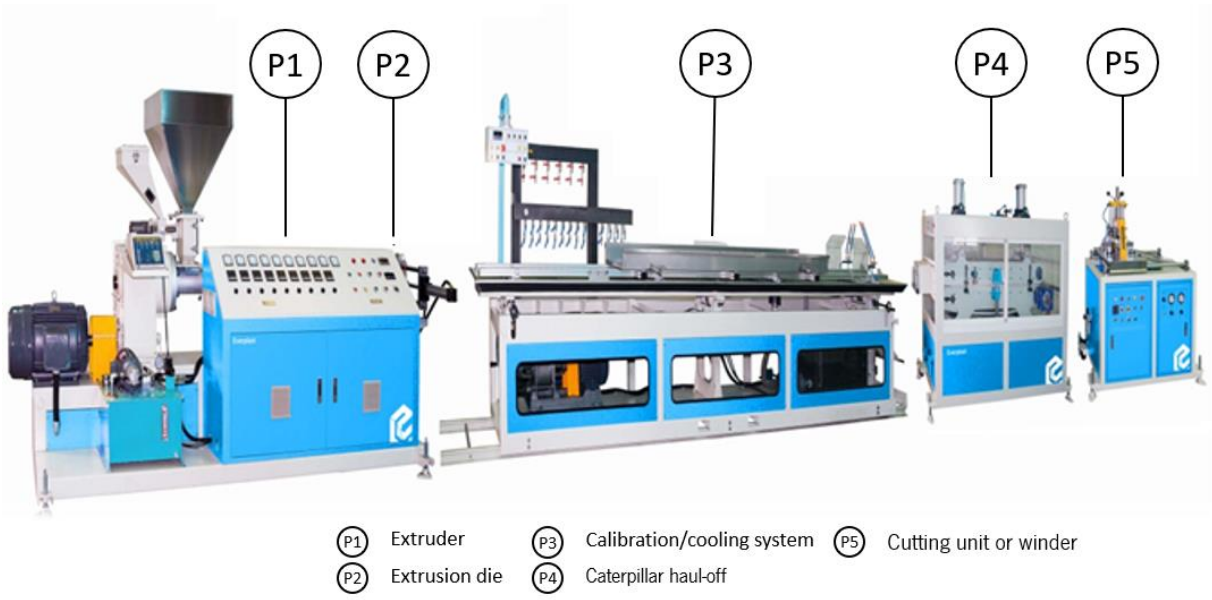

Figure 1.1: Typical profile extrusion line components (adapted from [4]*)*

Each unit has the following particular functions:

- **Extruder** - melting the solid material fed through the hopper, and homogenizing and pushing the molten polymer through the extrusion die.
- **Extrusion die** - shaping the molten polymer into the desired cross-section.
- **Calibration/Cooling system** - cooling and sizing the molten polymer profile, to guarantee the required shape.
- **Caterpillar haul-off** - pulls the profile at a specified constant linear velocity.

- **Cutting unit or winder** - cuts the continuous profile into segments with the required length (for rigid profiles) or winds the continuous profile (for flexible profiles).

The extrusion die and the calibration/cooling system, the so-called extrusion line forming tools [3], are the main and most important components [5], since they play a central role in establishing the dimensions, morphology, and properties of the final product, determining also the maximum production rate [1,5].

Traditional profile die design methodologies are experimental and mainly rely on the designer's experience. These approaches are typically based on trial-and-error procedures, involving several iterations of die modification/extrusion tests, all of which are time-consuming, costly, and do not guarantee the achievement of an optimal solution. Recently, due to computational power enhancement and the increased data availability a great evolution to employ computer-aided design methodologies to design different parts of profile extrusion was observed.

In the past decades, employing computational modeling approach in die design process rise in widespread [2,6,15,16,7–14], due to the advancement of computer technology, as well as the major improvement of computational fluid dynamics, the rapid and precise development of numerical tools. Accordingly, there is a plethora of numerically based research on extrusion die design [2,6,15,16,7–14]. The initial experiments comprising computational modeling in profile extrusion started in the 1970s [17]. In these works, inelastic constitutive models [17] were employed. They have analyzed the flow distribution in flat sheet dies to describe the flow under isothermal flow conditions, using Power Law constitutive models. Wortberg et al. [18] used a Finite Element Method (FEM) approach to model the flow in Y and T shaped profile extrusion dies. Then, Rakos et al. [19] employed FEM to balance the flow in a L shaped profile extrusion die. The 3D modeling for the profiles with a converging rectangular and cylindrical shapes was addressed in Gupta et al. [20]. At the same time, Legat and Marchal [21,22] proposed a numerical approach known as the inverse extrusion problem (IEP) to predict the die geometry with varied simple shapes (cross, square, and rectangle). Later, Na and Lee [23] employed the same computational method in the framework of the FEM, for profile extrusion die geometry optimization purposes. Chen et al. [24] employed a new methodology, known as the Taguchi method, to examine the influence of various process parameters, such as materials, die geometry, and processing conditions, on the optimization of a manifold profile. Carneiro et al. [25] established a comprehensive methodology for optimizing the profile extrusion die design process. A 3D computational code based on the Finite Volume Method (FVM) was

devised for performing numerical modeling, and the different sections of flow channel were optimized aimed at achieving a balanced flow distribution in the confined flow. Moreover, the required steps for the automatic design process were demonstrated. Wu and Hsu [26] devised a numerical design approach based on FEM, to optimize the shape of extrusion dies. The optimization process was carried out using an improved genetic algorithm, resulting in an optimal shape with the least amount of the extrusion force and strain. During the same period, Gifford [27] used 3D numerical modeling to predict the side bending and the extrudate-swell phenomena in a T-shaped die. Carneiro et al. performed a series of simulations using the numerical code developed and advanced with the idea of automatic optimization design [28–31]. The optimization design methodologies employed were based on adjustments performed in the cross-section of the Pre-Parallel and Parallel Zones. However, due to the usage of structured computational meshes, the studies were limited to dies with simple shapes. Later, a numerical code based on unstructured meshes was devised, to cope with complex geometries, and a Generalized-Newtonian fluid (GNF) was utilized to represent the flow under isothermal conditions [13,32]. Lehnhäuser and Schäfer [33] employed numerical modeling to optimize the shape of a Newtonian fluid in profile extrusion. Sienz et al. [34] investigated the performance of a slit die using FEM-based modeling. In this work, the results obtained with three approaches were compared, to identify the best solution for melt flow distribution: a generic algorithm, a multipoint approximation optimization method, and a gradient-based optimization method. The same research group [35] employed a direct differentiation approach based on the FEM for performing sensitivity analysis in the profile extrusion die design process. According to the study, the data required to evaluate design sensitivity may be obtained in a post-processing phase, by utilizing the same code that solves the discretized governing equations. Vergnes et al. [36] investigated the challenges of the numerical modeling of forming tools for a more complex profile geometry, having an L-shape, when a non-isothermal generalized Newtonian constitutive model was employed. Mu and Guoqun [37] also resorted to numerical modeling to simulate a hollow rectangular profile with a rectangular metal insert, and they explored the relationship of flow rate with pressure drop and the occurrence of instabilities. A new numerical design methodology for shape optimization in profile extrusion dies was proposed by Elgeti et al. [38] when a simple slit profile and a complex floor skirting were employed. Moreover, the effects of Newtonian and GNF models were investigated [38]. Recently, a new and improved design methodology for the extrusion forming tools was developed by Rajkumar [2]. The proposed methodology provides simplified guidelines for the design of complex profile extrusion dies, which can be decomposed in L and T elementary geometries.

All the previous works employ GNF (inelastic) models, but some studies carried out in the past, also employed viscoelastic models [35,39–44]. The boundary element method was applied to simulate the extrudate swell in triangular and square shaped dies, using differential viscoelastic models by Tran-Cong and Phan-Tien [45]. Mu and Zhao [43] addressed a non-isothermal 3D modeling of a profile die with a hollow square shape using the Phan-Thien-Tanner (PTT) viscoelastic model. Afterwards, the same research group examined extrudate swell occurring in the same geometries. The results obtained were compared with experimental data at relatively high Weissenberg number flows [46]. Marin and Rasmussen [47] employed the Kaye–Bernstein-Kearsley-Zapas (K-BKZ) constitutive model to simulate a transient 3D flow based with a Lagrangian FEM formulation for a rectangular geometry.

Based on the above a major part of the available numerical works, related to profile extrusion die, been carried out using inelastic constitutive models (GNF) [27,36,56,57,48–55]. Viscoelastic models, the more realistic and complex ones, were only employed in a few works [35,39–44], dealing with fairly basic geometries with low relevance for industrial practice [38,43,44,58–61].

Nowadays, due to the growing complexity of the geometry of the profiles and the request for shorter times to market, computer-aided design methodologies are mostly employed, either using commercial or proprietary software. COMPUPLAST® Virtual Extrusion Laboratory™ [62], Plastic Flow [63], Plastics Technology [64], and Greiner Extrusion [65] are some of the most common commercial software, which are widely employed in profile extrusion die design.

Typically, two types of constitutive models are employed to model the polymer melts behavior in profile extrusion die design, and each of them has advantages and disadvantages. Consequently, the selection of the most appropriate constitutive model depends not only on the material itself, but also on the phenomena to be modeled [66]. As a consequence, although inelastic constitutive models can be sufficient to model the flow inside the flow channel for the confined flow [27,48,52,63,67], these types of constitutive models are not a good choice for modeling the flow outside the flow channel, because they are unable to appropriately predict the post-extrusion phenomenon [45,46,68–70], such as extrudate swell. Therefore, the information provided in the literature recommend the employment of viscoelastic constitutive models to appropriately predict the post-extrusion phenomena [45,46,68–70].

This should be noted that the material also should be characterized under conditions representative of the process to be modeled, and the most adequate constitutive model should be selected to fit the

experimental data. Indeed, material characterization performance and constitutive models must be selected based on the nature of the desired process to be numerically modeled.

Rheological characterization is an important step in profile extrusion die design [66,71], and several rheometry techniques are used to obtain the required material data [66,71]. These techniques comprise different types of experiments, such as shear flow tests, oscillatory (shear) tests, and extensional tests. In fact, each of the mentioned rheometry techniques has their own functionality and different properties/aspects of materials are determined by each of these tests [66,71].

The extensional flows were addressed for the first time in 1906 by Trouton [72]. Then, two works dealt with this type of flow in the late 1930s [73,74]. Finally, in the late 1960s, the extensional flows topic became well-known [75–80].

Actually, though extensional flows are dominant in some relevant polymer processing technologies such as blow molding, fiber spinning, thermoforming, film blowing, and extrusion coating, these particular types of flows have not already been thoroughly investigated. This results from the fact that there are additional difficulties involved in the characterization of extensional flows, such as converging flow lines and complex experimental methodologies required to achieve steady-state flow conditions and to ensure appropriate conditions like test temperature, sample dimensions, etc.

Although various platforms were developed by different research groups [81–88], aiming at reducing the complexity of the measurement process as well as collecting highly accurate data [81–88], dealing with these types of flows is still a challenging task.

Recently, a new platform, known as the Sentmanat Extensional Rheometer (SER), was developed by Sentmanat et al. [87,89]. This platform is a multi-functional device, which can be used to perform not only extensional tests but also other types of tests such as peeling, among others [87,89]. The easy operation procedure of the SER when compared to previously developed platforms is its main advantage [87,89], which leads to its widespread use in industry and academia [89-105] [89,90,99–105,91–98].

A collection of rheological tests addressed above, including the characterization of viscous and elastic behavior components, is performed in an integrated manner in order to comprehensively characterize the material and determine all relevant parameters. Figure 1.2 illustrates typical procedures for obtaining the required rheological data, which later will be used to fit inelastic and viscoelastic models. Afterwards, the parameters obtained from fitting will be employed in the numerical modeling.

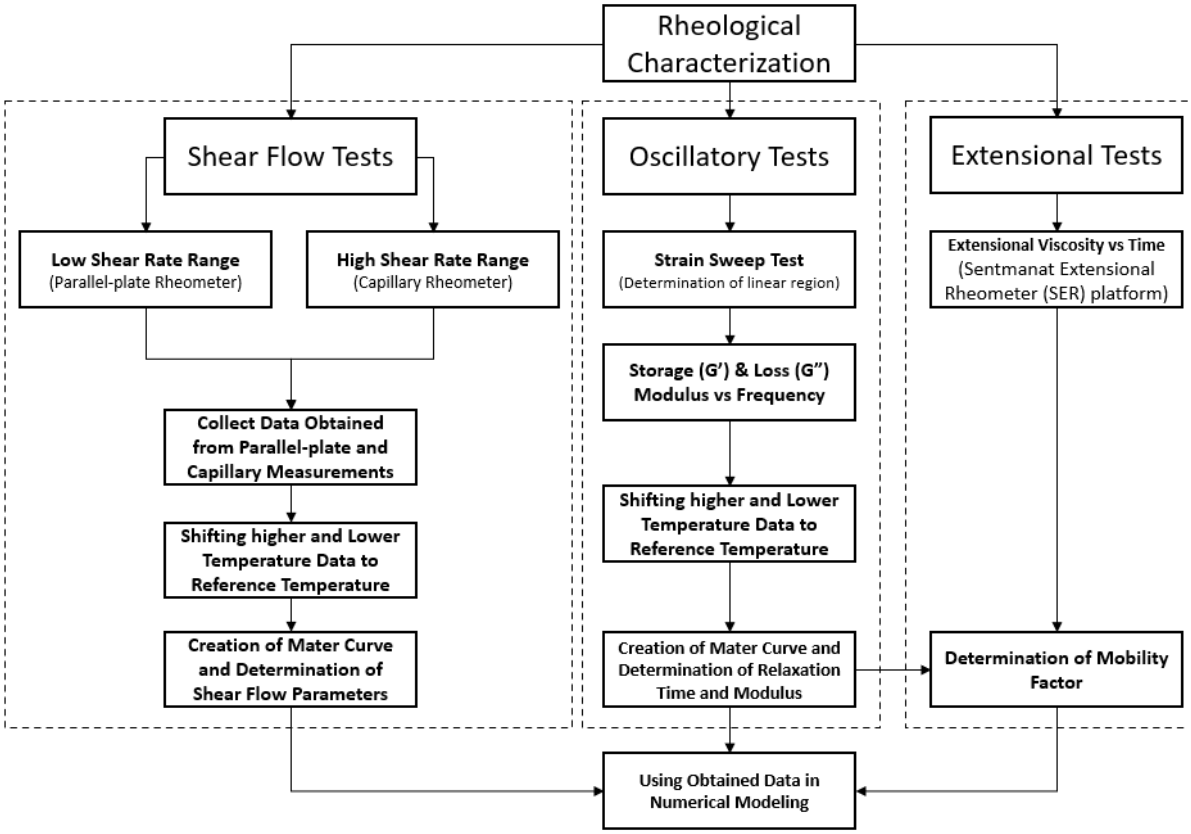

Figure 1.2: Typical sequences of the rheological characterization of non-isothermal inelastic and viscoelastic fluids

As depicted in Figure 1.2, the rheological characterization of the material consists of three set of rheometry techniques. First, the shear flow tests are typically performed to determine the viscous behavior of the material at a wide range of shear rates and at different temperatures [66,71]. Shear flow is important in confined flow and in mixing applications [66,71]. In shear flow tests, a shear rate is imposed, and the induced shear stress is measured or vice-versa [66,71]. The final data of shear flow tests are a collection of results obtained in parallel-plate/cone and-plate rotational rheometers (used for viscosity measurement at the low shear rate range), and in capillary/slit rheometers (used for viscosity measurement at high shear rates).

Second, the small-amplitude oscillatory shear tests provide information on the linear viscoelastic behavior of the material [66,71], mainly the relaxation times spectrum and relaxation modulus, or moduli when several modes are considered at frequencies and temperatures of interest [66,71,106]. These measurements consist of imposing an oscillatory shear strain, and monitoring the corresponding oscillatory shear stress, or vice-versa [66,71,106]. This allows determining the storage, G', and loss, G'', moduli [66,71,106], which give information on the elastic and viscous components, respectively, of the material [66,71,106]. These tests are performed at the linear region that should be first identified by performing a strain sweep test [66,71,106].

Generally, all the tests (shear flow and oscillatory tests) are performed at three different temperatures aimed to identify the temperature effect(s) in the material behavior and the flow activation energy [107]. Moreover, using three different temperatures can provide the results in a vast (non-tested) shear rate/frequency range, through the use of the time-temperature superposition principle, which helps to obtain better fittings.

Finally, contrarily to the oscillatory tests, the extensional rheometry tests are performed to characterize the material non-linear behavior [66,71], which are undertaken by measuring the material extensional viscosity in a range of extensional rates [66,71].

Extensional flows can be categorized into three different types, as depicted in Figure 1.3, namely: (i) uniaxial extensional flow (stretching in one direction, resulting in the compression of the other two directions), (ii) biaxial extensional flow (stretching in two directions, resulting in the compression of the third one), (iii) planar extensional flow (fixing the dimension of one of the directions, stretching in one direction that results in the compression of the remaining direction).

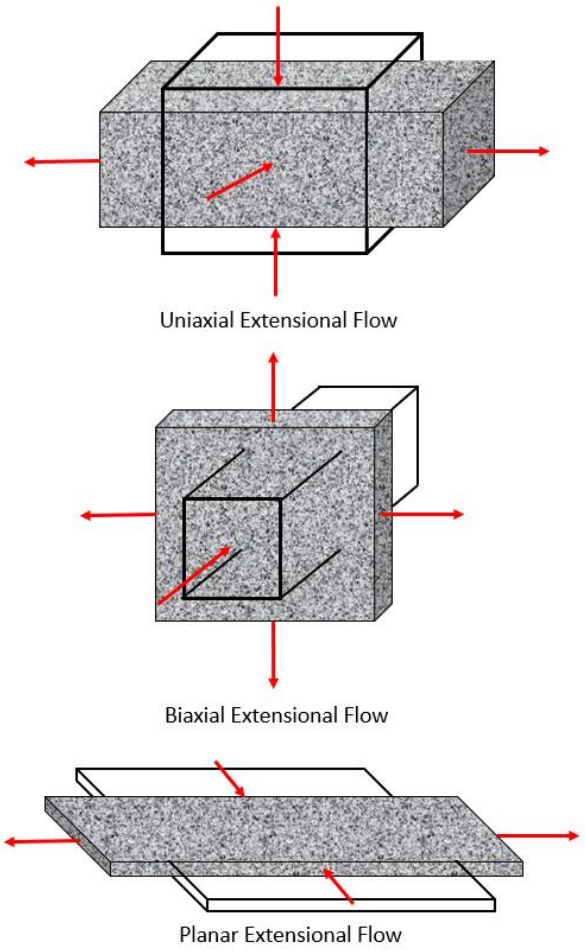

Figure 1.3: Schematic representation of the different types of extensional flows

The uniaxial extensional flow is the least difficult one among them [66] being, therefore, the least difficult to promote for characterization purposes. In the steady-state uniaxial extension, one possible and common method is that a constant extensional rate should be applied. In this way, the sample is highly extended, meaning that a high degree of molecular stretching is induced [66].

Shear flows are well-established in polymeric material systems rheometry [66,71], and numerous studies have been published on the subject. Some of the works that have been carried out in this area deal with common errors that might arise during experimental characterization [108,109]. This constitutes useful guidelines for rheologists, to better plan their work. Common errors in shear rheometry tests are the following: instrument specification, instrument inertia, fluid inertia, secondary flows, surface tension forces, slip, and small volume and/or small gap in the parallel-plate. In order to obtain more insights into the mentioned source of error in shear flow and oscillatory tests, the work of Ewoldt et al. [108] is advised.

Sample dimensions uncertainty, sample clamping, and test temperature are the most important and common errors that typically occur on the uniaxial extensional rheometry tests using the SER platform [93,110]. The effect of the sample clamping and test temperature on the accuracy of the final data was experimentally studied in Svrcinova et al. [93] and Aho et al. [110]. The results obtained demonstrated that a small difference in the test temperature led to a considerable impact on the results obtained. However, it was found that the accuracy of the results was increased when the clamp was not used to fix the sample to the drum.

The works carried out with extensional rheometry [93,110] show that these tests are the most sensitive to the test conditions and samples used, which motivated numerical studies to identify the causes of errors and quantify their impact on the results.

The necking phenomenon in the SER was numerically modeled by Lyhne et al. [111] using a Lagrangian modeling approach. The effect of the rectangular sample thickness and width on the nature of the extensional flow test investigated by Yu et al. [112]. In another work, the same group [104] was investigated effects of the cylindrical sample initial diameter on the accuracy of the uniaxial extensional flow. Hassager et al. [105] also studied the 3D numerical necking phenomenon during the uniaxial extensional tests using the SER.

1.2. Motivation and Objectives

The main motivations of the present thesis were the following:

- It is known that viscoelastic models are mandatory to predict accurately post-extrusion phenomena, like extrudate swell, but most of the available numerical codes (or undertaken approaches), for profile extrusion, model the confined flow with inelastic constitutive models. However, it is not clear how the assumption of an inelastic model in confined flow affects the results accuracy.
- Extensional flows are dominant in many processes such as blow molding, etc. Moreover, several platforms, like SER, were developed to characterize the materials in (uniaxial) extensional flow conditions. However, the information that can help the rheologists to be aware of the error sources and their effects on the accuracy of the results obtained from uniaxial extensional rheometry tests is scarce. Indeed, more effort is required to quantify the relevance errors that might arise in such flows, particularly when the SER is used, in order to avoid the most detrimental ones in the experimental tests.

As a consequence, the two main objectives of this thesis were the following:

1. Assess the effect of viscoelasticity on the confined flow in profile extrusion dies.

For this purpose, first, a methodology has to be developed to obtain inelastic constitutive models and their respective parameters based on the viscoelastic constitutive model parameters.

Then a computational framework must be set up to model and analyze the flow inside complex and simple profile extrusion dies (under steady-state conditions) employing both viscoelastic and inelastic fluids.

Finally, numerical modeling of confined flow must be performed using viscoelastic and equivalent inelastic fluids, and the results obtained should be compared.

2. Assess the effect of possible experimental sources of error on the precision of uniaxial extensional rheometry results, for the SER platform.

First, a computational framework must be devised, including the programming of the modeling code and the definition of the geometry and appropriate initial and boundary conditions representative of the uniaxial

extensional rheometry test, in order to appropriately model the uniaxial extensional rheometry tests through the SER platform. Moreover, a code should be developed to calculate the forces and torques in desired regions of the domain, for incompressible multimode viscoelastic fluids.

The devised computational tools should be used to replicate the extensional viscosity calculation employed experimentally in the SER platform. For this purpose, forces/torque computed by the developed code should be employed to calculate the extensional viscosity.

The calculation framework should be then used to diagnose and quantify the effect of each source of error, namely: sample dimensions (width and thickness) and test temperature on the results accuracy of the extensional rheometry tests. For this purpose, the numerical calculation should be performed with induced errors on the referred variables (sample thickness and width and test temperature), and the predicted extensional viscosities should be compared with the correct materials data. To obtain a better insight, the effect of the error sources should be assessed first for inelastic fluid models and then for the viscoelastic counterpart.

1.3. Thesis Structure

The outline of the present thesis is organized as follows:

- General information about the profile extrusion die design, including common challenges, approaches, and constitutive models employed are addressed in **Chapter 1**. Moreover, this chapter also comprises a brief illustration of the rheological characterization methods and common errors that occur in the experimental rheological characterization. The first chapter ends with a presentation of the motivations and objectives of the present thesis.
- The viscoelasticity effects on the flow distribution and pressure drop in profile extrusion dies are investigated in **Chapter 2**.
- The development of a new computational modeling framework, setup to simulate the SER uniaxial extensional rheometry tests, and the work carried out to identify the effect of the typical sources of error, when an **inelastic** fluid model is employed, are described in **Chapter 3**.
- The previous studies are extended to a **viscoelastic** fluid model in **Chapter 4**.
- Finally, the main conclusions of present thesis, as well as recommendations for future work, are drawn in **Chapter 5**.

References

[1] C. Rauwendaal, Polymer Extrusion, 5th ed., Hanser Publishers, Munich, 2012.

[2] A. Rajkumar, Improved methodologies for the design of extrusion forming tools, Ph.D. Thesis, University of Minho, 2017.

[3] O.S. Carneiro, J.M. Nóbrega, Design of Extrusion Forming Tools, Chapter 1, Smithers RAPRA, 2012.

[4] Everplast Mashinery Co. Ltd, Industrial PE Recycle Plastic Timber Machine Line Manufacturing - Everplast, (2017). https://www.everplast.com.tw/en/product/PE-Recycle-Plastic-Timber-Machine-Line/pe_recycle_machine_line.html (accessed December 5, 2017).

[5] P.G. Lafleur, B. Vergnes, Polymer Extrusion, 2nd ed., John Wiley & Sons, Inc, Great Britain, 2014.

[6] M. Schäfer, Computational engineering: Introduction to numerical methods, 2006. https://link.springer.com/content/pdf/10.1007/978-3-030-76027-4.pdf (accessed April 3, 2022).

[7] M.A. Meyers, K.K. Chawla, Mechanical Behavior of Materials, 2009. http://www.smesfair.com/pdf/mechanical eng/smesfair09.pdf.

[8] J.M. Nóbrega, O.S. Carneiro, A.C. Gaspar, N.D. Gonçalves, Design of Calibrators for Profile Extrusion - Optimizing Multi-step Systems, Int. Polym. Process. 23 (2008) 331–338.

[9] J.M. Nóbrega, O.S. Carneiro, Optimising cooling performance of calibrators for extruded profiles, Plast. Rubber Compos. 35(9) (2006) 387–392. https://doi.org/10.1179/174328906X128216.

[10] D.E. Smith, Design sensitivity analysis and optimization for polymer sheet extrusion and mold filling processes, Int. J. Numer. Methods Eng. 57 (2003) 1381–1411. https://doi.org/10.1002/nme.782.

[11] J. Nizami, C. Batur, Stability analysis and controller design for polymer sheet extrusion, JVC/Journal Vib. Control. 6 (2000) 1083–1105. https://doi.org/10.1177/107754630000600708.

[12] P. Lin, Y. Jaluria, Conjugate thermal transport in the channel of an extruder for non-newtonian fluids, Int. J. Heat Mass Transf. 41 (1998) 3239–3253. https://doi.org/10.1016/S0017-9310(98)00030-1.

[13] N.D.F. Gonçalves, Computer Aided Design of Extrusion Forming Tools for Complex Geometry Profiles, Ph.D. Thesis, University of Mino, 2013.

[14] F. Habla, C. Fernandes, M. Maier, L. Densky, L.L. Ferrás, A. Rajkumar, O.S. Carneiro, O. Hinrichsen, J.M. Nóbrega, Development and validation of a model for the temperature distribution in the extrusion calibration stage, Appl. Therm. Eng. 100 (2016) 538–552. https://doi.org/10.1016/J.APPLTHERMALENG.2016.01.166.

[15] F. Marques, S. Clain, G.J. MacHado, B. Martins, O.S. Carneiro, J.M. Nóbrega, A novel heat transfer coefficient identification methodology for the profile extrusion calibration stage, Appl. Therm. Eng. 103 (2016) 102–111. https://doi.org/10.1016/J.APPLTHERMALENG.2016.04.013.

[16] H. Yang, Conjugate thermal simulation for sheet extrusion die, Polym. Eng. Sci. 54 (2014) 682–694. https://doi.org/10.1002/pen.23609.

[17] J.M. McKelvey, K. Ito, Uniformity of flow from sheeting dies, Polym. Eng. Sci. 11 (1971) 258–263. https://doi.org/10.1002/PEN.760110314.

[18] J. Wortberg, E. Haberstroh, J. Lutterbeck, U. Masberg, J. Schmidt, G. Targiel, Designing of extrusion lines, Adv. Polym. Technol. 2 (1982) 75–106. https://doi.org/10.1002/ADV.1993.060020203.

[19] A.K.H.S. R. Rakos, Computer design aids for non-axis-symmetric profile dies, Annu. Tech. Conf. - Soc. Plast. Eng. (1989) 66–68. https://doi.org/10.2/JQUERY.MIN.JS.

[20] M. Gupta, Y. Jaluria, V. Sernas, M. Esseghir, T.H. Kwon, Numerical and experimental investigation of three-dimensional flow in extrusion dies, Polym. Eng. Sci. 33 (1993) 393–399. https://doi.org/10.1002/PEN.760330704.

[21] V. Legat, J.-M. Marchal, Die design: An implicit formulation for the inverse problem, Int. J. Numer. Methods Fluids. 16 (1993) 29–42. https://doi.org/10.1002/fld.1650160103.

[22] V. Legat, J.-M. Marchal, Prediction of three-dimensional general shape extrudates by an implicit iterative scheme, Int. J. Numer. Methods Fluids. 14 (1992) 609–625. https://doi.org/10.1002/fld.1650140507.

[23] S.Y. Na, T. yong Lee, Shape optimization of polymer extrusion die by three-dimensional flow simulation, Proc. Conf. High Perform. Comput. Inf. Superhighway, HPC Asia'97. (1997) 601–604. https://doi.org/10.1109/HPC.1997.592216.

[24] C. Chen, P. Jen, F.S. Lai, Optimization of the coathanger manifold via computer simulation and an orthogonal array method, Polym. Eng. Sci. 37 (1997) 188–196. https://doi.org/10.1002/PEN.11661.

[25] O.S. Carneiro, J.M. Nóbrega, F.T. Pinho, P.J. Oliveira, Computer aided rheological design of extrusion dies for profiles, J. Mater. Process. Technol. 114 (2001) 75–86. https://doi.org/10.1016/S0924-0136(01)00574-X.

[26] C.Y. Wu, Y.C. Hsu, Optimal shape design of an extrusion die using polynomial networks and genetic algorithms, Int. J. Adv. Manuf. Technol. 19 (2002) 79–87. https://doi.org/10.1007/S001700200000.

[27] W.A. Gifford, Compensating for Die Swell in the Design of Profile Dies, Polym. Eng. Sci. 43 (2003) 1657–1665. https://doi.org/10.1002/PEN.10139.

[28] J.M. Nóbrega, O.S. Carneiro, P.J. Oliveira, F.T. Pinho, Flow balancing in extrusion dies for thermoplastic profiles: Part I: Automatic design, Int. Polym. Process. 18 (2003) 298–306. https://doi.org/10.3139/217.1745.

[29] O.S. Carneiro, J.M. Nóbrega, P.J. Oliveira, F.T. Pinho, Flow balancing in extrusion dies for thermoplastic profiles. Part II: Influence of the design strategy, Int. Polym. Process. 18 (2003) 307–312. https://doi.org/10.3139/217.1746.

[30] J.M. Nóbrega, O.S. Carneiro, F.T. Pinho, P.J. Oliveira, Flow balancing in extrusion dies for thermoplastic profiles, Part III: Experimental assessment, Int. Polym. Process. 19 (2004) 225–235. https://doi.org/10.3139/217.1825.

[31] J.M. Nóbrega, Computer Aided Design of Forming Tools for the Production of Extruded Profiles, Ph.D. Thesis, 2004.

[32] J.M. Nóbrega, O.S. Carneiro, A. Gaspar-Cunha, N.D. Gonçalves, Design of calibrators for profile extrusion - Optimizing multi-step systems, Int. Polym. Process. 23 (2008) 331–338. https://doi.org/10.3139/217.2148/HTML.

[33] T. Lehnhäuser, M. Schäfer, A numerical approach for shape optimization of fluid flow domains, Comput. Methods Appl. Mech. Eng. 194 (2005) 5221–5241. https://doi.org/10.1016/J.CMA.2005.01.008.

[34] J. Sienz, S.J. Bates, J.F.T. Pittman, Flow restrictor design for extrusion slit dies for a range of materials: Simulation and comparison of optimization techniques, Finite Elem. Anal. Des. 42 (2006) 430–453. https://doi.org/10.1016/J.FINEL.2005.06.008.

[35] J. Sienz, A. Goublomme, M. Luege, Sensitivity analysis for the design of profile extrusion dies, Comput. Struct. 88 (2010) 610–624. https://doi.org/10.1016/J.COMPSTRUC.2010.02.003.

[36] M. Vincent, B. Vergnes, Y. Demay, T. Coupez, N. Billon, J.-F. Agassant, Present Challenges in the Numerical Modeling of Polymer-forming Processes, Can. J. Chem. Eng. 80 (2002) 1143–1152. https://doi.org/10.1002/CJCE.5450800616.

[37] Y. and G.Z. Mu, Modeling and simulation of the complex flows in the extrusion process of plastic profile with metal insert, in: Proc. ANTEC, Cincinnati, Ohio, 2007: pp. 352–358.

[38] S. Elgeti, M. Probst, C. Windeck, M. Behr, W. Michaeli, C. Hopmann, Numerical shape optimization as an approach to extrusion die design, Finite Elem. Anal. Des. 61 (2012) 35–43. https://doi.org/10.1016/j.finel.2012.06.008.

[39] D. Tang, F.H. Marchesini, L. Cardon, D.R. D'hooge, State of the-Art for Extrudate Swell of Molten Polymers: From Fundamental Understanding at Molecular Scale toward Optimal Die Design at Final Product Scale, Macromol. Mater. Eng. 305 (2020) 2000340. https://doi.org/10.1002/MAME.202000340.

[40] B. Debbaut, T. Marchal, Numerical simulation of extrusion process and die design for industrial profile, using multimode pom–pom model, Taylor Fr. 37 (2013) 142–150. https://doi.org/10.1179/174328908X283311.

[41] T. Marchal, Challenges of modelling the extrusion process, Taylor Fr. 34 (2013) 265–270. https://doi.org/10.1179/174328905X64786.

[42] R. I.Tanner, A theory of die-swell revisited, Elsevier. 129 (2005) 85–87.

[43] Y. Mu, G. Zhao, C. Zhang, Numerical investigation of die geometry effect on LDPE annular extrudate swell, J. Appl. Polym. Sci. 117 (2010) 91–109. https://doi.org/10.1002/app.31490.

[44] C. Béraudo, A. Fortin, T. Coupez, Y. Demay, B. Vergnes, J.F. Agassant, A finite element method for computing the flow of multi-mode viscoelastic fluids: comparison with experiments, J. Nonnewton. Fluid Mech. 75 (1998) 1–23. https://doi.org/10.1016/S0377-0257(97)00083-9.

[45] T. Tran-Cong, N. Phan-Thien, Three-dimensional study of extrusion processes by Boundary Element Method., Rheol. Acta 1988 276. 27 (1988) 639–648. https://doi.org/10.1007/BF01337460.

[46] M. Yue, Z. Guoqun, Numerical study of nonisothermal polymer extrusion flow with a differential viscoelastic model, Polym. Eng. Sci. 48 (2008) 316–328. https://doi.org/10.1002/PEN.20928.

[47] J.M.R. Marín, H.K. Rasmussen, Lagrangian finite element method for 3D time-dependent non-isothermal flow of K-BKZ fluids, J. Nonnewton. Fluid Mech. 162 (2009) 45–53. https://doi.org/10.1016/J.JNNFM.2009.05.008.

[48] J. Xing, M. Alsarheed, A. Kundu, J.P. Coulter, Internal flow optimization in a complex profile extrusion die using flow restrictors and flow separators, Int. J. Adv. Manuf. Technol. 119 (2022) 4939–4950. https://doi.org/10.1007/S00170-021-08306-6.

[49] P. Hurez, P.A. Tanguy, D. Blouin, A New design procedure for profile extrusion dies, Polym. Eng. Sci. 36 (1996) 626–635. https://doi.org/10.1002/PEN.10450.

[50] P. Hurez, P.A. Tanguy, D. Blouin, Numerical simulation of profile extrusion dies without flow separation, Polym. Eng. Sci. 33 (1993) 971–979. https://doi.org/10.1002/PEN.760331506.

[51] N.D. Gonçalves, O.S. Carneiro, J.M. Nóbrega, Design of complex profile extrusion dies through numerical modeling, J. Nonnewton. Fluid Mech. 200 (2013) 103–110. https://doi.org/10.1016/j.jnnfm.2013.02.007.

[52] M. Gupta, Y. Jaluria, V. Sernas, M. Esseghir, T.H. Kwon, Numerical and experimental investigation of three-dimensional flow in extrusion dies, Polym. Eng. Sci. 33 (1993) 393–399.

https://doi.org/10.1002/PEN.760330704.

[53] A.R. Shahreza, A.H. Behravesh, M.B. Jooybari, E. Soury, Design, optimization, and manufacturing of a multiple-thickness profile extrusion die with a cross flow, Polym. Eng. Sci. 50 (2010) 2417–2424. https://doi.org/10.1002/pen.21770.

[54] I. Szarvasy, J. Sienz, J.F.T. Pittman, E. Hinton, Computer Aided Optimisation of Profile Extrusion Dies: Definition and Assessment of the Objective Function, Int. Polym. Process. 15 (2000) 28–39. https://doi.org/10.3139/217.1577/.

[55] B.V. and J.F.A. Gobeau, J.F., T. Coupez, Computations of Profile Dies for Thermoplastic Polymers using Anisotropic Meshing, in Simulation of Materials Processing: Theory, Methodsand Applications, in: ANTEC 2011 Plast. Annu. Tech. Conf. Proc., S.F. Shen, P. Dawson Eds., Balkema, Rotterdam,The Netherlands, 1995: p. 1360.

[56] A. Rajkumar, L.L. Ferrás, C. Fernandes, O.S. Carneiro, A. Sacramento, J.M. Nóbrega, An open-source framework for the computer aided design of complex profile extrusion dies, Int. Polym. Process. 33 (2018) 276–285. https://doi.org/10.3139/217.3514/MACHINEREADABLECITATION/RIS.

[57] S. Sharma, M. Goswami, A. Deb, B. Padhan, S. Chattopadhyay, Structural deformation/instability of the co-extrudate rubber profiles due to die swell: Experimental and CFD studies with 3D models, Chem. Eng. J. 424 (2021) 130504. https://doi.org/10.1016/J.CEJ.2021.130504.

[58] L. Pauli, M. Behr, S. Elgeti, Towards shape optimization of profile extrusion dies with respect to homogeneous die swell, J. Nonnewton. Fluid Mech. 200 (2013) 79–87. https://doi.org/10.1016/j.jnnfm.2012.12.002.

[59] E. Mitsoulis, Annular extrudate swell of pseudoplastic and viscoplastic fluids, J. Nonnewton. Fluid Mech. 141 (2007) 138–147. https://doi.org/10.1016/J.JNNFM.2006.10.004.

[60] M.M.A. Spanjaards, M.A. Hulsen, P.D. Anderson, Computational analysis of the extrudate shape of three-dimensional viscoelastic, non-isothermal extrusion flows, J. Nonnewton. Fluid Mech. 282 (2020) 104310. https://doi.org/10.1016/J.JNNFM.2020.104310.

[61] M. Zhang, C.Z. Huang, Y.X. Jia, J.L. Liu, The Inverse Prediction for Profile Extrusion Die Based

on the Finite Element Method, Adv. Mater. Res. 941–944 (2014) 2332–2335. https://doi.org/10.4028/WWW.SCIENTIFIC.NET/AMR.941-944.2332.

[62] B. Touré, J. Svabik, M. Veaux, W. Bahloul, J.P. Mascia, M. Abéguilé, T. Seux, S.J. Hauko, Numerical simulation of extrusion: A good tool for troubleshooting extrusion problems, AIP Conf. Proc. 1526 (2013) 128. https://doi.org/10.1063/1.4802608.

[63] M. Gupta, Accurate simulation of the four modes of post-die extrudate shape distortion, Int. Polym. Process. 36 (2021) 69–78. https://doi.org/10.1515/IPP-2020-3995/MACHINEREADABLECITATION/RIS.

[64] Helping Plastics Processors Do Things Better | Plastics Technology, (n.d.). https://www.ptonline.com/ (accessed April 7, 2022).

[65] Automated extrusion process – Greiner Extrusion, (n.d.). https://www.greinerextrusion.com/en/extrusion/digitalisation-automation (accessed April 7, 2022).

[66] F.A. Morrison, understanding rheology, Oxford university press, New York, 2001.

[67] J. Lee, J.S. Allen, M. Gupta, Observations of liquid-liquid encapsulation in coextrusion of inelastic Newtonian fluids, in: Soc. Plast. Eng. Annu. Tech., 2011: pp. 1360–1366.

[68] M. Gupta, VISCOELASTIC SIMULATION OF BI-LAYER COEXTRUSION IN A SQUARE DIE: AN ANALYSIS OF VISCOUS ENCAPSULATION, in: Soc. Plast. Eng. Annu. Tech., 2013: pp. 1227–1231.

[69] H. Coupez, Y. Isaac, A., and Nouatin, Optimisation in forming using the simplex method and prelimi- nary results on an explicit 3D viscoelastic solution, in: Proc. 2nd ESAFORM, 1999: 477–480.

[70] Y. Mu, G. Zhao, C. Zhang, Numerical Investigation of Viscoelastic Flow and Swell Behaviors of Polymer Melts in the Hollow Profile Extrusion Process, Adv. Mater. Res. 97–101 (2010) 209–213. https://doi.org/10.4028/WWW.SCIENTIFIC.NET/AMR.97-101.209.

[71] C.W. Macosko, Rheology: Principles, Measurements, and Applications, Wiley, NEW YORK, 1994.

[72] F.T. Trouton, On the Coefficient of Viscous Traction and Its Relation to that of Viscosity, Proc. R. Soc. A Math. Phys. Eng. Sci. 77 (1906) 426–440. https://doi.org/10.1098/rspa.1906.0038.

[73] E.N. da C. Andrade, B. Chalmers, The Resistivity of Polycrystalline Wires in Relation to Plastic Deformation, and the Mechanism of Plastic Flow, Proc. R. Soc. A Math. Phys. Eng. Sci. 138 (1932) 348–374. https://doi.org/10.1098/rspa.1932.0189.

[74] E. Jenckel, K. Ueberreiter, Über Polystyrolgläser verschiedener Kettenlänge, Zeitschrift Für Phys. Chemie. 182A (2017) 361–383. https://doi.org/10.1515/zpch-1938-18240.

[75] H.J. Karam, J.C. Bellinger, Tensile Creep of Polystyrene at Elevated Temperatures. Part I., Trans. Soc. Rheol. 8 (1964) 61–72. https://doi.org/10.1122/1.548969.

[76] G. V. Vinogradov, A.I. Leonov, A.N. Prokunin, On uniaxial extension of an elasto-viscous cylinder, Rheol. Acta. 8 (1969) 482–490. https://doi.org/10.1007/BF01976233.

[77] R.L. Ballman, Extensional flow of polystyrene melt, Rheol. Acta. 4 (1965) 137–140. https://doi.org/10.1007/BF01984710.

[78] A. Ziabicki, K. Kedzierska, Studies on the orientation phenomena by fiber formation from polymer melts. IV. Effect of molecular structure on orientation. Polyethylene and polystyrene, J. Appl. Polym. Sci. 6 (1962) 361–367. https://doi.org/10.1002/app.1962.070062114.

[79] R. Takserman-Krozer, A. Ziabicki, Behavior of polymer solutions in a velocity field with parallel gradient. I. Orientation of rigid ellipsoids in a dilute solution, J. Polym. Sci. Part A Gen. Pap. 1 (1963) 491–506. https://doi.org/10.1002/pol.1963.100010143.

[80] F.H. Müller, C. Engelter, Zur Spannungsabhängigkeit des Fließens Polymerer, Kolloid-Zeitschrift Zeitschrift Für Polym. 186 (1962) 36–41. https://doi.org/10.1007/BF01797951.

[81] F.N. Cogswell, The rheology of polymer melts under tension, Plast. Polym. 36 (1968) 109–111.

[82] H. Münstedt, New Universal Extensional Rheometer for Polymer Melts. Measurements on a Polystyrene Sample, J. Rheol. (N. Y. N. Y). 23 (1979) 421–436. https://doi.org/10.1122/1.549544.

[83] T. Raible, A. Demarmels, J. Meissner, Stress and recovery maxima in LDPE melt elongation, Polym. Bull. 1 (1979) 397–402. https://doi.org/10.1007/BF00284409.

[84] J. Meissner, Development of a Universal Extensional Rheometer for the Uniaxial Extension of Polymer Melts., Trans Soc Rheol. 16 (1972) 405–420. https://doi.org/10.1122/1.549258.

[85] J. Meissner, J. Hostettler, A new elongational rheometer for polymer melts and other highly viscoelastic liquids, Rheol. Acta. 33 (1994) 1–21. https://doi.org/10.1007/BF00453459.

[86] G.H. McKinley, T. Sridhar, F ILAMENT -S TRETCHING R HEOMETRY OF C OMPLEX F LUIDS , Annu. Rev. Fluid Mech. 34 (2002) 375–415. https://doi.org/10.1146/annurev.fluid.34.083001.125207.

[87] M.L. Sentmanat, Miniature universal testing platform: From extensional melt rheology to solid-state deformation behavior, Rheol. Acta. 43 (2004) 657–669. https://doi.org/10.1007/s00397-004-0405-4.

[88] B. Li, W. Yu, X. Cao, Q. Chen, Horizontal extensional rheometry (HER) for low viscosity polymer melts, J. Rheol. (N. Y. N. Y). 64 (2020) 177–190. https://doi.org/10.1122/1.5134532.

[89] M. Sentmanat, B.N. Wang, G.H. McKinley, Measuring the transient extensional rheology of polyethylene melts using the SER universal testing platform, J. Rheol. (N. Y. N. Y). 49 (2005) 585–606. https://doi.org/10.1122/1.1896956.

[90] M. Sentmanat, B.N. Wang, G.H. McKinley, Measuring the transient extensional rheology of polyethylene melts using the SER universal testing platform, J. Rheol. (N. Y. N. Y). 49 (2005) 585–606. https://doi.org/10.1122/1.1896956.

[91] R. Pivokonsky, M. Zatloukal, P. Filip, On the predictive/fitting capabilities of the advanced differential constitutive equations for branched LDPE melts, J. Nonnewton. Fluid Mech. 135 (2006) 58–67. https://doi.org/10.1016/j.jnnfm.2006.01.001.

[92] T.S.K. Ng, G.H. McKinley, M. Padmanabhan, Linear to non-linear rheology of wheat flour dough, Appl. Rheol. 16 (2006) 265–274. https://doi.org/10.1515/arh-2006-0019.

[93] P. Svrcinova, A. Kharlamov, P. Filip, On the measurement of elongational viscosity of polyethylene materials, Acta Tech. CSAV (Ceskoslovensk Akad. Ved). 54 (2009) 49–57.

[94] R. Pivokonsky, M. Zatloukal, P. Filip, On the predictive/fitting capabilities of the advanced differential constitutive equations for linear polyethylene melts, J. Nonnewton. Fluid Mech. 150

(2008) 56–64. https://doi.org/10.1016/j.jnnfm.2007.10.005.

[95] R. Pivokonsky, M. Zatloukal, P. Filip, C. Tzoganakis, Rheological characterization and modeling of linear and branched metallocene polypropylenes prepared by reactive processing, J. Nonnewton. Fluid Mech. 156 (2009) 1–6. https://doi.org/10.1016/j.jnnfm.2008.06.001.

[96] O. Delgadillo-Velázquez, S.G. Hatzikiriakos, M. Sentmanat, Thermorheological properties of LLDPE/LDPE blends, Rheol. Acta. 47 (2008) 19–31. https://doi.org/10.1007/s00397-007-0193-8.

[97] Y. Wang, S.-Q. Wang, From elastic deformation to terminal flow of a monodisperse entangled melt in uniaxial extension, J. Rheol. (N. Y. N. Y). 52 (2008) 1275–1290. https://doi.org/10.1122/1.2995858.

[98] E. Garofalo, G.M. Russo, P. Scarfato, L. Incarnato, Nanostructural modifications of polyamide/MMT hybrids under isothermal and nonisothermal elongational flow, J. Polym. Sci. Part B Polym. Phys. 47 (2009) 981–993. https://doi.org/10.1002/polb.21706.

[99] E.B. Muliawan, S.G. Hatzikiriakos, Rheology of mozzarella cheese, Int. Dairy J. 17 (2007) 1063–1072. https://doi.org/10.1016/j.idairyj.2007.01.003.

[100] E. Mitsoulis, S.G. Hatzikiriakos, Rolling of bread dough: Experiments and simulations, Food Bioprod. Process. 87 (2009) 124–138. https://doi.org/10.1016/j.fbp.2008.07.001.

[101] J. Aho, V.H. Rolón-Garrido, S. Syrjälä, M.H. Wagner, Measurement technique and data analysis of extensional viscosity for polymer melts by Sentmanat extensional rheometer (SER), Rheol. Acta. 49 (2010) 359–370. https://doi.org/10.1007/s00397-010-0439-8.

[102] A. Oseli, B. Bizjan, E. Król, B. Širok, L. Slemenik Perše, Tensile properties of mineral fibers determined with Sentmanat extensional rheometer, Constr. Build. Mater. 253 (2020) 119215. https://doi.org/10.1016/J.CONBUILDMAT.2020.119215.

[103] E. Garofalo, L. Di Maio, P. Scarfato, A. Pietrosanto, A. Protopapa, L. Incarnato, Study on Improving the Processability and Properties of Mixed Polyolefin Post-Consumer Plastics for Piping Applications, Polym. 2021, Vol. 13, Page 71. 13 (2020) 71. https://doi.org/10.3390/POLYM13010071.

[104] K. Yu, H.K. Rasmussen, J.M.R. Marín, O. Hassager, The dynamics of cylindrical samples in dual wind-up extensional rheometers, J. Rheol. (N. Y. N. Y). 55 (2011) 571. https://doi.org/10.1122/1.3568816.

[105] O. Hassager, J.M.R. Marin, K. Yu, H.K. Rasmussen, Polymeric liquids in extension: Fluid mechanics or rheometry?, Rheol. Acta. 49 (2010) 543–554. https://doi.org/10.1007/s00397-010-0444-y.

[106] T. Osswald, N. Rudolph, Polymer rheology, Hanser, Madison, Wisconsin, USA, 2014. https://doi.org/10.1002/app.1961.070051418.

[107] Z. Tadmor, C.G. Gogos, PRINCIPLES OF POLYMER PROCESSING, Second Edi, 2006.

[108] R.H. Ewoldt, M.T. Johnston, L.M. Caretta, Experimental Challenges of Shear Rheology: How to Avoid Bad Data, (2015) 207–241. https://doi.org/10.1007/978-1-4939-2065-5_6.

[109] K. Hyun, M. Wilhelm, C.O. Klein, K.S. Cho, J.G. Nam, K.H. Ahn, S.J. Lee, R.H. Ewoldt, G.H. McKinley, A review of nonlinear oscillatory shear tests: Analysis and application of large amplitude oscillatory shear (LAOS), Prog. Polym. Sci. 36 (2011) 1697–1753. https://doi.org/10.1016/J.PROGPOLYMSCI.2011.02.002.

[110] J. Aho, V.H. Rolón-Garrido, S. Syrjälä, M.H. Wagner, Measurement technique and data analysis of extensional viscosity for polymer melts by Sentmanat extensional rheometer (SER), Rheol. Acta. 49 (2010) 359–370. https://doi.org/10.1007/s00397-010-0439-8.

[111] A. Lyhne, H.K. Rasmussen, O. Hassager, Simulation of elastic rupture in extension of entangled monodisperse polymer melts, Phys. Rev. Lett. 102 (2009). https://doi.org/10.1103/PhysRevLett.102.138301.

[112] K. Yu, J.M.R. Marín, H.K. Rasmussen, O. Hassager, 3D modeling of dual wind-up extensional rheometers, J. Nonnewton. Fluid Mech. 165 (2010) 14–23. https://doi.org/10.1016/j.jnnfm.2009.08.006.

CHAPTER 2

PROFILE EXTRUSION DIE DESIGN: A COMPARATIVE STUDY BETWEEN ELASTIC AND INELASTIC FLUIDS

This chapter was adapted from:
M. Aali, O.S. Carneiro, J.M. Nóbrega, Profile extrusion die design: A comparative study between elastic and inelastic fluids, Polym. Eng. Sci. 62 (2022) 497–509. https://doi.org/10.1002/PEN.25862.

Abstract

Computational modeling is widely used to support the design of profile extrusion dies. However, despite the viscoelastic nature of the polymer melts, the majority of the computational approaches resort to inelastic models. With the aim of assessing the accuracy of the approach usually employed on the modeling of profile extrusion dies, this work aims at comparing the behavior of profile extrusion dies when interrelated viscoelastic (elastic) and generalized Newtonian (inelastic) constitutive models are used. For this purpose, the polymer melt employed in the study was experimentally characterized, being the data collected used to fit a non-linear multimode viscoelastic (elastic) Giesekus constitutive model. Subsequently, the fitted model was used to generate the material shear flow curve, which was then used to fit a Bird-Carreau (inelastic) constitutive model. The numerical studies undertaken were focused on the extrusion die of two profiles: a simple one, with a rectangular cross-section, and a complex swimming pool cover profile. The results obtained showed that in realistic case studies the effect of elasticity might be relevant, even when modeling just the flow in the extrusion die flow channel and should be considered when designing profile extrusion dies.

Keywords: Profile extrusion, elastic fluid, inelastic fluid, flow distribution, pressure drop

2.1. Introduction

Extrusion is a steady-state process used to produce constant cross-section products [1]. Some examples of extruded products include pipes, films, sheets, and profiles. The latter has a significant industrial relevance, since it is the most challenging, and encompasses a huge range of complex shaped cross-section geometries for several applications, e.g., home siding, window frames, medical catheters, among several others [2].

In profile extrusion, the pellets of the polymeric raw material are melted in an extruder and then shaped in the extrusion die, to reach a cross-section close to the one required for the final profile. Subsequently, the profile is cooled in a calibration system, which promotes the polymer solidification and allows slight adjustments of the relevant dimensions [3,4]. The extrusion die is one of the most important tools of the extrusion line, and has an essential role in the quality of the final product and production rate [5,6].

The design of the extrusion die comprises the solution of two main problems: the flow balance and the compensation of the extrudate swell [7,8]. For the first, the flow channel must be conceived to assure an even average velocity distribution at its outlet cross-section [9–11], otherwise it would distort after leaving the flow channel, when subjected to the uniform velocity promoted by the caterpillar haul-off unit. Moreover, and mainly motivated by the viscoelastic nature of the polymeric melts, after leaving the flow channel the extrudate dimensions change and its cross-section might also distort [12–14]. Ideally, all these changes should be anticipated at the flow channel design phase. Therefore, to determine the effect of extrudate swell on the extrudate final dimensions, or to anticipate its effect on the parallel zone cross-section geometry, the viscoelastic nature of the material behavior should be taken into account.

The complexity of the profile extrusion die design task motivated the use of computer aided design approaches, carried out either with commercial or proprietary codes. However, the clear majority of the works covering the design of profile extrusion dies employ generalized Newtonian (inelastic) constitutive models [15–23]. There are a few works available in the literature that resort to viscoelastic models to tackle industrially relevant extruded profiles [24,25]. However, most of the works where viscoelastic models are used deal with simple geometries [26–29].

Based on the above, most of the modeling approaches used to support the design of profile extrusion dies, consider inelastic fluids, when the prediction of extrudate swell is not an issue or when the polymer melt has low elasticity or exhibits slip at the wall, as does rigid (unplasticised) PVC, for example. This can be one of the reasons behind the need to perform some additional experimental trial-and-error iterations,

to correct the extrusion die flow channel that results from numerical studies, before being able to produce the desired profile in stable conditions.

The main purpose of this work is to investigate the effect of the fluid model (viscoelastic and inelastic) on the accuracy of the numerical predictions of confined flow, including flow distribution and total pressure drop (that affects the selection of the extruder). For numerical modeling purposes, simpleFoam [30] and rheoTool [31,32] solvers based on the OpenFOAM computational library [33] were used for the elastic and inelastic fluid flow simulations, respectively. The viscoelastic constitutive model employed in the study is the non-linear Giesekus [34], being the parameters of the polymer melt obtained in a detailed experimental characterization. Subsequently, the fitted viscoelastic Giesekus model was used to predict the parameters of the analogous inelastic Bird-Carreau model [35]. These two models, Giesekus and Bird-Carreau, and their corresponding parameters, were the ones used in the hereinafter designated by elastic and inelastic studies, respectively. The investigation starts with a simple extrusion die, which allows identifying the most significant parameters and better understanding their effects. Subsequently, aiming at identifying the effects of the polymer melt constitutive model in a realistic problem, the same elastic and inelastic comparison will be extended to a complex industrial profile extrusion die.

The innovative character of this study is, thus, to better understand the importance of the melt elasticity in confined flow that take place in profile extrusion, in what concerns to the total pressure drop and flow distribution. Moreover, the methodology developed and used to carry out the elastic/inelastic fluid comparison, is also an original contribution.

The contents of the present chapter are organized as follows. All the experimental data and numerical information related to the case studies are addressed in Section 2.2. The results obtained for the simple and complex extrusion dies, and corresponding discussions, are presented in Section 2.3. The chapter ends with conclusions in Section 2.4.

2.2. Case Study

This section consists of three subsections, namely: (i) geometry and processing conditions, (ii) constitutive model, and (iii) numerical modeling. The geometries, processing conditions, and division of the flow channel outlet in Elemental Sections (ES), for flow distribution assessment purposes [9], will be presented in the first subsection. Subsequently, the constitutive models used, experimental data, and fitting procedure will be addressed in the second subsection. The information about the numerical modeling such as solvers used, applied boundary conditions, and mesh sensitivity studies is described in the last subsection.

2.2.1. Geometries and Processing Conditions

Two extrusion dies were employed in this work: a simple geometry (**SG**) for the production of a rectangular profile, and a complex geometry (**CG**) for the extrusion of a swimming pool cover profile, which is more representative of the industrial reality. This last one was designed assuming inelastic constitutive models [36].

The computational domains, dimensions, and patches (boundary groups) for the two case studies considered are depicted in Figure 2.1. SG comprises a 3D flow channel that converts the circular cross-section from the extruder outlet to a rectangular profile with (2×15) mm, comprising adapter, convergent and parallel zones. The angle of the convergent zone (β) affects the fluid acceleration and the tool length, being a value of 30° a typical one employed in extrusion dies [3]. For this reason, that was the convergence angle used in the reference case study (**Ref**). Two symmetry planes were considered (a vertical one, **symV**, and a horizontal one, **symH**). Thus, as illustrated in Figure 2.1(a), only a quarter of the SG was considered in the computational model, which allows reducing substantially the calculation time. For the CG, the full geometry had to be considered on the computational model (see Figure 2.1(b)). The ratio of the flow channel length to thickness (L/t) at the parallel zone is 10 in both geometries, which is a typical value used in industrial practice [3].

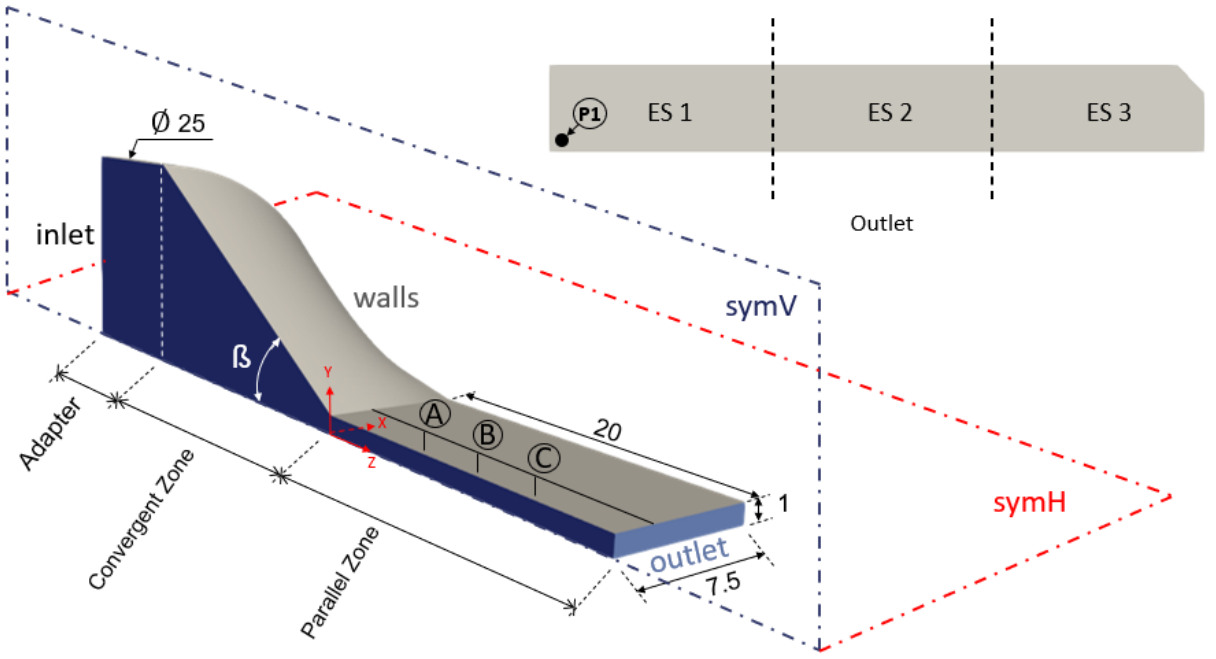

(a)

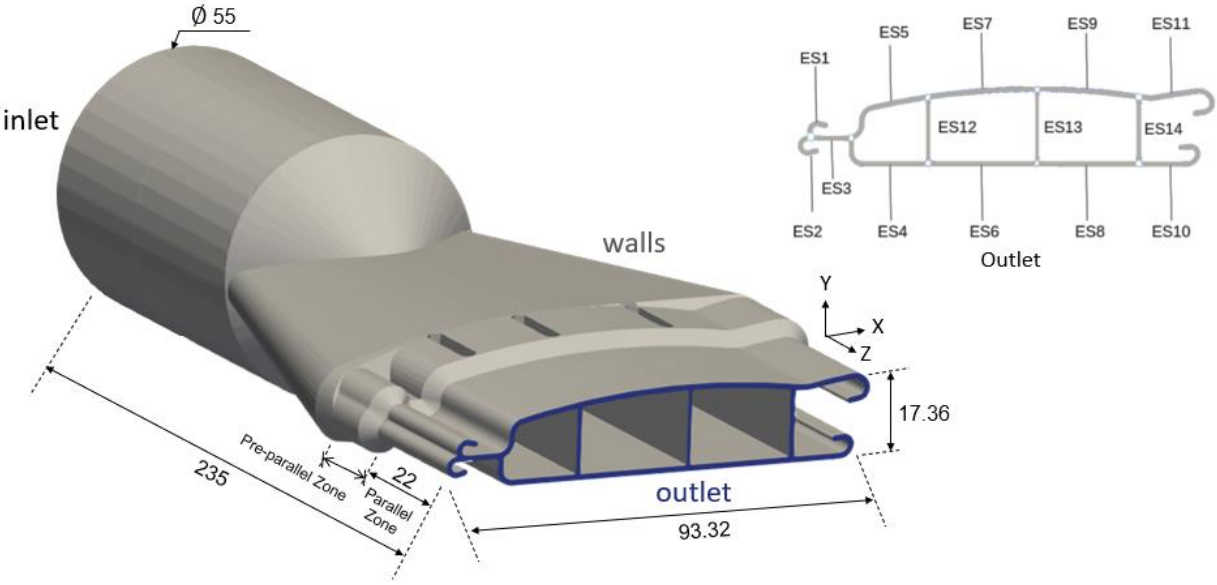

(b)

Figure 2.1: Case studies computational domains, and division of the outlet cross-section into ESs; (a) Simple Geometry - SG (Point P1 shows the location in which some results will be plotted), (b) Complex Geometry - CG, where the white zones are intersections that are not considered in the flow distribution assessment. (Note: dimensions are expressed in mm)

As indicated in Table 2.1, the Ref case for the SG has an outlet average velocity of 2 m/min, a typical industrial value in profile extrusion. Additionally, to improve the process insights, four additional case studies were considered, which aim at understanding the effect of the

average outlet velocity (U+ and U-) and of the convergence angle (β+ and β-). In the CG, just one condition was considered, corresponding to an outlet average velocity of 2 m/min.

Table 2.1: Conditions used in the SG case study

Parameters	**SG case**				
	Ref	**U+**	**U-**	**β+**	**β-**
Average velocity, U (m/min)	2	4	0.5	2	2
Convergence angle, β (°)	30	30	30	60	10

Aiming at quantifying the flow distribution, the outlet cross-sections of both SG and CG were divided into ESs [9], as depicted in Figure 2.1, in which the polymer melt average velocity was calculated. This was carried out by dividing the flow rate calculated in each ES by its area. In the CG, there are intersection zones (white sections in Figure 2.1(b)) that were not considered in the flow distribution assessment.

2.2.2. Material Characterization and Constitutive Model Fitting

The material used in this work is an extrusion grade of polycarbonate (Trirex 3027U(M1) [PC], supplied by Samyang Corporation, South Korea), which is also employed by the partner extrusion company, Soprefa SA, to produce the swimming pool cover profile (see Figure 2.1(b)). The rheological characterization of the material encompassed shear flow (parallel-plate), oscillatory, and (uniaxial) extensional rheometry tests. The shear flow test was performed at 250 °C (reference temperature) with the AR-G2 rheometer, from TA Instruments (New Castle, USA) to determine the shear viscosity Newtonian plateau. The oscillatory tests were performed with the ARES rheometer, from TA Instruments, at three different temperatures, the reference one, 230 °C, and 270 °C. The time-temperature superposition principle was applied to enlarge the characterization range. These tests were performed at the linear range of the material to determine the relaxation times spectrum and relaxation moduli (linear viscoelastic properties - LVE). The extensional rheometry tests were undertaken at the reference temperature (250 °C), with the AR-G2 rheometer, using the Sentmanat Extensional Rheometer (SER) platform [37]. In contrast with the oscillatory tests, these tests were performed at the non-linear range, and aimed to determine the material mobility factors (α) for the different modes.

The rheometry samples were all produced by compression molding, at the reference temperature. According to the datasheet of the PC, a hygroscopic material, it was dried for three hours at 120 °C in a vacuum assisted oven. Then, the dried material was used to produce samples for the shear

flow/oscillatory and extensional rheometry tests, namely disks with 25 mm diameter and 1 mm thickness, and rectangular sheets for laser-cutting strips of (17×10×0.7 mm), respectively.

Prior to the oscillatory tests, a strain sweep test was performed, at a frequency of 62.83 rad/s and reference temperature, to identify the material linear range, as depicted in Figure 2.2. Considering the results, a strain of 6% was selected for characterizing the linear behavior of the polymer melt. The storage (G') and loss (G'') moduli master curves are depicted in Figure 2.3. The experimental data collected was then fitted to small-amplitude oscillatory shear (SAOS) material functions for a multimode Maxwell fluid (Equations. (2.1) and (2.2)), given by

$$G'(\omega) = \sum_{k=1}^{N} \frac{G_k \omega^2 \lambda_k^2}{1+\omega^2 \lambda_k^2} \tag{2.1}$$

$$G''(\omega) = \sum_{k=1}^{N} \frac{G_k \omega \lambda_k}{1+\omega^2 \lambda_k^2} \tag{2.2}$$

where N is the number of modes, G_k is the relaxation modulus of the k_{th} mode, λ_k is the relaxation time of the k_{th} mode, and ω is the angular frequency

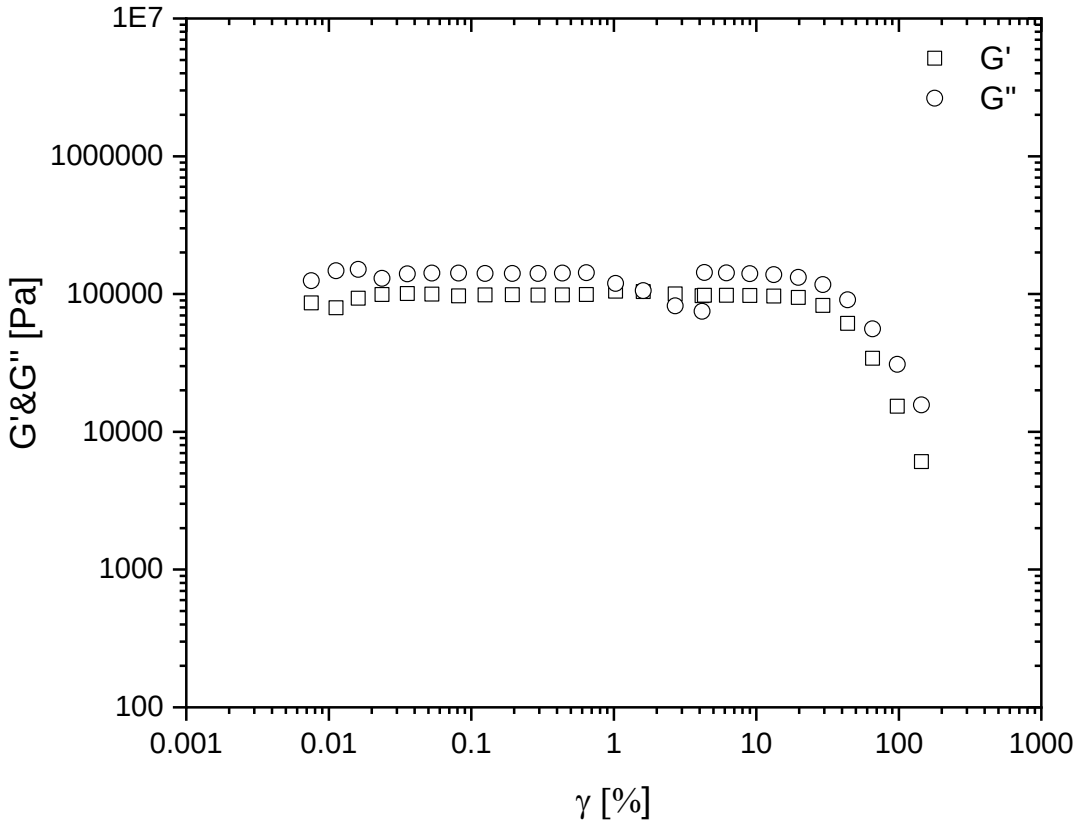

Figure 2.2: Strain sweep test

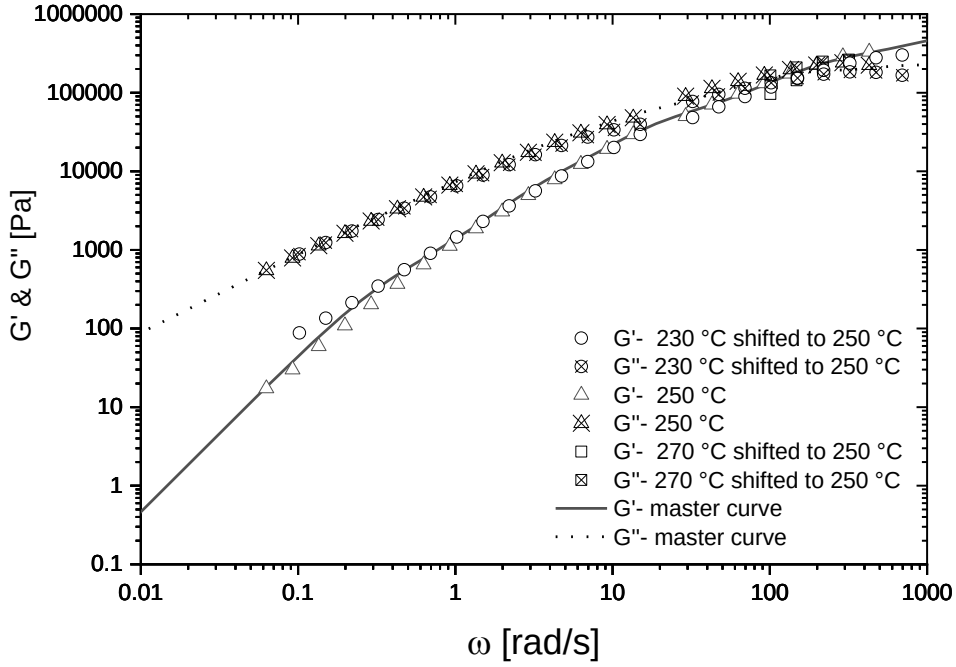

Figure 2.3: Dynamic shear moduli, G' and G'' of PC. Symbols represent experimental data, and lines represent the corresponding fitting (master curves)

The fitting procedure was carried out by minimizing the relative difference between the experimental and predicted values, using an evolutionary algorithm in an in-house developed fitting tool. A set of relaxation times was defined, and the corresponding relaxation moduli were determined (the required number of modes defined based on covering the experimental data purposes. So that, each mode covered a part of the data, and next modes were added to cover the remaining parts, and this procedure continued to cover all data), allowing for a maximum relative difference of 10^{-6} between the experimental and predicted data. It should be mentioned that the number of modes was successively increased until five, which was the number that allowed a proper fit of the experimental data. The resulting relaxation spectrum is listed in Table 2.2.

Table 2.2: Relaxation spectrum for the polymer melt (PC Trirex 3027U(M1))

Mode	G **(Pa)**	λ **(s)**	η_k **(Pa.s)**
1	400000	0.0008	320
2	250000	0.00685	1625
3	50000	0.06	3000
4	8000	0.3	2400
5	600	2.5	1500

The extensional characterization of the material was performed at different deformation rates. Considering that the extensional viscosity (η_E) measurement is highly sensitive to temperature, the convection oven temperature was allowed to stabilize for 2 h. During the test, the time available for

heating homogeneously the sample was set to 20 s. The test duration time was mainly defined based on the imposed extensional rate ranging from 2 s to 20 min, respectively, for the extensional rates of 2.5 and 0.001 1/s.

An in-house developed code was used for fitting purposes. The fitting methodology was based on the minimization of the relative difference between the experimental and predicted data, which reached values lower than 10^{-6}. In the fitting procedure, G_k and λ_k (obtained in the oscillatory tests), were used with different trial values for the mobility factors (α_k). Each α_k was adjusted until reaching values capable of generating an adequate fitting covering the whole experimental data range. Figure 2.4 depicts the fitting resulting from a 5-mode Giesekus model given by

$$\underline{\underline{\tau_k}} + \lambda_k \overset{\nabla}{\underline{\underline{\tau_k}}} + \frac{\alpha_k \lambda_k}{\eta_{0_k}} \underline{\underline{\tau_k}} \bullet \underline{\underline{\tau_k}} = \eta_{0_k} \underline{\underline{\dot{\gamma}}} \qquad 2.3$$

where $\underline{\underline{\tau_k}}$ is the stress tensor, λ_k is the relaxation time, $\overset{\nabla}{\underline{\underline{\tau_k}}}$ is the upper-convective shear stress tensor, α_k is the mobility factor, η_{0_k} is the zero-shear viscosity of the material (multiplication of G_k and λ_k), and $\underline{\underline{\dot{\gamma}}}$ is the rate of deformation tensor.

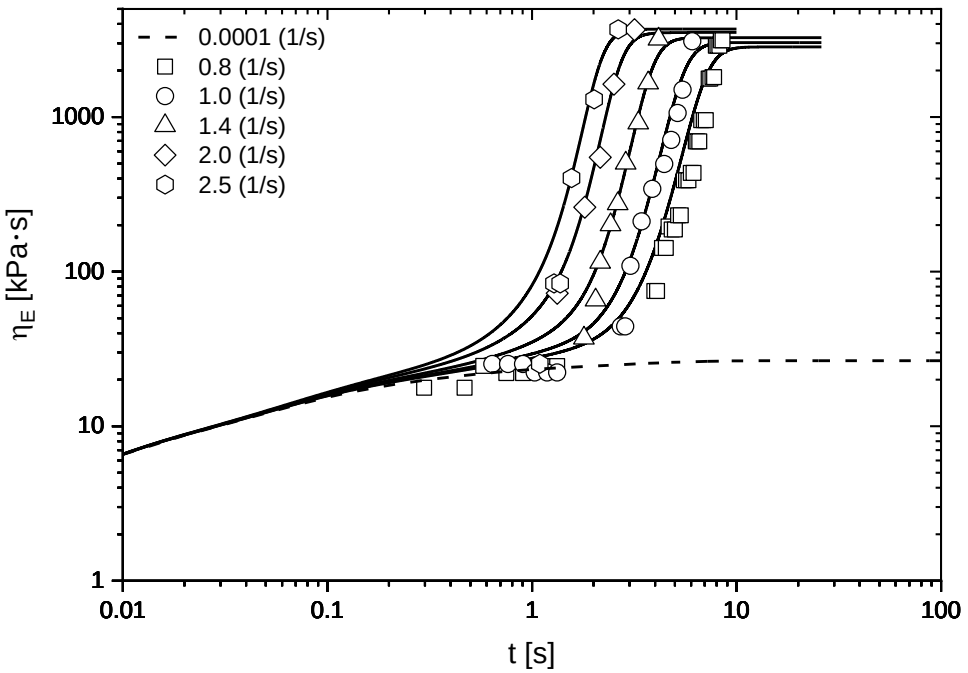

Figure 2.4: Extensional viscosity of PC obtained at the reference temperature for different extensional rates: symbols represent experimental data, solid-lines represent the corresponding fitting, and the dashed-line represents a very low extensional rate (linear range representation)

For the multimode case, the total stress tensor, $\underline{\underline{\tau_T}}$ is computed as the sum of the stress tensors for each mode (5, in the present case) given by

$$\underline{\underline{\tau_T}} = \sum_{k=1}^{N} \underline{\underline{\tau_k}} \tag{2.4}$$

where N is the number of modes, and $\underline{\underline{\tau_k}}$ is the k_{th} element of the stress tensor.

The extensional viscosity was determined as the first normal stress difference divided by the extensional rate [38]. The mobility factors obtained in the fitting are listed in Table 2.3.

Table 2.3: Mobility factor obtained for each mode

Mode	α
1	0.1
2	0.6
3	0.001
4	0.007
5	0.0008

Subsequently, the fitted Giesekus model was used to calculate the shear flow curve (η vs $\dot{\gamma}$) of the material. For this purpose, the in-house code developed for the fitting of the extensional rheometry data was modified to predict the shear viscosity. For each shear rate considered, the calculation was performed until reaching steady-state conditions (constant viscosity). The methodology was repeated to obtain a set of flow curve points covering the range 0.001 - 1000 1/s, illustrated in Figure 2.5. Then, the Bird-Carreau model (Equation (2.5)) was used to fit the predicted data, given by

$$\eta = \eta_\infty + (\eta_0 - \eta_\infty)[1 + (\lambda\dot{\gamma}^2]^{\left(\frac{n-1}{2}\right)} \tag{2.5}$$

where η_∞ is the infinite shear rate viscosity, which is assumed to be zero, λ is a characteristic time, $\dot{\gamma}$ is the shear rate, and n is the power-law index.

The resulting parameters are listed in Table 2.4. The fitting methodology was based on the minimization of the relative difference between the values calculated by the code and those predicted data by the Bird-Carreau model, which reached values lower than 10^{-6}.

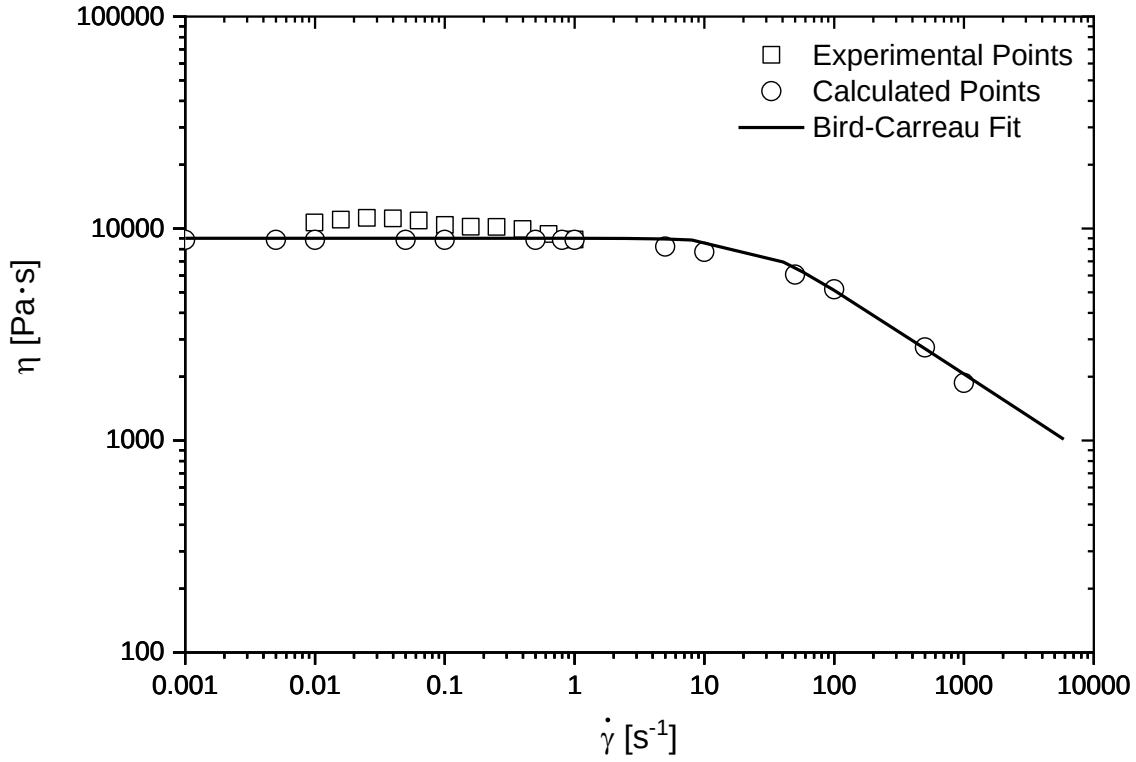

Figure 2.5: Calculated shear viscosity, based on the extensional rheometry data, and fitting. Comparison of the parallel-plate results (shear flow test) with the calculated ones

Table 2.4: Bird-Carreau model parameters obtained from the fitting

η_∞ **(Pa.s)**	η_0 **(Pa.s)**	λ **(s)**	n
0	9000	0.04	0.6

It should be mentioned that, for assessment purposes, the data predicted by the code was compared to the existing experimental data (corresponding to the plateau region). As depicted in Figure 2.5, there is a very good agreement between the predicted data and the experimental ones.

The obtained parameters for the Giesekus (Tables 2.2 and 2.3) and Bird-Carreau (Table 2.4) constitutive models were subsequently used in the numerical studies of the elastic and inelastic fluids, respectively

2.2.3. Numerical Modeling

As previously referred, the simpleFoam [30] and rheoTool [31,32] solvers, available at the OpenFOAM computational library, were used to model the flow of elastic and inelastic fluids, respectively. These solvers were selected based on the fact that a steady-state process (profile extrusion) is being considered. The boundary conditions employed for SG were the following: for the velocity field, a fully developed flow condition (using the mapped boundary condition [39] provided in OpenFOAM) was imposed at the inlet, a null (no-slip) boundary condition was used at the walls, and a null normal gradient boundary condition

was considered at the outlet. Concerning the pressure field, null normal gradient was imposed at the inlet and walls, and a null pressure was considered at the outlet. For the stress field, a null normal gradient was imposed at the outlet and walls, and a fully developed flow condition at the inlet. Symmetry plane boundary condition was imposed at patches **symV** and **symH** (see Figure 2.1(a)) for the velocity, pressure, and stress fields. The boundary conditions imposed in the CG were similar to those corresponding to SG, with the exception of the symmetry planes that do not exist in this geometry.

The number of cells of the computational meshes used for the SG in the mesh sensitivity analysis are presented in Table 2.5, being the reference mesh (M3) depicted in Figure 2.6(a). These computational meshes were generated with the cfMesh utility [40].

Table 2.5: Meshes used for the SG

Mesh	Number of cells
M1	19,180
M2	64,018
M3	1,075,526

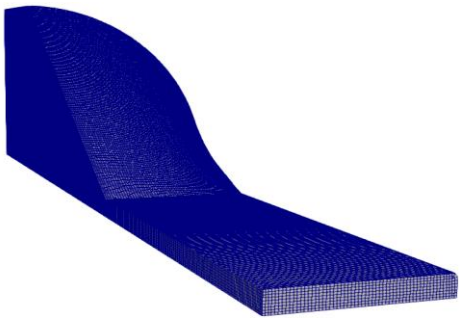

(a)

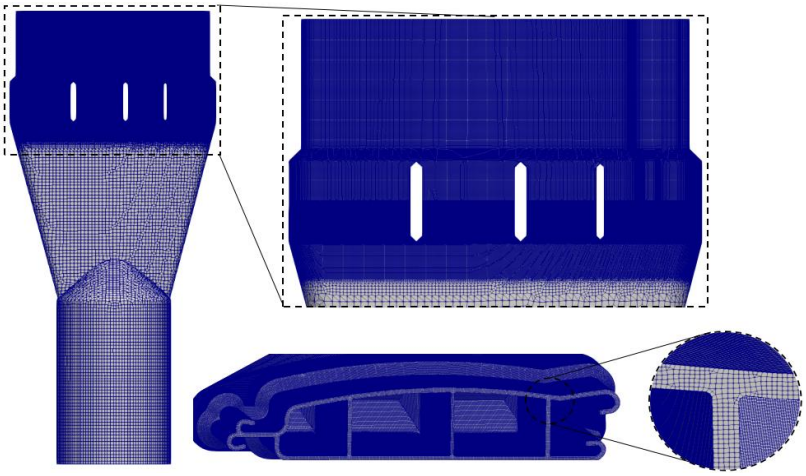

(b)

Figure 2.6: Schematic representation of the meshes selected for the modellng studies: (a) M3 for SG, and (b) equivalent to M3 mesh density for CG

In the CG, and due to the larger dimensions of the domain, the mesh was essentially refined at the pre-parallel and parallel zones, where the higher gradients occur, as depicted in Figure 2.6(b). In these zones, the density of the mesh was similar to that of mesh M3 used for the SG.

To select the appropriate level of mesh refinement in the SG, the total pressure drop and the flow distribution at each ES at the outlet (see Figure 2.1(a)), were compared with the ones obtained for the most refined mesh (M3) used in the study. As depicted in Figure 2.7, in terms of the pressure drop and the flow distribution, M3 predictions present a considerable difference when compared to those obtained with M1, especially for the elastic fluid, while there is no significant difference identified between the M3 and M2 predictions. Based on these results, all the subsequent numerical runs were made using meshes with a similar refinement level to the one employed in M3. For the CG, this resulted in a mesh with approximately 12.8 million cells (Figure 2.6(b)).

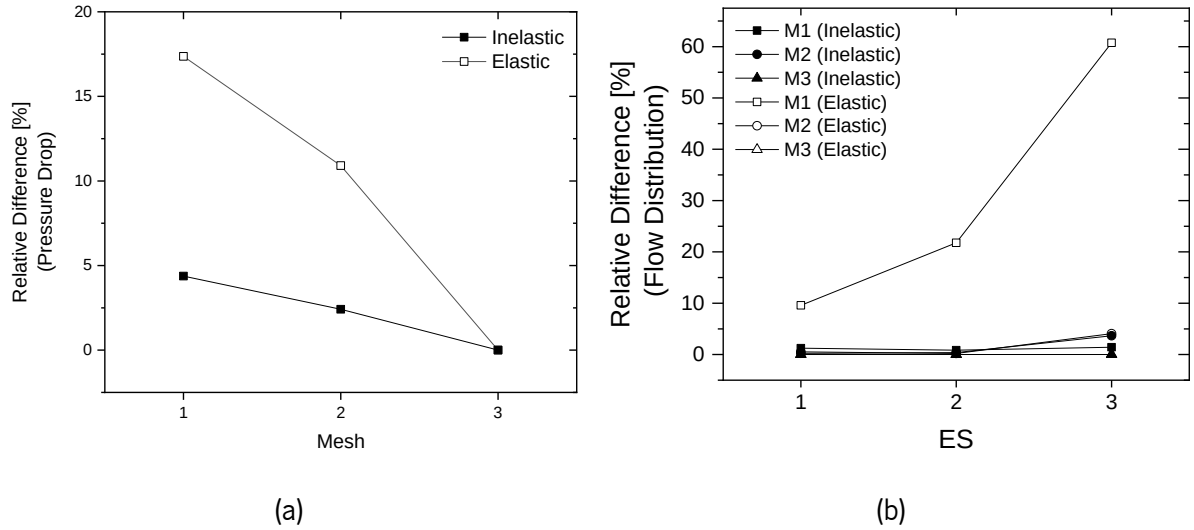

Figure 2.7: Mesh sensitivity analysis results for SG: relative differences corresponding to: (a) pressure drop, (b) flow distribution in each ES

For the mesh employed for CG the calculation time for the elastic fluid model was 7 days, using 20 cores; for the inelastic fluid model only 1 core was used, and the calculation time was just 1 hour.

2.3. Results and Discussion

In this section, the obtained results will be presented and the differences between elastic and inelastic fluids will be discussed, focusing mainly on both the flow distribution at the flow channel outlet and the total pressure drop along the flow channel. First, SG will be addressed since it is expected to provide useful insights about the underlying phenomena. The conclusions taken with this simple case will then be used to understand the results obtained for the CG case study.

2.3.1. Simple Geometry (SG) Case Study

The velocity and the pressure contours for both elastic and inelastic fluids for Ref case are depicted in Figure 2.8. As can be seen, the results obtained for both cases are quite similar. This was observed for all the test cases (with different average outlet velocities and different convergence angles). The only difference between the two types of fluid is that the velocity is higher in the central zone of the flow channel for the elastic fluid. In contrast, it seems that a fully developed flow was achieved in the inelastic fluid. These hypotheses require confirmation, and thus further investigations will be addressed in the following.

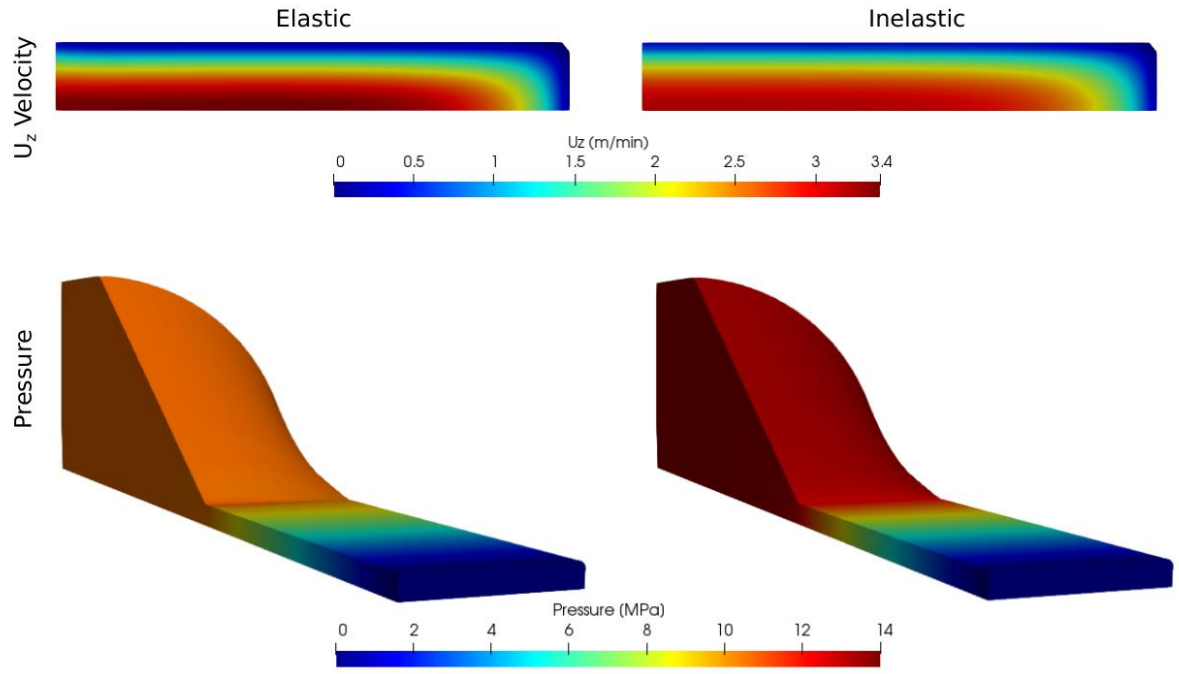

Figure 2.8: Velocity in z direction at the flow channel outlet and pressure distribution along the flow channel for both elastic and inelastic fluids

As expected, the highest pressure drop occurs in the parallel zone, in both cases, being negligible in the ones along the upstream zones. However, it can be seen that there is a significant difference between the results obtained for the two fluids.

In order to identify the reason for the above-mentioned differences, the pressure evolution in location **P1** (see Figure 2.1(a)) along the total length of the domain was plotted, for both elastic and inelastic fluids, being the results depicted in Figure 2.9. The pressure drops obtained for all the cases considered for the SG, and differences between the elastic and inelastic fluids are listed in Table 2.6.

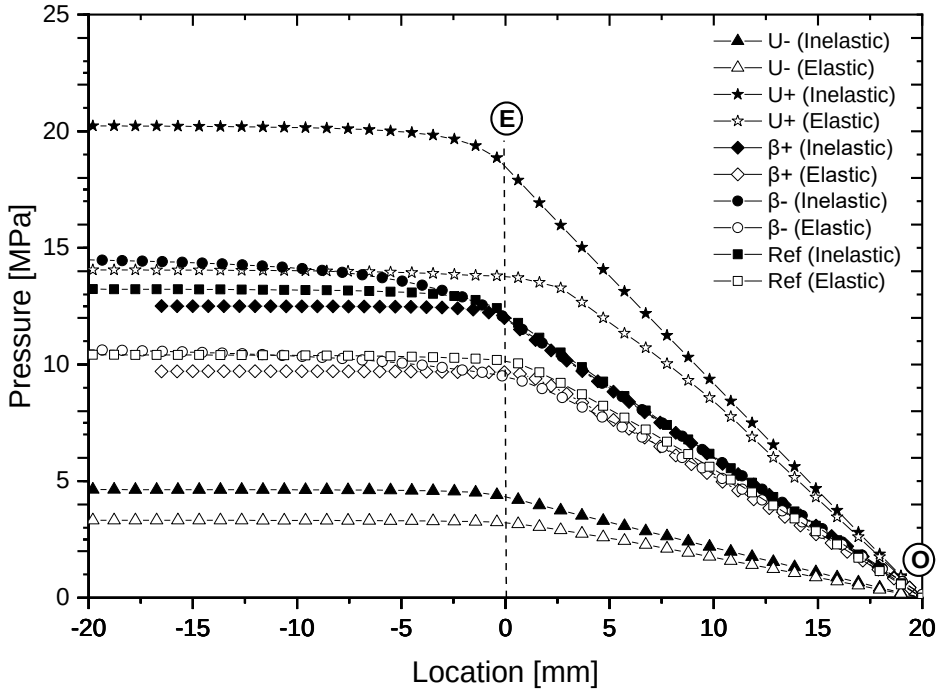

Figure 2.9: Pressure evolution along the total length of the SG (Ⓔ is the entrance of the parallel zone, and Ⓞ is the flow channel outlet)

According to the obtained results (see Figure 2.9 and Table 2.6), there is a systematic difference between the pressure drops obtained for the elastic and inelastic fluids, being significantly lower for the elastic counterpart. Furthermore, this difference increases with the average outlet velocity. Also, at the transition between the convergent and parallel zones, there is a delay in the pressure decay when the elastic fluid is considered. The elasticity of the fluid can justify the observed behavior, which is in accordance with results provided in Oliveira et al. [41]. In fact, elastic fluids have finite memory (relaxation behavior), which means that all the parameters (stresses, velocities, and pressure) require a finite time to evolve, when geometry changes occur in the flow channel, whereas for the inelastic fluid the adaption to flow conditions is almost instantaneous. Accordingly, in the case of the elastic fluid, the length required to the above-mentioned adaptation is longer for the higher velocities (higher magnitude of the deformation). The convergence angle (**β**) does not have a considerable effect on the total pressure drop obtained.

Table 2.6: Pressure drops obtained for all the cases considered for the SG, and differences between the elastic and inelastic fluids

Cases	Elastic (MPa) (E)	Inelastic (MPa) (I)	Relative difference (%) ((I-E)/I)
Ref	10.54	13.26	20.51
U-	3.83	4.64	17.45
U+	14.03	20.25	30.71
β-	10.92	14.71	25.76
β+	9.16	12.50	26.72

In order to better understand these results, the velocity profiles and the stresses were examined at different locations of the parallel zone, as depicted in Figure 2.10.

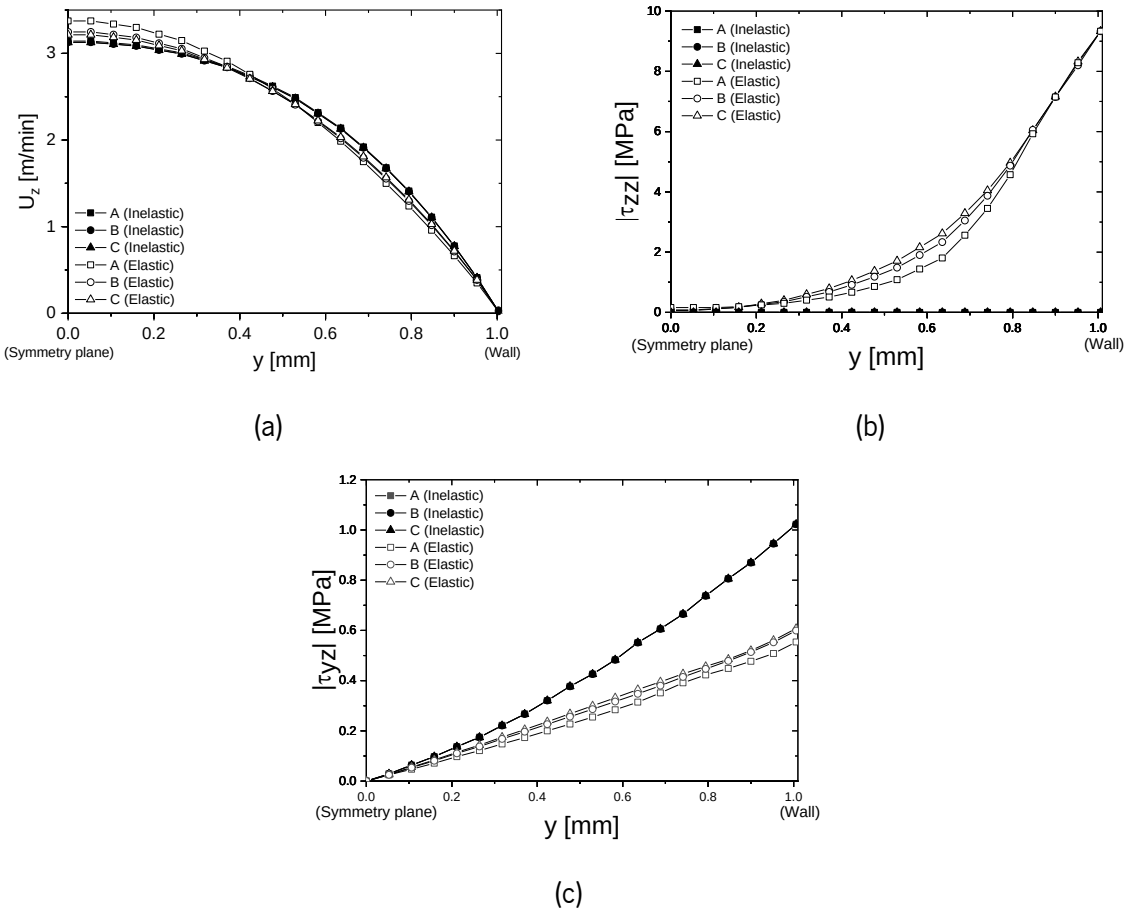

Figure 2.10: Velocity in z direction and stress tensor component profiles, along the channel thickness, at different locations of the parallel zone (see Figure 2.1); (a) velocity profile, (b) normal stress τ_{zz}, and (c) shear stress τ_{yz}

As depicted in Figure 2.10(a), the velocity profiles in z direction seem to evolve quickly for the elastic and inelastic fluids, reaching a similar shape. A small difference is visible at the center of the channel that can promote the difference observed for the velocity contours presented in Figure 2.8. As expected, and shown in Figure 2.10(b), the normal stress is zero for all the cases of the inelastic fluid, which corresponds to fully developed flow, and does not reach steady state conditions for the cases where the elastic behavior is considered. The lack of fully developed flow conditions can be also confirmed for the shear stress distribution, shown in Figure 2.10(c); the lower velocity gradient near the walls, observed for the elastic fluid, results in substantially lower shear stresses along the parallel zone (see Figure 2.10(a)). Having all the results shown into consideration, it may be concluded that the lower shear stress at the wall is the cause of the lower pressure drop obtained for the elastic fluid. Moreover, it seems that for the elastic fluid, a longer channel is required to attain fully developed flow conditions.

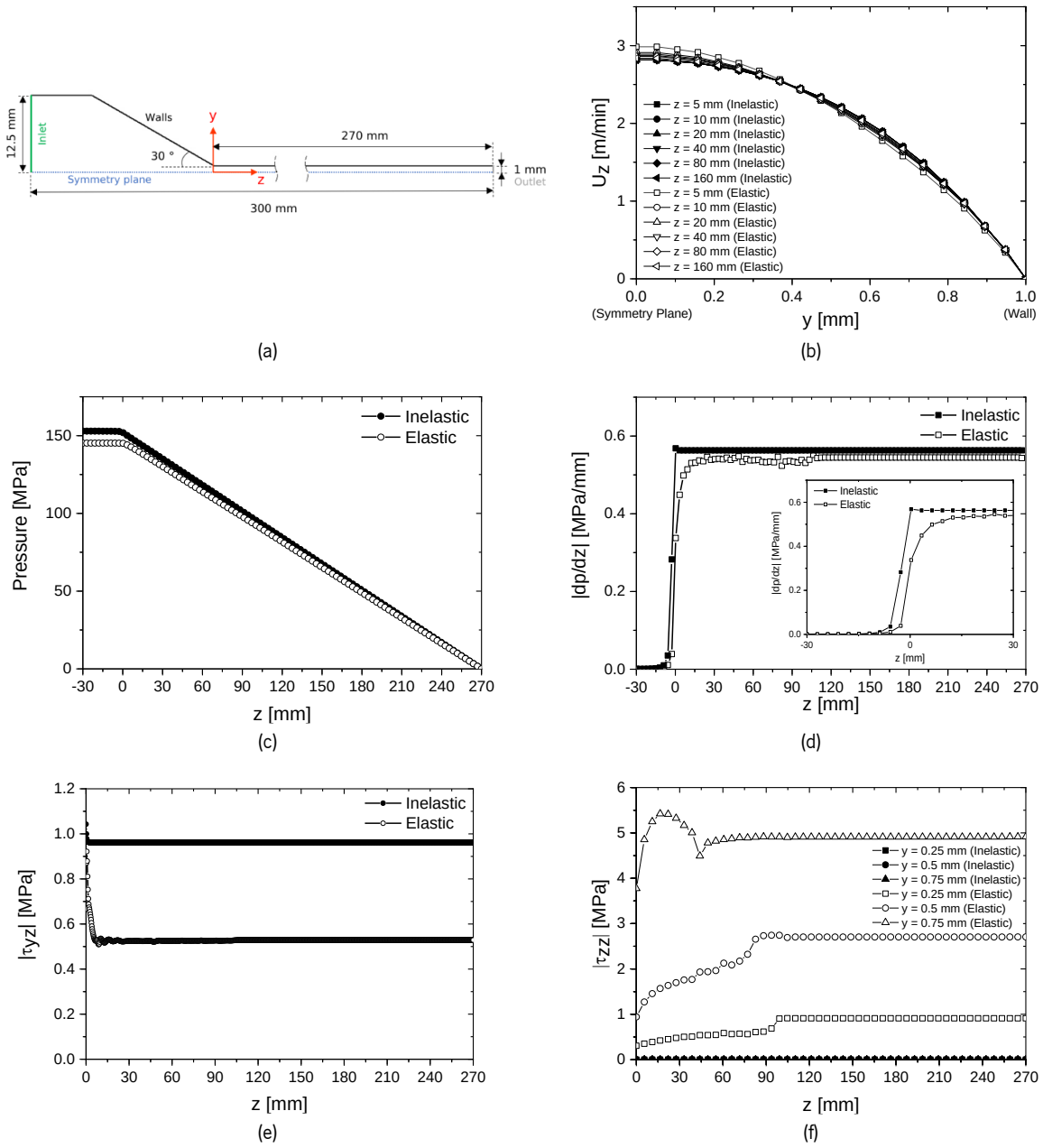

Figure 2.11: 2D-SG geometry and results obtained: (a) a schematic representation, (b) z component of velocity along the thickness at different locations of the parallel zone, (c) pressure evolution along the length, (d) pressure gradient evolution along the length, (e) shear stress at the wall along the parallel zone, and (f) normal stress along the thickness at different locations of the parallel zone

In order to confirm the above hypothesis, a 2D version of the SG (2D-SG), depicted in Figure 2.11(a), was set up to determine the length of the parallel zone required to reach a fully developed flow. The same mesh refinement level of the SG was employed for this case, together with a much longer parallel zone (270 mm). The applied boundary conditions were similar to those imposed in the SG; the only difference was that the flow was modeled as 2D.

For the 2D-SG, the velocity profiles, and stresses (shear and normal) along the parallel zone thickness, at different locations along its length, and the pressure gradient (dp/dz) along the parallel zone, are depicted in Figure 2.11.

As depicted in Figure 2.11(b), the velocity profiles in z direction evolve quickly both for the elastic and inelastic fluids, reaching a similar shape. This was also observed for the SG (3D) (see Figure 2.10(a)). Again, the main difference is that the value of the velocity for the elastic fluid is slightly higher at the center of the channel, mostly near the transition between the convergent and parallel zones. As already referred, this induces a lower velocity gradient at the wall and thus a lower shear stress at the same location (see Figure 2.11(e)), which justifies the lower pressure gradient for the elastic fluid. As depicted in Figure 2.11(c), the slope of the pressure drop for the elastic fluid is slightly lower than that of the inelastic one, from the entrance of the parallel zone until z = 120 mm, which means that the flow in this region is still developing. As soon as the stresses are fully developed (for z ≥ 120 mm), the slope of the pressure gradient for the elastic and inelastic fluids are quite similar, as shown in Figure 2.11(d). In order to further understand the exhibited pressure drop trends, the shear stress at the wall along the parallel zone was examined for both fluids, as depicted in Figure 2.11(e). For the elastic fluid, an oscillatory behavior of the shear stress, prior to z = 120 mm, is observed. A stable condition is reached just beyond z = 120 mm, which corresponds to a length over thickness ratio of 60, as soon as the flow reaches a fully developed condition. Again, this is more evident in the dp/dz graph (Figure 2.11(d)). The same behavior is observed for the normal stresses of the elastic fluid (Figure 2.11(f)) that only stabilizes for z ≥ 120 mm. This means that a longer parallel zone (z ≥ 120 mm) would be required in SG to reach fully developed flow conditions.

According to the results depicted in Figures 2.11(c) to (f), it can be concluded that although the velocity profile evolved quickly along the parallel zone, the flow is not fully developed prior to a flow channel length of 120 mm, for the elastic fluid. Downstream this location, all the flow variables (pressure gradient, and shear and normal stresses) reached a stable condition. It also should be mentioned that the dp/dz value is almost the same for the elastic and inelastic fluids when the flow is fully developed. In these conditions, the relative difference of the total pressure drop is quite small, being around 4.0%. The results obtained for the 2D-SG allowed us to conclude that a partially developed flow condition was the main reason for the difference observed in the pressure drop obtained for the elastic and inelastic fluids in the SG.

Figure 2.12 depicts the effects of different average velocity and convergent angle on the flow distribution at the flow channel outlet. As can be seen, the differences between the elastic and inelastic fluids with

the average flow velocity, mainly in the ES3 (Figure 2.12(a)). In all the cases, the average velocity is higher for ES1 and ES2, as expected, since these sections are less affected by the restriction promoted by the flow channel lateral wall, than ES3. As a consequence, the velocity is lower in the ES3. It should be mentioned that, similarly to what happened with the pressure drop, the convergence angle did not considerably affect the flow distribution (see Figure 2.12(b)).

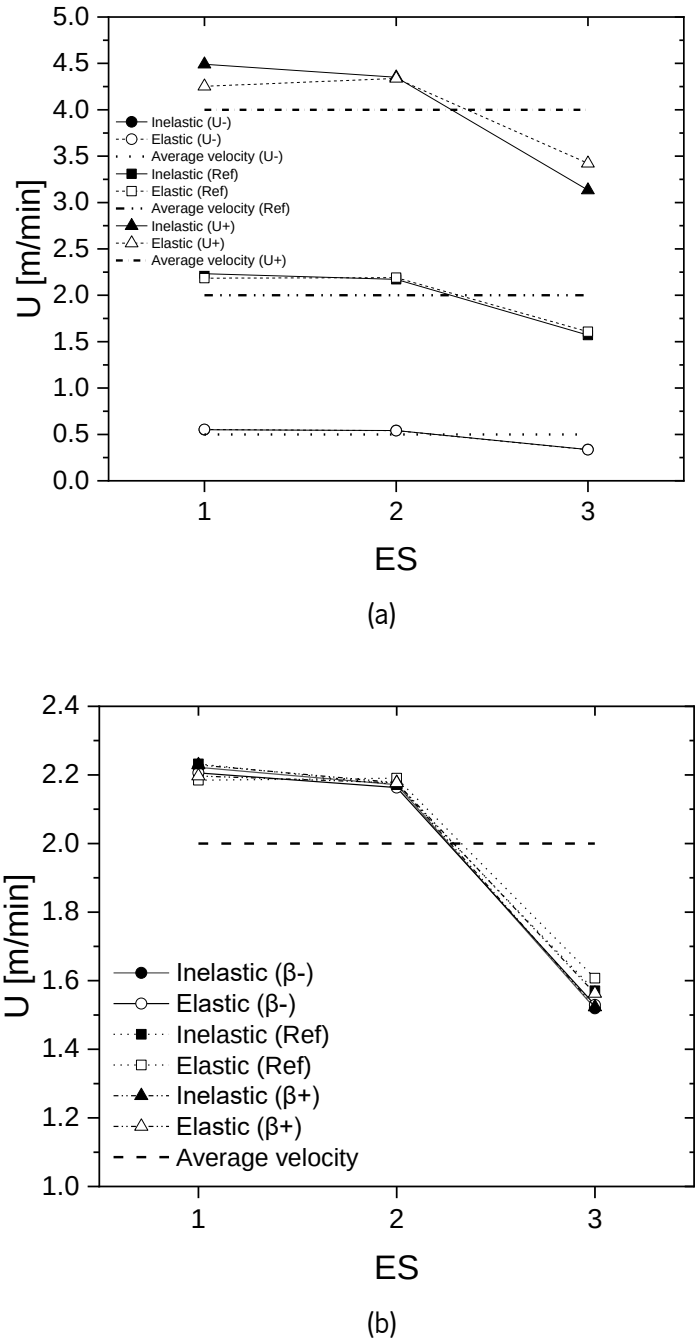

Figure 2.12: Flow distribution at the flow channel outlet: (a) effect of the average flow velocity, (b) effect of the convergence angle

2.3.2. Complex Geometry (CG) Case Study

In this section, the flow distribution and pressure drop for the CG will be analyzed, comparing the effect of the two fluid models under consideration. The main motivations are the following: (i) to verify the qualitative extension of the conclusions obtained for the SG, and (ii) to quantify the differences obtained between the elastic and inelastic constitutive models for a geometrically complex industrial extrusion die.

The velocity field at the flow channel outlet, the flow distribution, and their differences in each ES, are depicted in Figure 2.13, for both elastic and inelastic fluids.

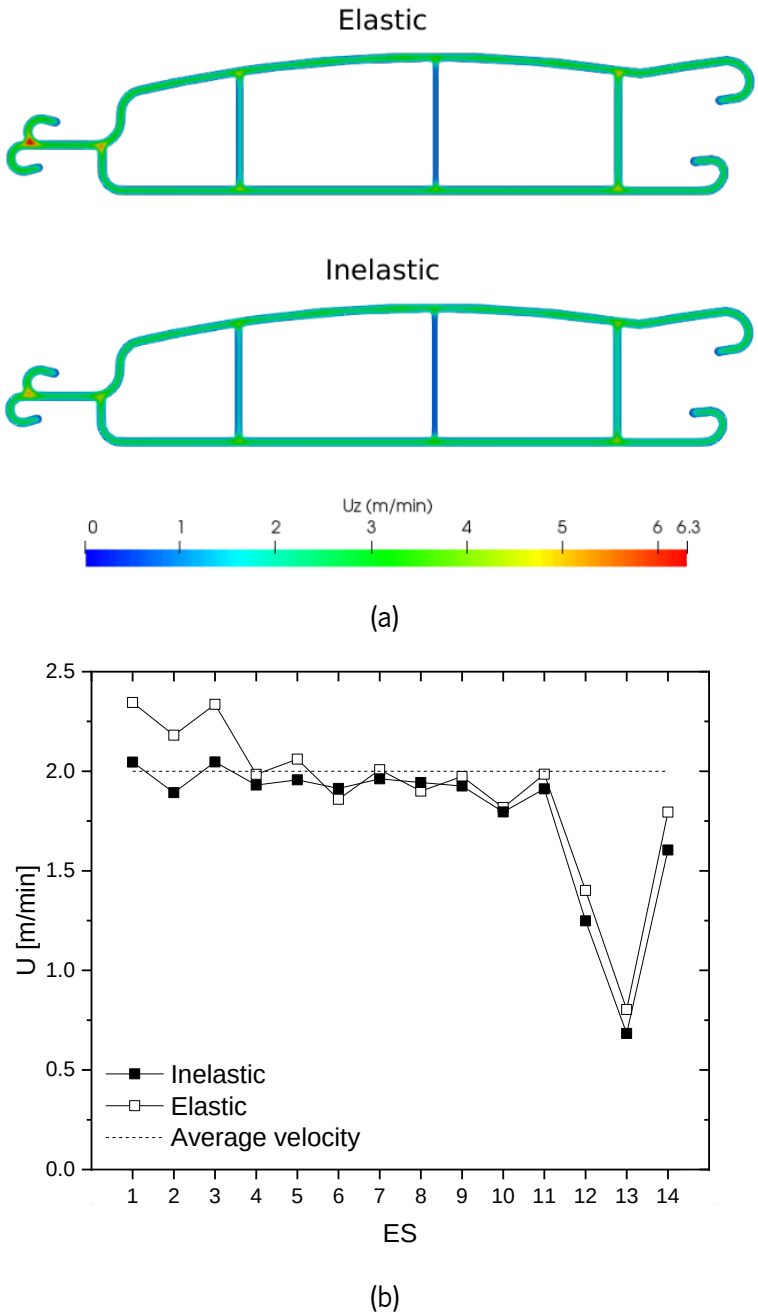

Figure 2.13: Results obtained for the CG: (a) velocity profile at the flow channel outlet, (b) flow distribution at each ESs of the flow channel outlet

As for the SG, there are no considerable differences on the velocity contours. Concerning the flow distribution, and as depicted in Figure 2.13, the extrusion die is well-balanced for most of the ESs, for the inelastic fluid (as expected since the die was designed assuming inelastic fluids [36]), with the exception of ESs 12 to 14 (the thinner interior walls). The complexity of the flow channel in the CG is the reason for the higher differences observed in terms of the flow distribution. For the elastic fluid, there are three ESs (1 to 3) that evidence a reasonable difference from the average value. It should be mentioned that this also happened in practice, when the first version of the die was tested at the extrusion company. The problem was then solved by performing some trial-and-error modifications on the flow channel geometry and use of differential heating [36] on the die external faces. Therefore, it can be concluded that elasticity also affects the flow distribution, and it would be advantageous to consider the elastic behavior on the design stage.

The pressure contours for the elastic and inelastic fluids are illustrated in Figure 2.14. Similarly, to the SG, a significant difference was observed between the elastic and inelastic fluids.

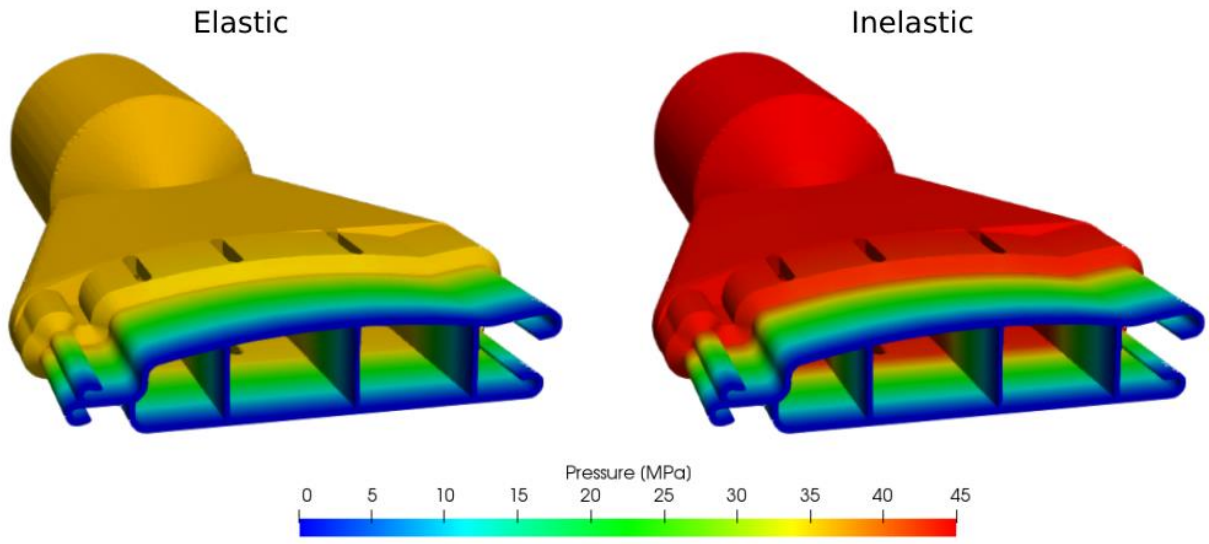

Figure 2.14: Pressure at the CG

The total calculated pressure drops were 36.4 MPa and 44.7 MPa for the elastic and inelastic fluids, respectively. The conclusions taken with the SG still applies in this case, being clear now that, for the elastic fluid, a longer parallel zone would be required to achieve a fully developed flow condition, and, therefore, similar total pressure gradients.

2.4. Conclusion

In the present work, the differences between elastic and inelastic fluids in terms of flow distribution and pressure drop in simple and complex extrusion dies, were investigated through the experimental characterization of the polymer rheology and a detailed numerical modeling study. The parameters of the constitutive model corresponding to the elastic fluid were determined by fitting the data collected in oscillatory and uniaxial extensional rheometries, using a multimode elastic (Giesekus) constitutive model. The fitted viscoelastic model was then employed to generate the shear flow curve (shear viscosity versus shear rate), being the generated data employed to fit the inelastic (Bird-Carreau) constitutive model.

The fitted models were employed in the subsequent numerical studies performed with the simpleFoam and rheoTool solvers, available in the OpenFOAM framework. Two geometries were considered in the numerical studies, one for the production of a simple rectangular profile and another employed in industry, to produce a swimming pool cover profile. The length over thickness ratio (L/t) considered for the parallel zone was 10 (a typical value used in industrial practice) in both geometries.

The investigation started with the simple extrusion die, which allowed performing a detailed study aiming at identifying the effect of the most relevant/significant process parameters (flow rate and convergence angle) on the flow distribution obtained at the flow channel outlet and the pressure drop. It was shown that the differences in the flow distribution increase with the flow rate, in particular for the elastic fluid. Concerning the convergence angle, it did not significantly affect the flow distribution. On the other hand, the results obtained showed that the velocity profiles evolved quickly, along the parallel zone, both for the elastic and inelastic fluids. A systematic difference between elastic and inelastic fluids was found in terms of the pressure drop in both simple and complex geometries. To find out the cause for this result, a simple 2D case with a very long parallel zone (L/t of 135) was set up. For the elastic fluid, at the initial length of the parallel zone, although the velocity profile quickly evolved, the stresses required a longer parallel region to reach fully developed flow conditions. Above that length (corresponding to a L/t of 60), the pressure drop gradients for the elastic and inelastic fluids were similar. Therefore, this allowed us to conclude that a very long parallel zone is required to attain the fully developed flow condition when elasticity is taken into account, a condition that does not occur in the simple and complex geometries (where the L/t was 10). According to the results obtained in the simple 2D and 3D cases, although the velocity profile quickly evolved, the stresses were not fully developed for the elastic fluid, because of the finite relaxation time of the material and the lack of a sufficient length of the parallel zone (residence time). This was identified as the main cause for the differences obtained in terms of pressure drop. As a

consequence, it was shown that in the development region, the velocity gradient near the channel walls was lower for the elastic fluid case, being, therefore, the corresponding shear stress and pressure drop also lower than that corresponding to the inelastic fluid.

The conclusions in terms of the pressure drop and flow distribution in the complex geometry were similar to the ones that were taken from the simple geometry. Again, the pressure drop was around 20% higher when the elastic fluid was considered. In terms of the flow distribution, some differences were observed between elastic and inelastic fluids, which are expected to affect the performance of the forming tool.

According to the results of the present work, the design stage can be considerably shorter when an inelastic constitutive model is used in the numerical modeling process. In fact, in this case each run took about 1 hour in one core whereas when the elastic constitutive model was used each run took circa 7 days, using 20 cores, which would obviously imply a longer design stage and more computational resources. However, since the elastic model is more accurate, fewer corrections would be expected on the experimental trial-and-error stage that follows the design stage.

References

[1] C. Rauwendaal, Polymer Extrusion, 5th ed., Hanser Publishers, Munich, 2012.

[2] A. Rajkumar, Improved methodologies for the design of extrusion forming tools, Ph.D. Thesis, University of Minho, 2017.

[3] O.S. Carneiro, J.M. Nóbrega, Design of Extrusion Forming Tools, Chapter 1, Smithers RAPRA, 2012.

[4] J.M. Nóbrega, O.S. Carneiro, J.A. Covas, F.T. Pinho, P.J. Oliveira, Design of calibrators for extruded profiles. Part I: Modeling the thermal interchanges, Polym. Eng. Sci. 44 (2004) 2216–2228. https://doi.org/10.1002/pen.20249.

[5] N.D. Gonçalves, P. Teixeira, L.L. Ferrás, A.M. Afonso, J.M. Nóbrega, O.S. Carneiro, Design and optimization of an extrusion die for the production of wood-plastic composite profiles, Polym. Eng. Sci. 55 (2015) 1849–1855. https://doi.org/10.1002/PEN.24024.

[6] N.D.F. Gonçalves, Computer Aided Design of Extrusion Forming Tools for Complex Geometry Profiles, Ph.D. Thesis, University of Mino, 2013.

[7] C. Hopmann, W. Michaeli, Extrusion Dies for Plastics and Rubber, 3th Editio, Hanser Publishers, Munich, 2003. http://www.hanserpublications.com/SampleChapters/9781569906231_9781569906231 Extrusion Dies 4E sample pages.pdf (accessed December 5, 2017).

[8] O.S. Carneiro, J.M. Nóbrega, F.T. Pinho, P.J. Oliveira, Computer aided rheological design of extrusion dies for profiles, J. Mater. Process. Technol. 114 (2001) 75–86. https://doi.org/10.1016/S0924-0136(01)00574-X.

[9] J.M. Nóbrega, O.S. Carneiro, P.J. Oliveira, F.T. Pinho, Flow balancing in extrusion dies for thermoplastic profiles: Part I: Automatic design, Int. Polym. Process. 18 (2003) 298–306. https://doi.org/10.3139/217.1745.

[10] O.S. Carneiro, J.M. Nóbrega, P.J. Oliveira, F.T. Pinho, Flow balancing in extrusion dies for thermoplastic profiles. Part II: Influence of the design strategy, Int. Polym. Process. 18 (2003) 307–312. https://doi.org/10.3139/217.1746.

[11] J.M. Nóbrega, O.S. Carneiro, F.T. Pinho, P.J. Oliveira, Flow balancing in extrusion dies for thermoplastic profiles, Part III: Experimental assessment, Int. Polym. Process. 19 (2004) 225–235. https://doi.org/10.3139/217.1825.

[12] V. Legat, J.-M. Marchal, Die design: An implicit formulation for the inverse problem, Int. J. Numer. Methods Fluids. 16 (1993) 29–42. https://doi.org/10.1002/fld.1650160103.

[13] M.M.A. Spanjaards, M.A. Hulsen, P.D. Anderson, Die shape optimization for extrudate swell using feedback control, J. Nonnewton. Fluid Mech. 293 (2021) 104552. https://doi.org/10.1016/J.JNNFM.2021.104552.

[14] V. Legat, J.-M. Marchal, Prediction of three-dimensional general shape extrudates by an implicit

iterative scheme, Int. J. Numer. Methods Fluids. 14 (1992) 609–625. https://doi.org/10.1002/fld.1650140507.

[15] P. Hurez, P.A. Tanguy, D. Blouin, A New design procedure for profile extrusion dies, Polym. Eng. Sci. 36 (1996) 626–635. https://doi.org/10.1002/PEN.10450.

[16] P. Hurez, P.A. Tanguy, D. Blouin, Numerical simulation of profile extrusion dies without flow separation, Polym. Eng. Sci. 33 (1993) 971–979. https://doi.org/10.1002/PEN.760331506.

[17] W.A. Gifford, Compensating for Die Swell in the Design of Profile Dies, Polym. Eng. Sci. 43 (2003) 1657–1665. https://doi.org/10.1002/PEN.10139.

[18] N.D. Gonçalves, O.S. Carneiro, J.M. Nóbrega, Design of complex profile extrusion dies through numerical modeling, J. Nonnewton. Fluid Mech. 200 (2013) 103–110. https://doi.org/10.1016/j.jnnfm.2013.02.007.

[19] M. Gupta, Y. Jaluria, V. Sernas, M. Esseghir, T.H. Kwon, Numerical and experimental investigation of three-dimensional flow in extrusion dies, Polym. Eng. Sci. 33 (1993) 393–399. https://doi.org/10.1002/PEN.760330704.

[20] A.R. Shahreza, A.H. Behravesh, M.B. Jooybari, E. Soury, Design, optimization, and manufacturing of a multiple-thickness profile extrusion die with a cross flow, Polym. Eng. Sci. 50 (2010) 2417–2424. https://doi.org/10.1002/pen.21770.

[21] I. Szarvasy, J. Sienz, J.F.T. Pittman, E. Hinton, Computer Aided Optimisation of Profile Extrusion Dies: Definition and Assessment of the Objective Function, Int. Polym. Process. 15 (2000) 28–39. https://doi.org/10.3139/217.1577/.

[22] M. Vincent, B. Vergnes, Y. Demay, T. Coupez, N. Billon, J.-F. Agassant, Present Challenges in the Numerical Modeling of Polymer-forming Processes, Can. J. Chem. Eng. 80 (2002) 1143–1152. https://doi.org/10.1002/CJCE.5450800616.

[23] B.V. and J.F.A. Gobeau, J.F., T. Coupez, Computations of Profile Dies for Thermoplastic Polymers using Anisotropic Meshing, in Simulation of Materials Processing: Theory, Methodsand Applications, in: ANTEC 2011 Plast. Annu. Tech. Conf. Proc., S.F. Shen, P. Dawson Eds., Balkema, Rotterdam,The Netherlands, 1995: p. 1360.

[24] B. Debbaut, T. Marchal, Numerical simulation of extrusion process and die design for industrial profile, using multimode pom–pom model, Taylor Fr. 37 (2013) 142–150. https://doi.org/10.1179/174328908X283311.

[25] T. Marchal, Challenges of modelling the extrusion process, Taylor Fr. 34 (2013) 265–270. https://doi.org/10.1179/174328905X64786.

[26] L. Pauli, M. Behr, S. Elgeti, Towards shape optimization of profile extrusion dies with respect to homogeneous die swell, J. Nonnewton. Fluid Mech. 200 (2013) 79–87. https://doi.org/10.1016/j.jnnfm.2012.12.002.

[27] E. Mitsoulis, Annular extrudate swell of pseudoplastic and viscoplastic fluids, J. Nonnewton. Fluid Mech. 141 (2007) 138–147. https://doi.org/10.1016/J.JNNFM.2006.10.004.

[28] M.M.A. Spanjaards, M.A. Hulsen, P.D. Anderson, Computational analysis of the extrudate shape of three-dimensional viscoelastic, non-isothermal extrusion flows, J. Nonnewton. Fluid Mech. 282 (2020) 104310. https://doi.org/10.1016/J.JNNFM.2020.104310.

[29] M. Zhang, C.Z. Huang, Y.X. Jia, J.L. Liu, The Inverse Prediction for Profile Extrusion Die Based on the Finite Element Method, Adv. Mater. Res. 941–944 (2014) 2332–2335. https://doi.org/10.4028/WWW.SCIENTIFIC.NET/AMR.941-944.2332.

[30] Standard solvers, simpleFoam, ESI. (n.d.). https://www.openfoam.com/documentation/user-guide/a-reference/a.1-standard-solvers (accessed June 8, 2021).

[31] F. Pimenta, M.A. Alves, rheoTool, https://github.com/fppimenta/rheoTool, (n.d.).

[32] F. Pimenta, M.A. Alves, Stabilization of an open-source finite-volume solver for viscoelastic fluid flows, J. Nonnewton. Fluid Mech. 239 (2017) 85–104. https://doi.org/10.1016/J.JNNFM.2016.12.002.

[33] H. Jasak, Error Analysis and Estimation for the Finite Volume Method with Applications to Fluid Flows, Ph.D. Thesis, Imperial College, 1996.

[34] H. Giesekus, A simple constitutive equation for polymer fluids based on the concept of deformation-dependent tensorial mobility, J. Nonnewton. Fluid Mech. 11 (1982) 69–109. https://doi.org/10.1016/0377-0257(82)85016-7.

[35] P.J. Carreau, Rheological Equations from Molecular Network Theories, Trans. Soc. Rheol. 16 (1972) 99. https://doi.org/10.1122/1.549276.

[36] O.S. Carneiro, A. Rajkumar, L.L. Ferrás, C. Fernandes, A. Sacramento, J.M. Nóbrega, Computer aided die design: A new open-source methodology, AIP Conf. Proc. 1843 (2017) 030008. https://doi.org/10.1063/1.4982987.

[37] M.L. Sentmanat, Miniature universal testing platform: From extensional melt rheology to solid-state deformation behavior, Rheol. Acta. 43 (2004) 657–669. https://doi.org/10.1007/s00397-004-0405-4.

[38] F.A. Morrison, understanding rheology, Oxford university press, New York, 2001.

[39] OpenCFD, https://www.openfoam.com/documentation/user-guide/a-reference/a.4-standard-boundary-conditions, (2021).

[40] F. Juretic, cfMesh User Guide, in: 2015: pp. 1–62. http://www.springerreference.com/index/doi/10.1007/SpringerReference_27988.

[41] M.S.N. Oliveira, P.J. Oliveira, F.T. Pinho, M.A. Alves, Effect of contraction ratio upon viscoelastic flow in contractions: The axisymmetric case, J. Nonnewton. Fluid Mech. 147 (2007) 92–108. https://doi.org/10.1016/j.jnnfm.2007.07.009.

CHAPTER 3

USING COMPUTATIONAL MODELING TO STUDY EXTENSIONAL RHEOMETRY TESTS FOR INELASTIC FLUIDS

This chapter was adapted from:
M. Aali, C. Fernandes, O.S. Carneiro, J.M. Nóbrega, Using Computational Modelling to Study Extensional Rheometry Tests for Inelastic Fluids, Fluids. 6 (2021) 464. https://doi.org/10.3390/FLUIDS6120464.

Abstract

The present work focuses on the extensional rheometry test, performed with the Sentmanat Extensional Rheometer (SER) platform, and its main objectives are: (i) to establish the modeling requirements, such as the geometry of the computational domain, initial and boundary conditions, appropriate case setup, and (ii) to investigate the effect of self-induced errors, namely on the sample dimensions and test temperature, on the extensional viscosity obtained through the extensional rheometry tests. The definition of the modeling setup also comprised the selection of the appropriate mesh refinement level to model the process and the conclusion that gravity can be neglected without affecting the numerical predictions. The subsequent study allowed us to conclude that the errors on the sample dimensions have similar effects, originating differences on the extensional viscosity proportional to the induced variations. On the other hand, errors of a similar order of magnitude on the test temperature promote a significant difference in the predicted extensional viscosity.

Keywords: extensional rheometry, Sentmanat Extensional Rheometer (SER), computational modeling; inelastic fluid, Volume-of-Fluid (VOF), Eulerian, interFoam, interIsoFoam, OpenFOAM.

3.1. Introduction

Polymeric products are widely used in different application areas such as medical, packaging, civil construction, commodities, energy, etc., playing a crucial role in our daily life. Understanding their complex rheological behavior is essential for quality assurance and productivity maximization purposes. Accordingly, polymers have been dealt with in several studies from the past decades, aiming at their rheological characterization and modeling. Generally, the rheological characterization of polymer systems is divided into two different approaches, according to the type of flow to be characterized (and used), which can be shear and extensional. When subjected to a shear flow, polymer melts exhibit a shear-thinning behavior, i.e., they are pseudoplastic fluids, which means that their shear viscosity decreases as the shear rate is increased. In an ideal extensional flow, the deformation is measured as a response to the extensional stresses (normal stresses) applied, or vice versa. In this type of flow, polymer melts generally exhibit a strain-hardening behavior, being dilatant fluids [1], meaning that their extensional viscosity increases with increasing extensional strain rate.

Based on the research history on polymer systems rheology, shear flows were the most commonly addressed. Accordingly, numerous studies were published; thus, the subject is well documented [2,3]. On the other hand, viscometric extensional flows are difficult to achieve [4], and/or interpretation of experimental data is complex. As a consequence, there is a little commercial offer of extensional rheometers, and most of the knowledge about the materials is related to shear flow characterization [5]. However, extensional flows are dominant in some relevant polymer processing technologies such as blow-molding, fiber-spinning, thermoforming, film-blowing, and coating. Therefore, in these cases, the optimization of both the operating conditions and products requires proper characterization of polymer melt extensional properties. The main investigations about extensional flows started in the late 1960s [6–11], although the topic was introduced earlier by Trouton in 1906 [12], and few papers were published in the late 1930s [13,14]. At that time, the platform used to perform the extensional rheometry tests (tensile tester) showed several limitations. These led to the development of new platforms aimed at facilitating test performance. In the first attempt, Cogswell [15] used a stress-controlled platform, which later was improved by Münstedt [16]. In this device, a load is applied to the sample, and the length evolution along time is measured. In this way, the extensional viscosity was calculated based on the variation in the sample length. The proposed approach was considerably difficult to apply.

Aiming at facilitating the measurement process, as well as ensuring accurate data, various testing platforms, mainly developed for the characterization of uniaxial extensional flows, were proposed. Raible

et al. [17] presented a type of platform based on the rotary clamp technique, which later became known as the Meissner-type rheometer. In this platform, a sample immersed in an oil bath is stretched horizontally at a constant extensional rate. Although the oil bath helps to eliminate the sagging (gravity effect), especially for low viscosity materials, it might affect the results due to eventual physical-chemical interactions with the sample. On the other hand, contrarily to the tensile tester platform [18], a constant extensional rate was imposed by a constant rotational velocity of the gears (clamps). Furthermore, using two sets of rotary clamps with equal rotation velocity provided a homogeneous sample stretching, eliminating necking near the clamps. Later, the Rheometrics Melt Extensometer (RME) platform, which is the modified and commercialized version of the Meissner-type rheometer, was presented by Meissner and Hostettler [19]. Here, the small sample, supported by the cushion of inert gas, is stretched by a belt clamping system, and the maximum Hencky strain reaches a value up to seven [19]. Moreover, the test performance verification (Hencky strain checking) was possible by using the available video recording system, which was one of the main features of the RME. Münstedt Tensile Rheometer (MTR) is another variant of this type of platform, widely used not only for measuring the extensional viscosity but also for performing creep measurements [16]. In the MTR, the sample is stretched vertically, immersed in an oil bath. Moreover, attaching one of the ends of the sample to a flat carrier plate helped to eliminate the end-effect problem. The working principle of the MTR limits the testing temperature range [16]. Furthermore, a low value of maximum Hencky strain (up to 4) and a short-range of achievable extensional rates are the main limitations of the MTR.

The Filament-Stretching Rheometer (FSR) is another alternative platform presented by Mckinley and Sridhar [20] that aims at both facilitating the measurement process and increasing the accuracy of the measurements. In this platform, the sample is placed between circular endplates, and the required extensional rate is imposed by the relative motion of these plates. The FSR was essentially suitable for low and moderate viscosity material systems [20], such as polymer solutions, and it used small dimensions samples. Moreover, its operating principle leads to restrictions in the testing temperature range and applicable extensional rate (only up to 1 s^{-1}) [20].

As mentioned above, all the developed platforms present some limitations, which motivated the development of a new one, the Sentmanat Extensional Rheometer (SER) [21]. This platform is a multi-functional device, which can be used to perform not only extensional tests but also other types of tests such as peeling, etc. [21]. In this platform, the sample length is constant [21] (one of the main features of the SER), which means that a constant velocity is required to attain a constant Hencky strain rate [21],

i.e., velocity does not have to increase exponentially, as happens in the tensile tester and the RME platforms. Generally, in real experiments, it is quite difficult to generate a pure uniaxial extensional flow. Therefore, the availability of a video recording system in the SER helps to ensure the accuracy of the measurements by enabling visualizing and checking the process. Furthermore, the simple usage of SER when compared to other concepts proposed before is its main advantage [21], which leads to its widespread use in industry and academia [22–35]. Nonetheless, numerical studies carried out using SER are not considerable. The effect of the sample clamping system on the accuracy of extensional viscosity measurements was experimentally investigated by Svrcinova et al. [30]. This was the first research dealing with performance difficulties and fostering accurate measurements with SER. In their study, the authors demonstrated that, regardless of the required extensional rate and test temperature, the extensional viscosity was affected by the clamping system. Moreover, they demonstrated that using thin samples and mounting them onto the drums without clamping helps to achieve more accurate results. Later, the extensional flow measurement methodology and data analysis in the SER were studied by Aho et al. [25]. These authors claimed that mounting samples onto the drums without clamping the system, using a pre-heating stage prior to the actual test, and correcting the sample dimensions in the final data (considering the sample expansion phenomenon promoted by heating) is essential to achieve accurate results. Recently a new platform, known as Horizontal Extensional Rheometry (HER), was developed by Li et al. [36], whose mechanism is a combination of the SER and RME platforms. The advantages of the HER are as follows: (i) sample mounting and unmounting processes were easier when compared to the SER, (ii) characterization of very thin samples such as polymer films was possible, and (iii) the effect of gravity was eliminated.

Concerning the numerical modeling and simulation devoted to the extensional flows developed in the FSR, there are just a few works available [37–39]. A Lagrangian modeling approach was proposed by Kolte et al. [37], where the effects of the surface tension and gravity were neglected. The authors demonstrated that the simulated data were in good agreement with the experimental counterpart provided by Tirtaatmadja and Sridhar [40]. In a similar study, Sizaire and Legat [38] simulated the extensional experiment performed in the FSR, considering a Finite Extendable Non-linear Elastic–Chilcott and Rallison (FENE-CR) constitutive equation, and also neglecting the effects of inertia and gravity. The authors concluded that the neglected effects of inertia and gravity could play an effective role in the accuracy of the simulations, depending on the type of material tested.

Concerning the SER platform numerical modeling, a 2D numerical study of the necking phenomenon using a Lagrangian approach was presented by Lyhne et al. [28], which was one of the earlier modeling studies of extensional flow in this type of platform. The 3D numerical modeling of the extensional rheometry tests in the SER platform was carried out by Yu et al. [41]. In this work, a Lagrangian approach of the sample with low thickness and width was in good agreement with the ideal theoretical data, while higher values of thickness and width caused a remarkable deviation. Moreover, these authors concluded that at the lower Hencky strain values, the extensional behavior was not a pure uniaxial extensional flow, as it was a combination of uniaxial and planar extensional flows. In a subsequent stage, Hassager et al. [42] also used 3D numerical modeling to identify the flow type (dominant kinematic) and to illustrate the occurrence of the necking phenomenon during the extensional test. They concluded that the dominant kinematic in the SER is a mixture of uniaxial and planar extensional flows, confirming the conclusions of Yu et al. [41]. They were also able to predict the necking phenomenon.

Despite the efforts to develop new platforms for extensional rheometry with improved performance, the accuracy of the obtained results is still unclear. Moreover, the effect of the different parameters on the accuracy of the results was not satisfactorily diagnosed. In fact, systematic sensitivity studies on the effect (s) of errors occurring in different parameters such as sample dimensions, test temperature, and inertia on the accuracy of the results have not been yet investigated. In this work, the authors focus on the limitations of the previous studies and carry out a comprehensive study of the SER tests. The main objectives of the present chapter are (i) to establish the modeling setup such as the geometry of the computational domain, initial and boundary conditions, and modeling approach, and (ii) to investigate the effect of sample dimensions and test temperature errors on the accuracy of the extensional rheometry tests. Contrarily to the previous available modeling works, which employed Lagrangian approaches, an Eulerian-based algorithm will be used to capture the polymer-air interface. The studies performed in this work are undertaken with inelastic fluids since these simple rheological models allow a swift assessment of the proposed methodologies, without the need to deal with other numerical issues inherent to more complex constitutive models, as the viscoelastic ones. However, in future publications, the proposed modeling framework should be adapted to more complex constitutive models.

The contents of the present chapter are organized as follows. A brief explanation of the SER platform is presented in Section 3.2. The extensional rheometry tests modeling setup, which consists of materials rheological properties, the definition/selection of the system geometry, computational method, initial and boundary conditions used in the numerical modeling, case setup, mesh sensitivity analysis, and effect of

gravity, are addressed in Section 3.3. The case study and results obtained for the assessed error sources, and corresponding discussion, are presented in Section 3.4. The main conclusions of this chapter are presented in Section 3.5.

3.2. The Sentmanat Extensional Rheometer (SER) Platform

This section deals with the SER platform, presenting its geometry, operation, and calculation procedure. The SER can be easily mounted on any available rotational rheometer, and it consists of two rotating wind-up drums, which are connected by gears and rotate in opposite directions. The fundamental working principle of the SER is a transformation of a rotation motion of the rheometer top-head motor to a linear displacement [21], which stretches the mounted strip sample. Figure 3.1 depicts a schematic representation of the SER platform.

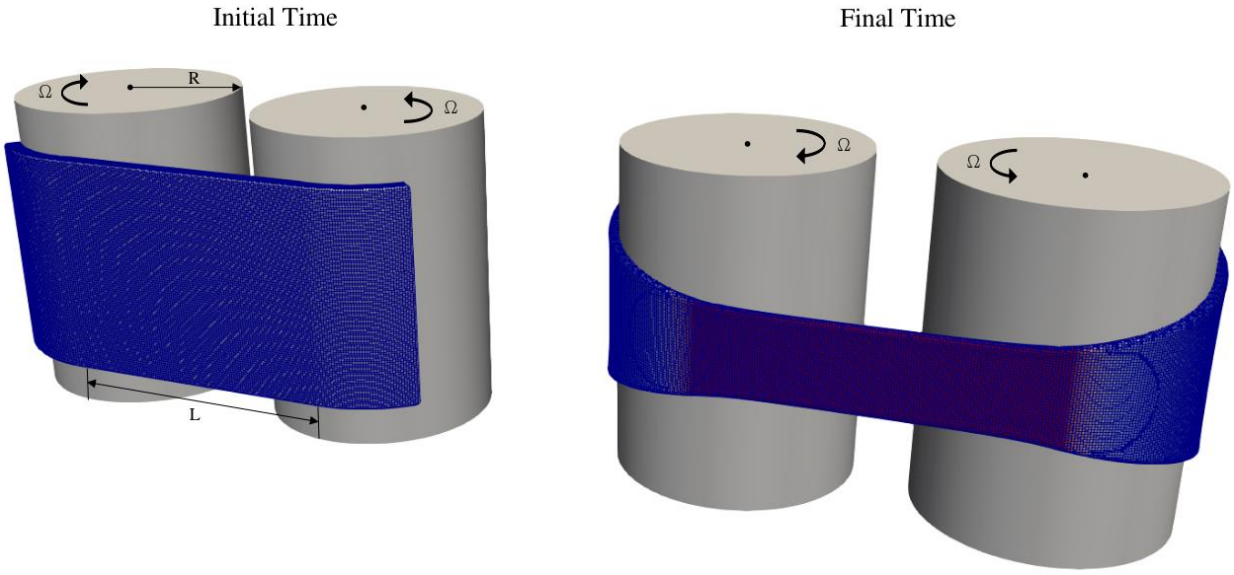

Figure 3.1: Schematic representation (3D view) of the extensional test in the SER platform

The imposed Hencky strain rate ($\dot{\varepsilon}_H$) in the SER is given by [21]

$$\dot{\varepsilon}_H = \frac{2\Omega R}{L} \tag{3.1}$$

where Ω is the drum angular velocity, R is the drum radius, and L is the sample length.

Since, as mentioned in the introduction section, the sample length is constant, the velocity does not have to vary to promote a constant extensional strain rate [21]. In this platform, the torque (T) is the only measured parameter, which is obtained by the rheometer torque transducer and can be related to the normal force applied to the sample, F , by [21]

$$T(t) = 2F(t)R \tag{3.2}$$

Then the stress (σ) is defined as [2,3]

$$\sigma = \frac{F(t)}{A(t)} \tag{3.3}$$

where A , is the cross-sectional area of the sample.

On the other hand, taking into account the constitutive model considered in this work, Newtonian (inelastic), the stress-induced in the material is given by [2,3]

$$\sigma = 3\mu\dot{\varepsilon}_{H} = \mu_{E}\dot{\varepsilon}_{H} \tag{3.4}$$

where μ and μ_E, are the material shear and extensional viscosities, respectively.

From Equations (3.3) and (3.4), the normal force, which is a function of time, can be obtained by

$$F(t) = \mu_{E}\dot{\varepsilon}_{H} A(t) \tag{3.5}$$

For isothermal conditions as happens in a typical extensional rheometry test, theoretically, the cross-sectional area, A , decreases exponentially along time, and it is a function of the Hencky strain and time as follows [21]

$$A(t) = A_0 \exp(-\dot{\varepsilon}_{H} t) \tag{3.6}$$

where A_0 is the initial cross-sectional area of the sample.

Finally, the extensional viscosity for a given Hencky strain rate can be obtained by [21]

$$\mu_{E}(t) = \frac{T(t)}{2RA(t)\dot{\varepsilon}_{H}} \tag{3.7}$$

The information provided above about the SER platform is required for the present work. In order to obtain more insights about the SER platform and its operation, the work of Sentmanat et al. [21] is advised.

3.3. Extensional Rheometry Tests Modeling Setup

This section aims at diagnosing the appropriate modeling setup for extensional rheometry tests, and it comprises the following subsections: (i) system geometry, (ii) computational method, (iii) initial and

boundary conditions, (iv) case setup, (v) mesh sensitivity analysis, and (vi) effect of gravity. The geometries used in this work are presented in the first subsection. The information about the numerical modeling, such as solvers definition, is addressed in the second subsection. Initial and applied boundary conditions are described in the third subsection. The case setup, where an appropriate configuration in terms of modeling is selected, is addressed in the fourth subsection. Subsequently, mesh sensitivity analysis will be addressed in the fifth subsection. Finally, the effect of gravity is assessed in the last subsection.

In the present work, a conventional Newtonian fluid constitutive model was considered for numerical modeling purposes, with the following properties: dynamic shear viscosity (μ_p) of 10,747 Pa·s and density (ρ_p) of 1200 kg·m^{-3} for the polymeric sample and dynamic shear viscosity (μ_A) of 1.48 × 10^{-5} Pa·s and density (ρ_A) of 1 kg·m^{-3} for the air.

3.3.1. System Geometry

The two geometries employed in this work are illustrated in Figure 3.2: **G1**, which was used on the initial modeling trials, and **G2**, which was proposed after diagnosing some limitations of G1. All the geometries, 2D and 3D, comprise two fluid regions: the polymeric sample (red region) and air (gray region). The parameters that define G1, which is 2D, are the height (H = 17 mm); total length (L_T = 14.86 mm); polymer sample initial length (L = 6.36 mm), which is the same as half of the distance between the two drums; and the drum radius (R = 5.155 mm). The parameters that define G2, in both 2D and 3D, are L and R, as defined for G1, and the outer radius (R_1 = 8.5 mm), which defines the modeled domain size. The 3D version of the G2 geometry comprises some additional parameters: the width (W = 14 mm), the sample width W_s = 10 mm), and the sample thickness (t_s = 0.7 mm).

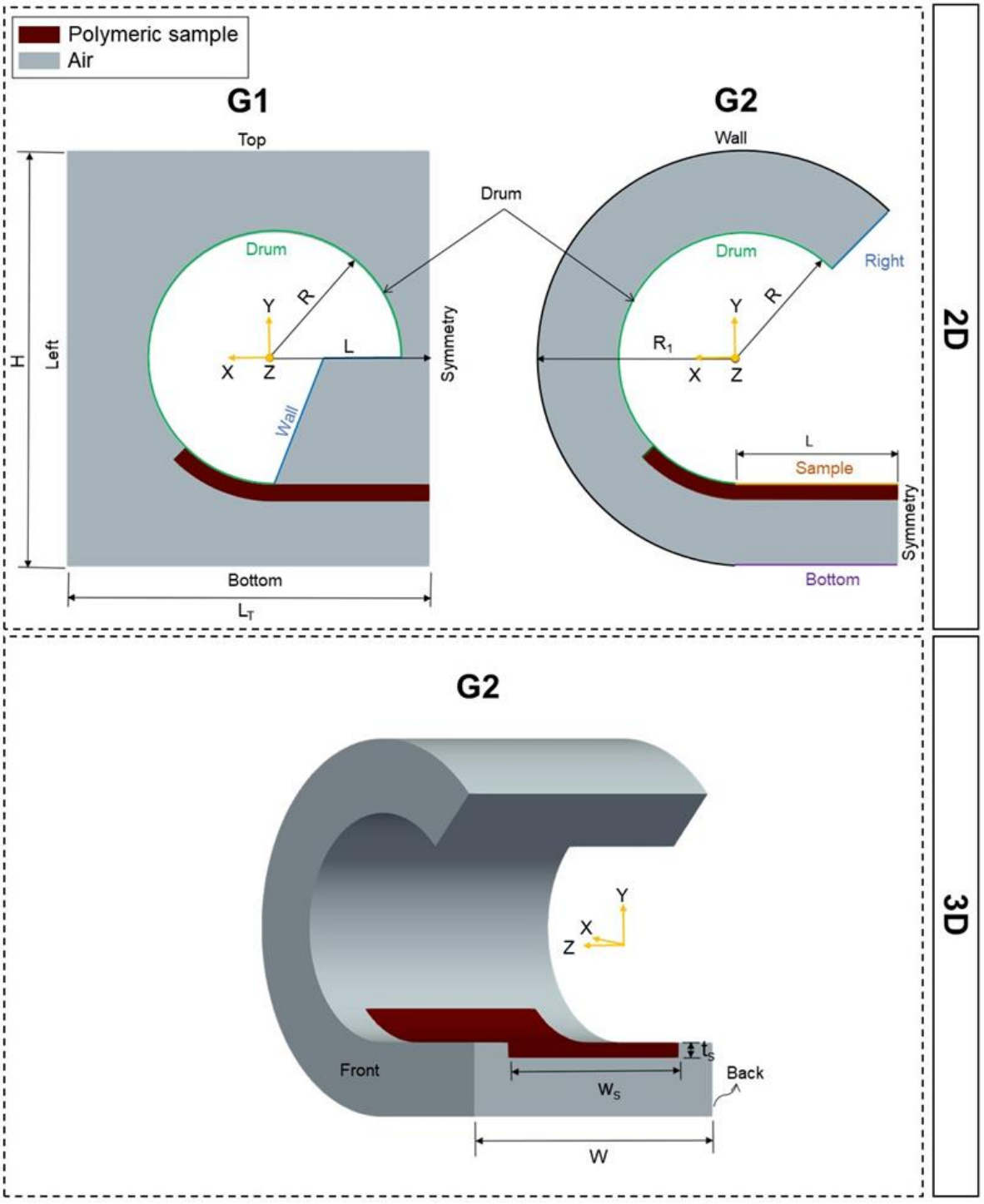

Figure 3.2: Geometries employed on the computational models

As illustrated in Figure 3.2, and due to symmetry reasons, only half of the system geometry (see Figure 3.1) was considered in the computational model, which allows substantially reducing the calculation time without affecting the results accuracy. As shown in Figure 3.2, an additional sample region that sticks at the drum surface was considered. This replicates what is carried out experimentally and aims at assuring that the drum surface speed is transmitted to the sample.

3.3.2. Computational Methods

The multiphase incompressible, isothermal, and immiscible flow solvers used in this work are the interFoam [43] and the interIsoFoam [44,45], both available in the open-source OpenFOAM computational library [46,47]. The location of the interface is known only at the initial time (see Figure 3.2), and along the modeling process its location must be calculated as part of the solution. The interFoam and interIsoFoam solvers follow the Volume-of-Fluid (VOF) method [48], the most popular variant of the interface capturing approaches [48,49], which correspond to an Eulerian approach. The main advantage of the Eulerian approach, when compared with the Lagrangian counterpart, is the use of static meshes, thus avoiding the need to deal with complex mesh manipulation algorithms. On the other hand, the main difficulty to be solved by the Eulerian-based methods is the minimization of the interface diffusion, which is inherent to these methods, while the ones that resort to moving meshes have sharp interfaces (boundaries).

In Eulerian approaches, a function value (α) is defined to capture the fraction of each cell occupied by each one of the fluids (air and polymer) [47,48]. In particular, in this work, a value of 1 for α corresponds to a cell full of one fluid, which in this work is the polymer, while α equal to 0 indicates that the cell is full of the other fluid, the air. Cells with α values between 0 and 1 are the ones where the interface is located. The interFoam solver uses an algebraic approach of the VOF method, while the interIsoFoam uses the isoAdvector [44,45] algorithm, a geometric approach of the VOF, to capture the interface. The isoAdvector algorithm computes the position of the fluids' interface surface, while the algebraic approach does not take that into account. Thus, the former is known to provide much sharper interfaces, with the disadvantage of requiring a larger computational time.

3.3.3. Initial and Boundary Conditions

Initial conditions are the initial values of the computational unknowns, being required in the modeling of unsteady cases, as the ones solved in this work. The following initial conditions were assumed for the velocity, pressure, and α : null values for velocity and pressure, for the α field a value of 1 was imposed at the polymeric sample cells, and a zero value was set for the remaining (air region).

The boundary conditions employed for geometry G1 (see Figure 3.2) were the following: for the velocity field, a rotating wall boundary condition with angular velocity of 0.987 rad·s^{-1} (corresponding to a 0.8 s^{-1} constant Hencky strain rate) was imposed at the drum, where the z-axis was the rotation axis; moreover, a null normal gradient boundary condition was used at the wall, top, left, and bottom surfaces.

Concerning the pressure field, a null normal gradient was imposed at all patches. For geometry G2, the boundary conditions imposed for the velocity field at the drum were equal to the ones considered for G1. Moreover, a null normal gradient boundary condition was used at the wall, right, and bottom faces in the 2D case and also at the front and back for the 3D case. Finally, a slip boundary condition was imposed at the sample face. Concerning the pressure field, a null normal gradient was used at all the patches, except the right, on which a null pressure was imposed. Regarding the α field, a null normal gradient boundary condition was used on all the faces. Symmetry plane boundary condition was imposed at patch symmetry (see Figure 3.2) for the velocity and pressure fields in both G1 and G2.

3.3.4. Case Setup

The work described in this section aimed to determine a proper setup, as well as select an appropriate configuration, to model the uniaxial extensional rheometry tests. In order to facilitate the modeling process, the investigation started with a 2D case study, where the gravity and surface tension were neglected, and 1 s was considered for the test duration time. The discussion starts with interFoam results obtained with G1, and all the limitations are diagnosed. Then the results obtained for the 3D geometry, G2, for both interFoam and interIsoFoam solvers, are presented and compared.

3.3.4.1. Initial 2D Trials

The modeling results of the interFoam solver for G1 (mesh with 79,947 cells) at a time of 1 s are depicted in Figure 3.3. Ideally, the sample should always stick to the drum surface during the test, as happens in practice. However, and as depicted in Figure 3.3(a), an unphysical code prediction was obtained, caused by air penetration between the polymeric sample and the drum surface. This phenomenon changed the nature of the test, promoting a significant difference between the velocity applied to the drum and that transmitted to the polymer surface, which led to a huge error (25%) in the velocity gradient calculated at the symmetry plane, as depicted in Figure 3.3(b).

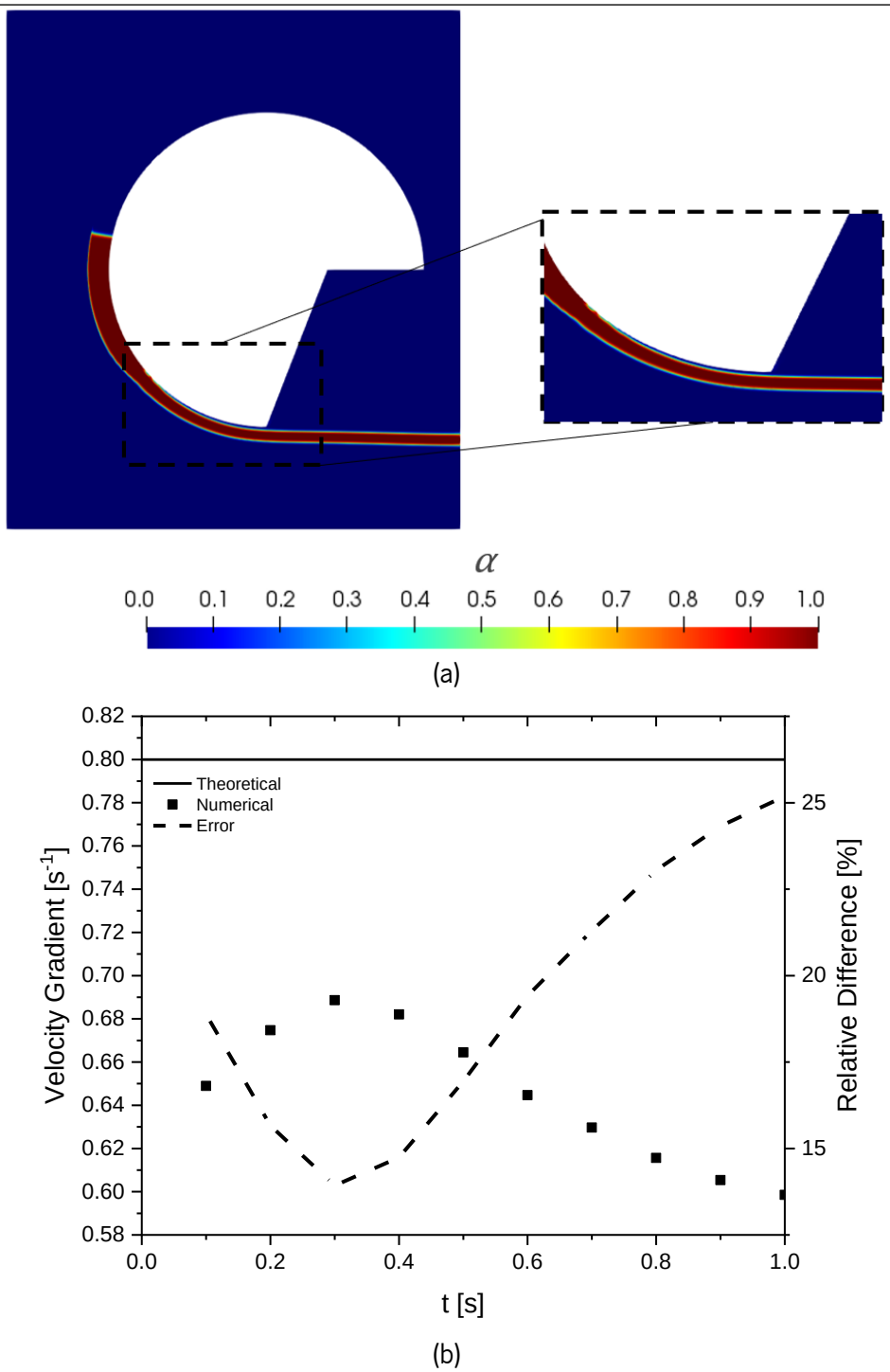

Figure 3.3: Modeling results using the interFoam solver with G1: (a) phase indicator distribution, showing the air penetration problem, (b) comparison of the numerical and theoretical average normal velocity gradient at the symmetry plane for the sample (α > 0.5)

After some unsuccessful trials with G1, which always involved the above-mentioned air penetration, the new geometry, G2 (mesh with 26,790 cells), was proposed in order to eliminate the problem described. As depicted in Figure 3.4(a), the air penetration problem was solved with this geometry. In these conditions, the predicted velocity gradient was in very good agreement with the theoretical one, and the error reduced considerably (≤ 5%), as can be seen in Figure 3.4(b). A small difference between the

numerical data and the theoretical ones, visible at the beginning of the calculation, seems to be promoted by the sample inertia, which also happens in practice.

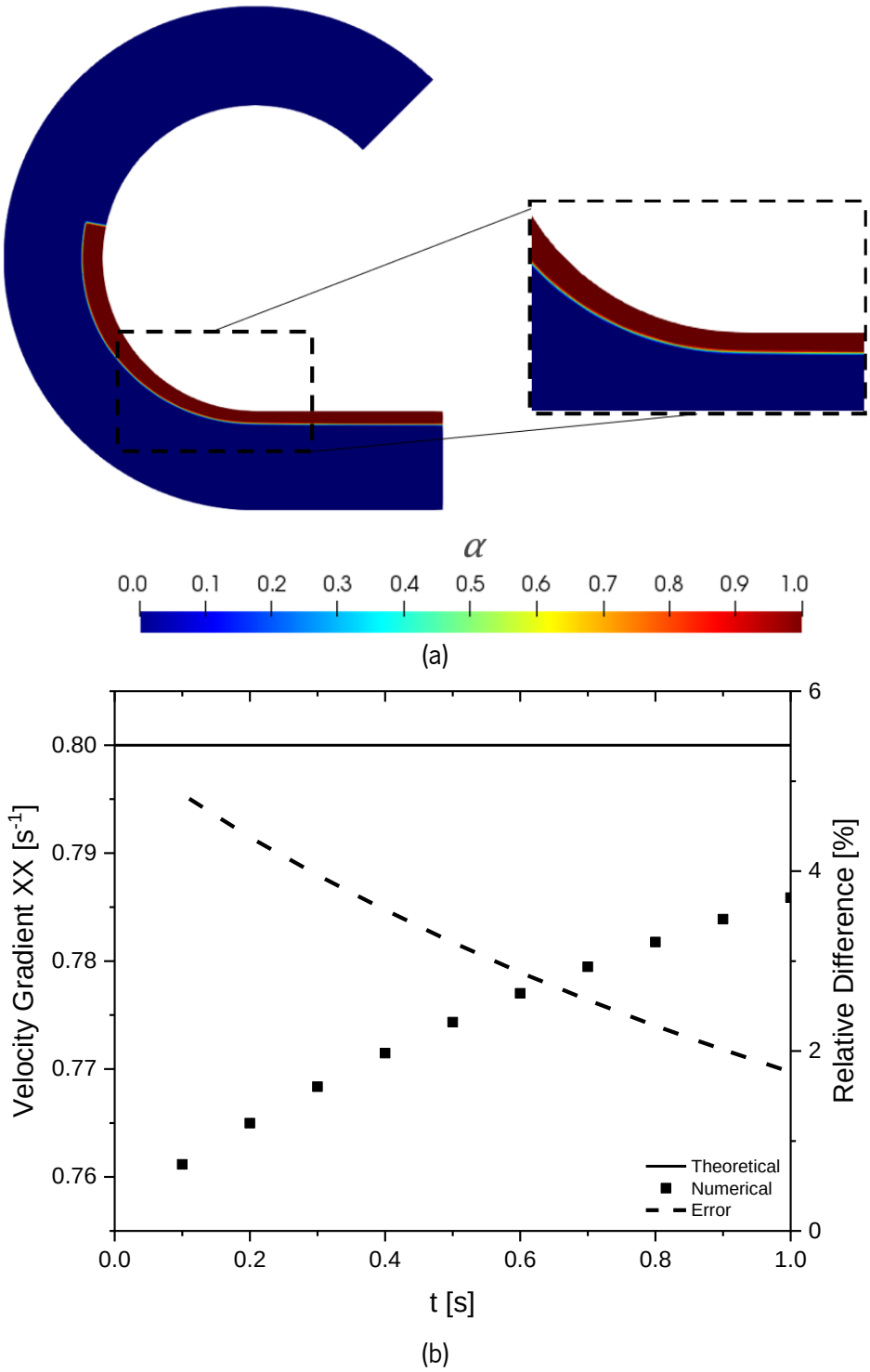

Figure 3.4: Modeling results using the interFoam solver with G2: (a) phase indicator distribution, (b) comparison of the numerical and theoretical average normal velocity gradient at the symmetry plane for the sample (α > 0.5)

According to the good numerical results obtained from G2 in the 2D case study, as well as the suppression of the air penetration problem, G2 and the respective boundary conditions were considered

as the most appropriate computational setup for performing the required modeling studies. Therefore, for the subsequent investigations, the corresponding 3D case study (see Figure 3.2), with 273,000 cells, was set up, and 2 s was considered as the test duration time.

3.3.4.2. Interface Capturing Method Selection

In this subsection, the numerical results obtained with the interFoam and interIsoFoam are compared in order to select the most appropriate approach for modeling the extensional rheometry test. According to the interFoam results depicted in Figure 3.5, although in the 3D case study the interface between the polymeric sample and air was wavy (not sharp), the numerical modeling results were in good agreement with the nature of the extensional rheometry test. First, our assumption was that the reported problem (wavy interface) resulted from an insufficient level of mesh refinement. Consequently, a higher level of mesh refinement (mesh with 1,856,400 cells) was used, but the wavy interface problem still remained, as depicted in Figure 3.5. Therefore, it was concluded that the algebraic VOF approach used in the interFoam solver was not capable of predicting the sharp interface for the present case study. Subsequently, the interIsoFoam solver was tested. As can be seen in Figure 3.5, for the same level of mesh refinement (1,856,400 cells), a sharp and physical sound interface was predicted with the interIsoFoam solver. For the most refined meshes (1,856,400 cells), the time required to reach converged results with both solvers was 1 day and 23 h, and 3 days and 19 h, respectively, for interFoam and interIsoFoam, using 192 cores. The additional time required for interIsoFoam solver, inherent to its more demanding calculation procedure, was necessary to predict a realistic sharp interface.

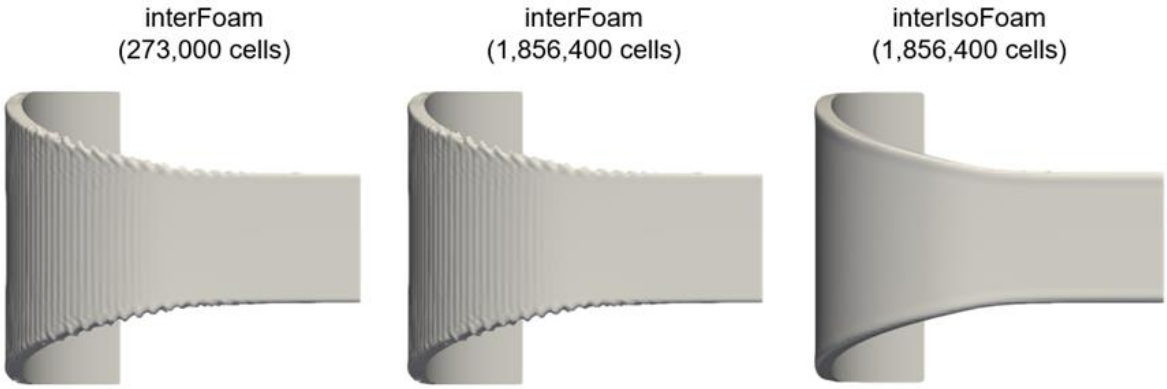

Figure 3.5: Polymeric sample geometry predicted by the modelIng code, using different meshes and interface capture ing approaches, at t = 2 s

3.3.4.3. Mesh Sensitivity Analysis

This section comprises the mesh sensitivity analysis carried out to select the most appropriate mesh refinement level to be used in the subsequent studies.

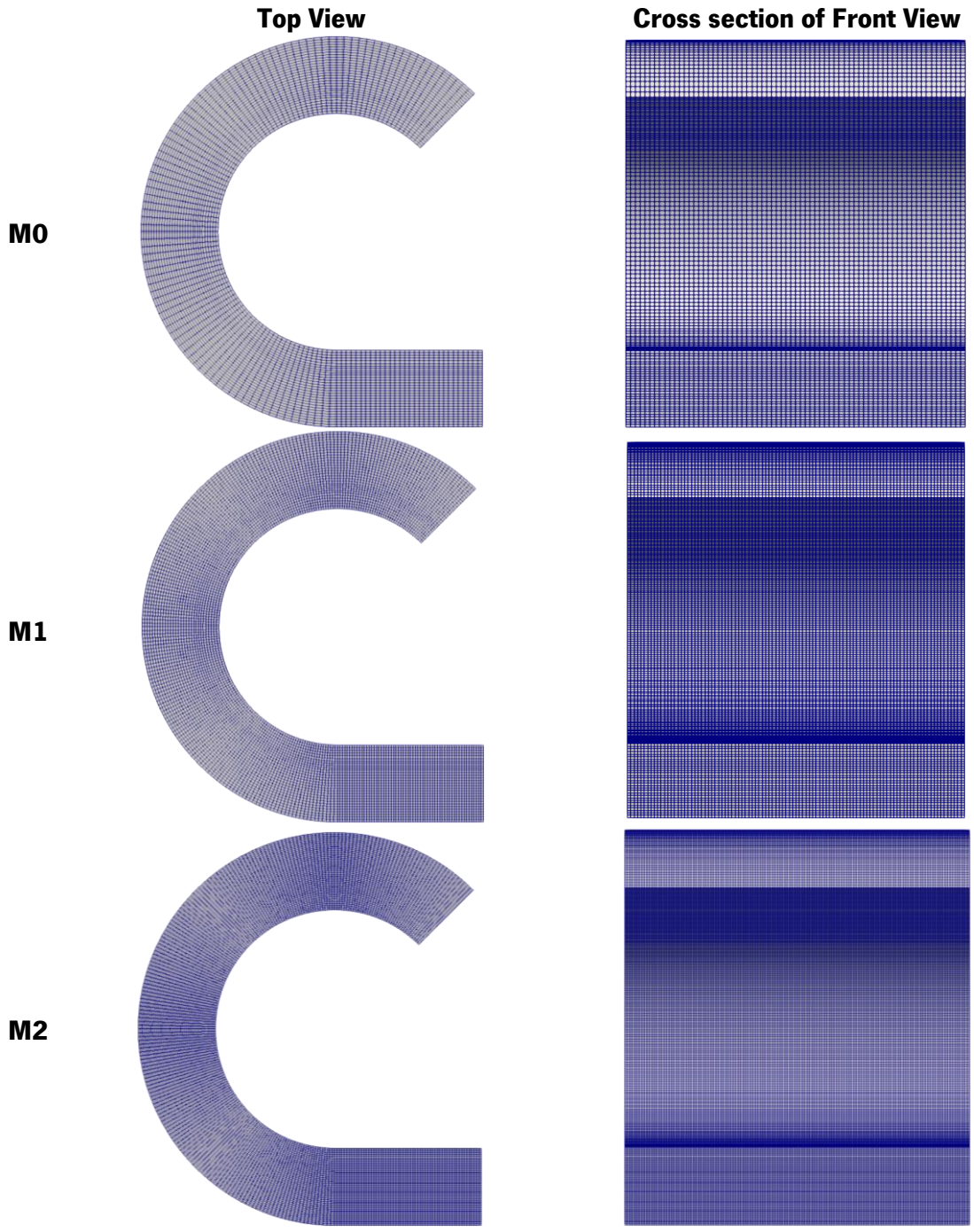

Figure 3.6: Schematic representation of the different meshes used

According to the conclusions achieved in the previous sections, all the subsequent numerical runs were made using interIsoFoam solver with G2. In the mesh sensitivity analysis, the number of cells of the computational meshes used is as follows: M0-273,000 cells; M1-780,000 cells; and M2-1,856,400 cells. All the meshes are depicted in Figure 3.6. These computational meshes were generated with the blockMesh utility [50] available in OpenFOAM. In order to select the appropriate level of mesh refinement, the numerical values of the cross-section area, forces, and extensional viscosities, obtained with the

different meshes were compared with the corresponding theoretical values. For this purpose, the theoretical cross-section area was calculated using Equation (3.6).

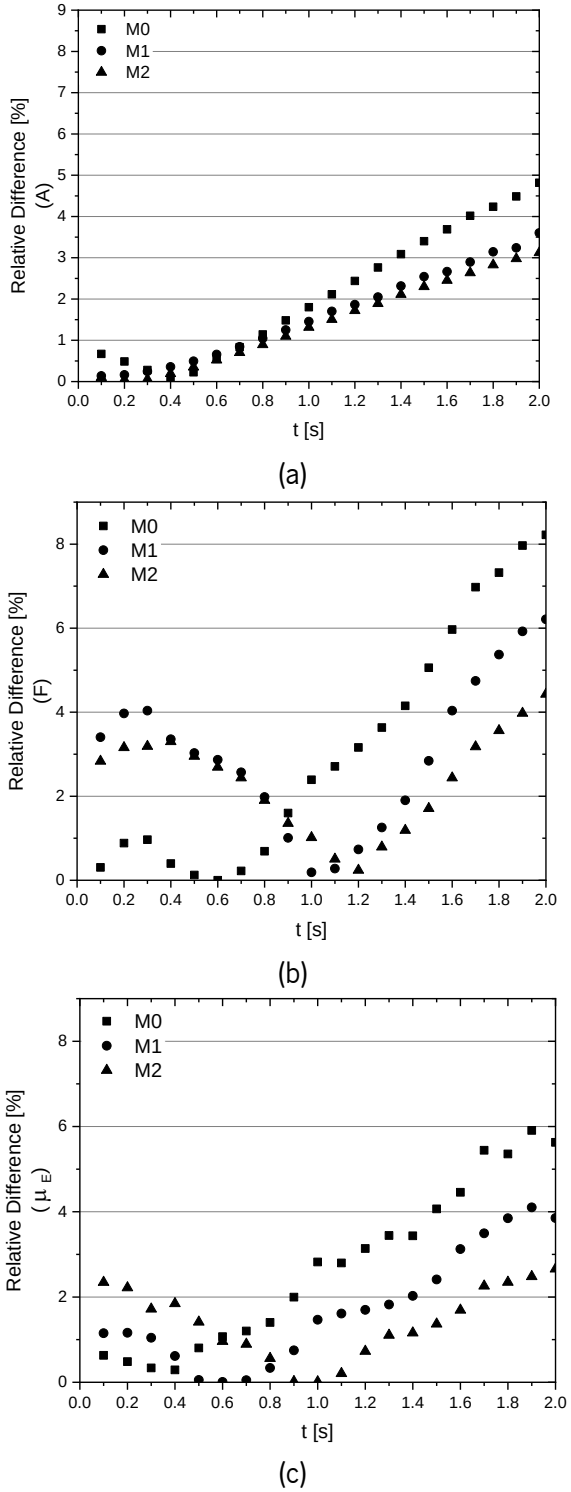

Figure 3.7: Mesh sensitivity analysis for G2. Relative differences between numerical and theoretical results corresponding to (a) cross-section area, (b) normal force, and (c) extensional viscosity

The Paraview [51] software was used to compute the numerical cross-section area, defined by the region where $\alpha > 0.5$ at the symmetry plane. The calculated theoretical normal force, using Equation (3.5),

was compared with the numerical counterpart computed with the torque at the drum surface, using Equation (3.2). Finally, the cross-section area and the theoretical and numerical torques were used in Equation (3.7) to compute the theoretical and numerical extensional viscosities, respectively.

As depicted in Figure 3.7, the M2 predictions for all the studied variables are considerably different from those obtained with M0, while there are smaller differences between the M2 and M1 results. In terms of the cross-section area data, the trends are the same for all meshes, and the difference reduces with mesh refinement level. Regarding the normal force and extensional viscosity data, a small difference is only visible at the initial part of the test. This behavior motivated a more detailed analysis of the numerical calculations carried out with M2.

The comparison of the numerical extensional viscosity and the theoretical one using M2 is depicted in Figure 3.8. As shown, the difference between the numerical and the theoretical extensional viscosities is very small. However, the numerical extensional viscosity started with a higher value, which reduces over time. This behavior seems to be related to the sample inertia, whose initial condition is at rest. To confirm this conjecture, the velocity evolution of one computational cell, whose location is depicted in Figure 3.9(a), was analyzed.

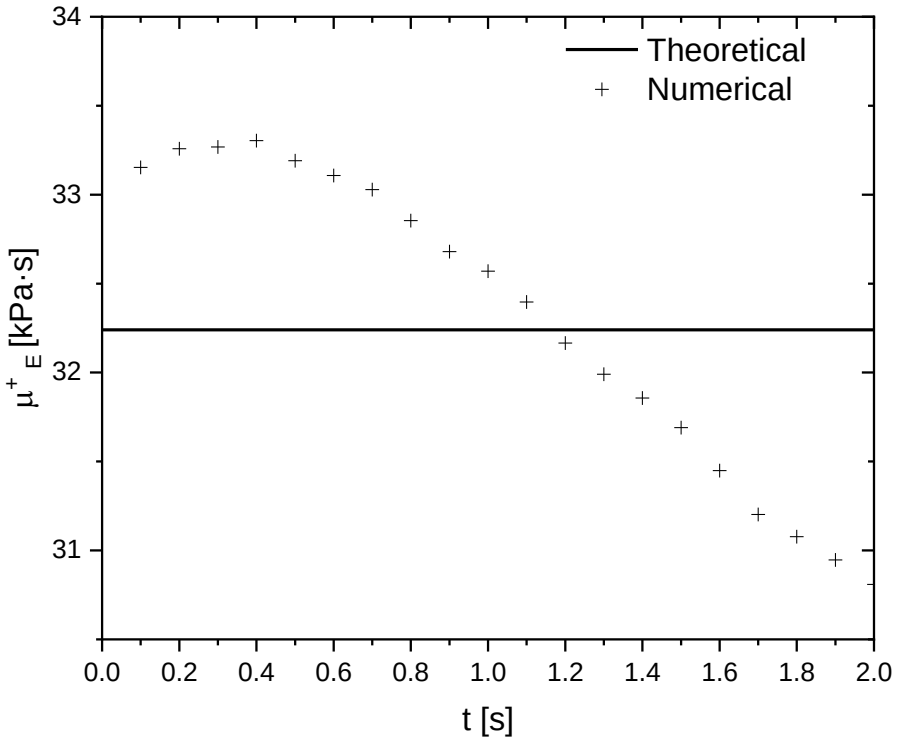

Figure 3.8: Extensional viscosity evolution: theoretical and numerical results

As shown in Figure 3.9(b), the velocity slope (acceleration) is high at the beginning of the test but reduces along with the test, i.e., the velocity tends to a constant value. In fact, in the numerical calculation a

sudden acceleration is imposed on the sample at t = 0 s. Consequently, due to inertia, the required torque is higher at the initial time steps since the polymer sample must be accelerated and deformed, which results in a higher extensional viscosity. Over time, the sample velocity tends to a steady-state distribution (null velocity slope) and, consequently, the extensional viscosity reduces and then stabilises. In fact, the time covered in the numerical case study was not enough to reach the referred steady-state conditions. These results show that inertia might affect extensional rheometry tests, which should be analysed in detail in future works.

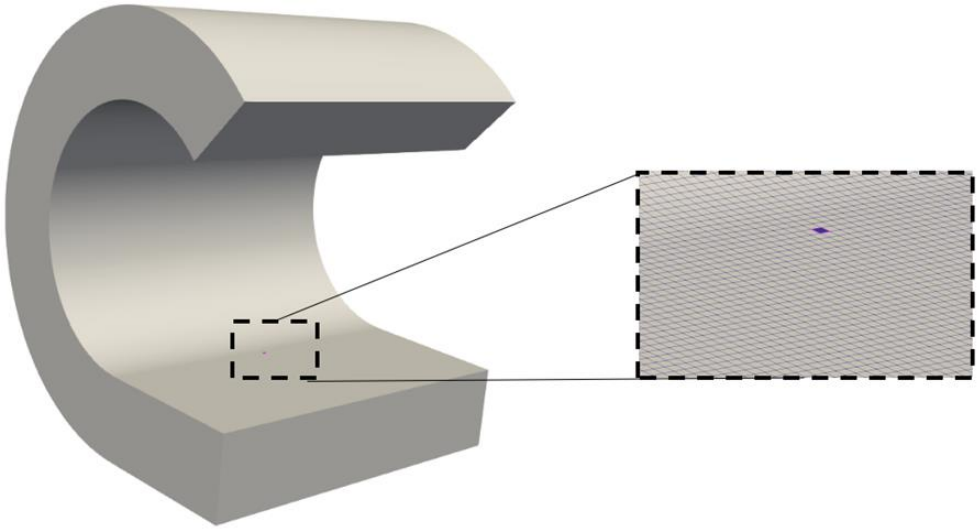

(a)

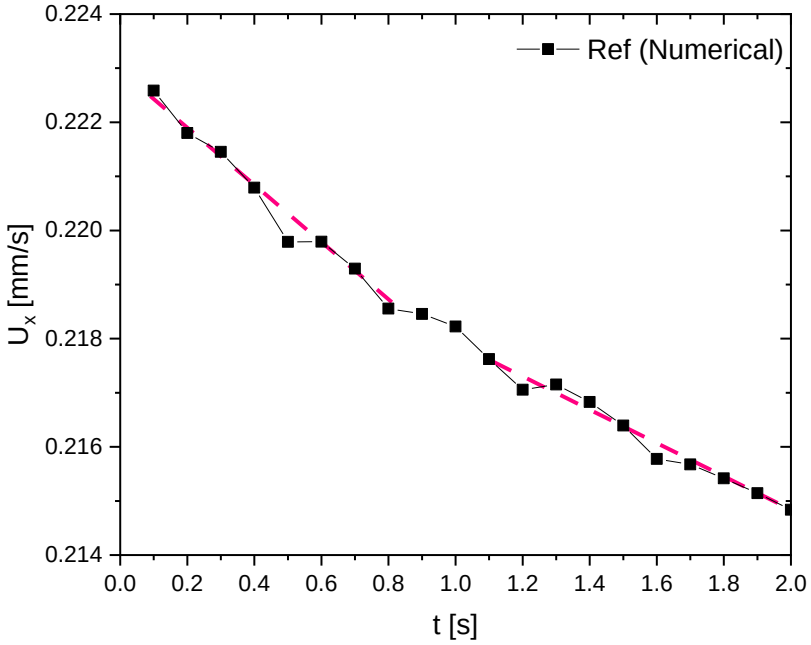

(b)

Figure 3.9: Detailed analysis of computational cell numerical results: (a) cell location and (b) x component of velocity evolution

According to the results obtained in the mesh sensitivity analysis, all the subsequent numerical runs were made using M2. For this level of mesh refinement, the calculation time was approximately 4 days, using 192 cores.

3.3.4.4. Effect of Gravity

The effect of considering or not gravity in the numerical modeling of SER tests was not studied before, despite it might influence the results, especially when low viscosity materials are considered. In order to diagnose the effect of this parameter, a case study was set up considering the gravity equal to 9.81 $m \cdot s^{-2}$ in the negative z direction. As depicted in Figure 3.10, the extensional viscosity obtained when gravity is considered, is exactly the same as the one obtained in the numerical case where gravity is neglected. Accordingly, gravity was not considered in the subsequent studies.

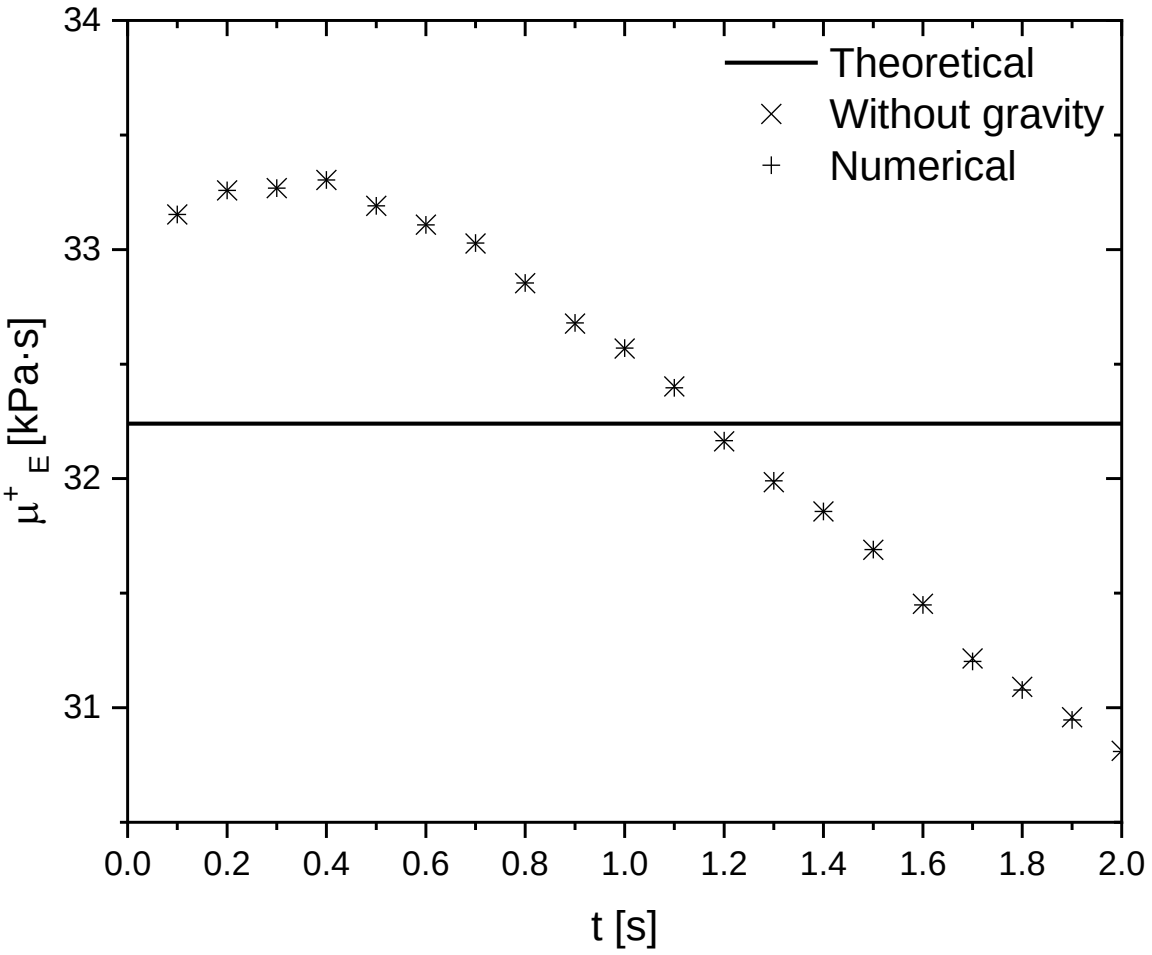

Figure 3.10: Effect of gravity on the numerical results of extensional viscosity

3.4. Case Studies

In this section, the effect of some errors that may occur in practice, namely on the (i) sample dimensions and (ii) test temperature, was investigated numerically, using the extensional rheometry tests setup defined in Section 3.3. For this purpose, we induced errors on the referred variables, performed the numerical calculation, and the erroneous predicted extensional viscosities were compared with the theoretical ones. Since the purpose of these case studies is to mimic the experimental procedure, where the experimentalist is unaware of the differences between the real and assumed parameters, the theoretical cross-sectional area evolution and Hencky strain rate were used in those calculations. In this case, the only variable that will be different from the theoretical one is the numerical torque (or normal force) used to calculate the extensional viscosity (see Equation (3.7)).

3.4.1. Sample Dimensions Error

Sample dimensions are a common experimental error source in the extensional rheometry tests due to difficulties inherent to the samples preparation procedure, usually based on hot compression molding. In these, the most probable errors occur on the sample thickness, which cannot be accurately controlled in this manufacturing process. Moreover, the sample width, defined by the employed cutting procedure, can also comprise some uncertainty. Finally, the sample length set by the rheometer drums distance is much less prone to experimental uncertainties and, thus, is not considered in this work. The sample dimensions used in this case study are presented in Table 3.1, which show variations of ±20% on the width and ±10% on the thickness.

Table 3.1: Values used in the sample dimensions case studies

Case Study	Sample Width [mm]	Sample Thickness [mm]
Ref case	10	0.7
Higher Width (↑W)	12 (+20% than the Ref case)	0.7
Lower Width (↓W)	8 (–20% than the Ref case)	0.7
Higher Thickness (↑T)	10	0.77 (+10% than the Ref case)
Lower Thickness (↓T)	10	0.63 (–10% than the Ref case)

The initial and final geometries of the samples considered in this work are depicted in Figure 3.11, where the induced differences in terms of sample width and thickness are clear.

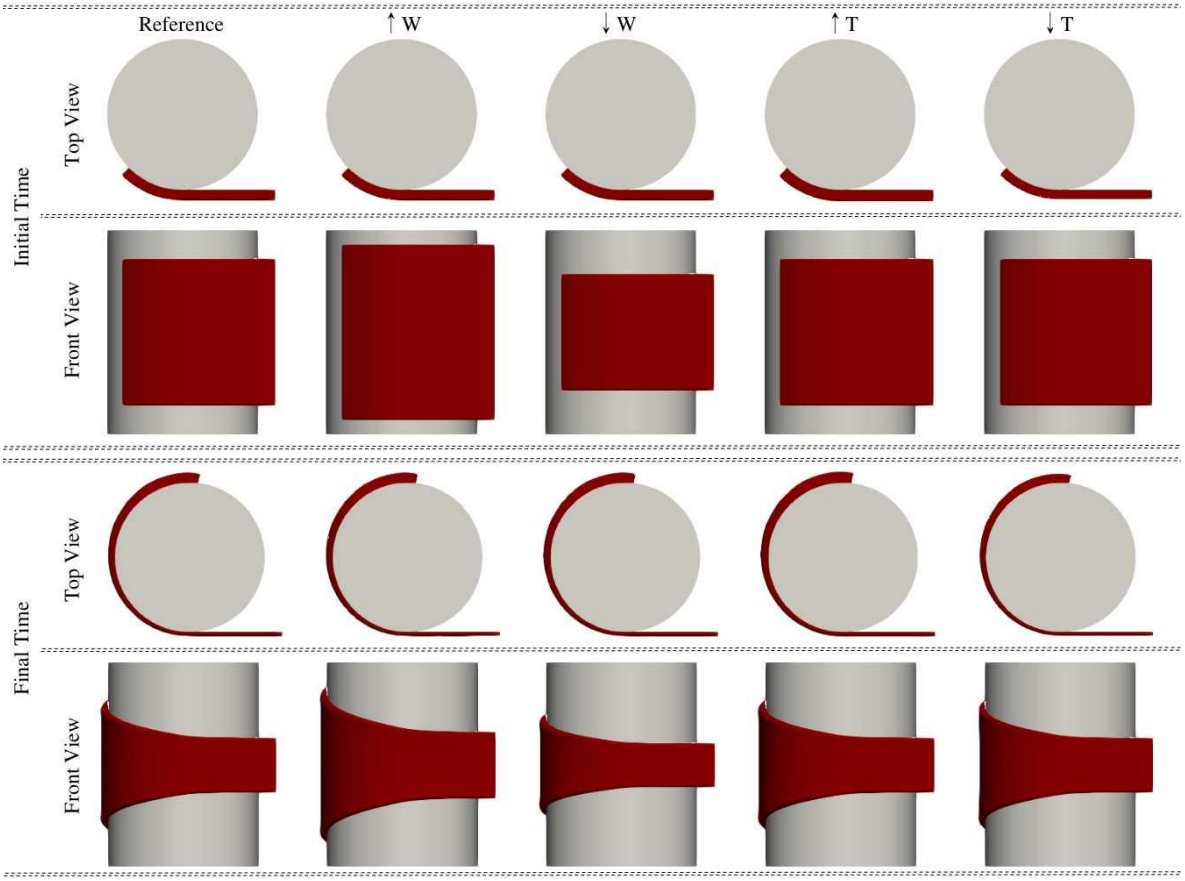

Figure 3.11: Schematic representation of the numerical results of the sample dimensions errors case studies compared to the reference one, Ref, at the initial and final times

As depicted in Figure 3.12(a), where the time evolution of the extensional viscosity is plotted, the trend is similar in all case studies. Due to the induced error, the predicted extensional viscosity is different from the theoretical one and initially has a high value that decreases over time. This trend is related to the effect of the sample inertia, as explained in Section 3.3. Concerning the impact of the specific induced errors, and as expected, for the ↑W and ↑T cases, the sample exhibited higher resistance to deformation due to its higher cross-sectional area, and, thus, the rheometer has to apply a higher torque to reach the specified Hencky strain rate. Accordingly, in these cases, both the force and the extensional viscosity in the numerical case are higher than the theoretical one. The opposite occurs for the ↓W and ↓T cases. In terms of the actual error obtained, as depicted in Figure 3.12(b), the predicted values are worse on the initial phase of the test ($t \simeq 0$ s) for larger sample dimensions (↑W and ↑T) than for the smaller samples (↓W and ↓T). Again, this problem is related to inertia, with a more pronounced effect for larger samples due to their higher mass. In what concerns the relevance of the erroneous variable, the results obtained show that thickness and width have a similar impact since the errors obtained are of the same order of magnitude of the induced variations, i.e., 10% and 20%, respectively.

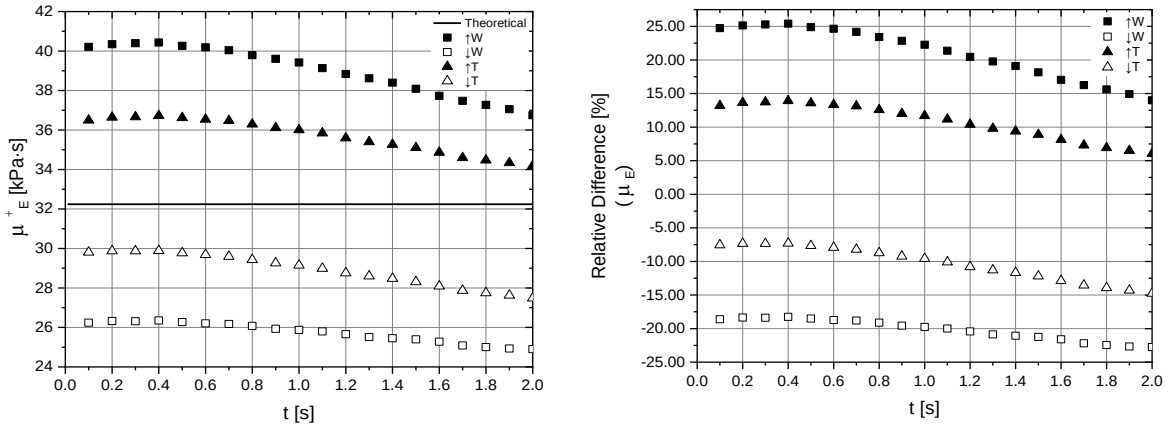

(a) (b)

Figure 3.12: Results for the sample dimensions errors case studies: (a) extensional viscosity, (b) relative difference between theoretical and numerical viscosities

3.4.2. Test Temperature Error

Test temperature is another important source of error when performing extensional rheometry tests. In order to eliminate this experimentally, some special procedures are applied, such as, for instance, allowing the temperature of the system to stabilise for a few hours [25]. However, if the experimentalist is not careful enough, the test temperature might not be the desired one. The relevance of this problem is emphasized in the experimental-based study of Aho et al. [25], which is focused on assessing the effect of errors on the test temperature. However, on the numerical side, the authors are not aware of any previous work carried out to assess the effect of temperature.

For this study, an error of +8% was considered on the temperature, from 250 °C to 270 °C, which changed the material shear viscosity employed in the calculations, obtained with an activation energy typical of thermoplastic polymers (107,044 J/mol). Therefore, the polymer shear viscosity considered in the new case study was 4,344 Pa·s, corresponding to a temperature of 270 °C (for the reference temperature, 250 °C, the polymer shear viscosity had a value of 10,747 Pa·s, which corresponds to a relative difference of 59.58%).

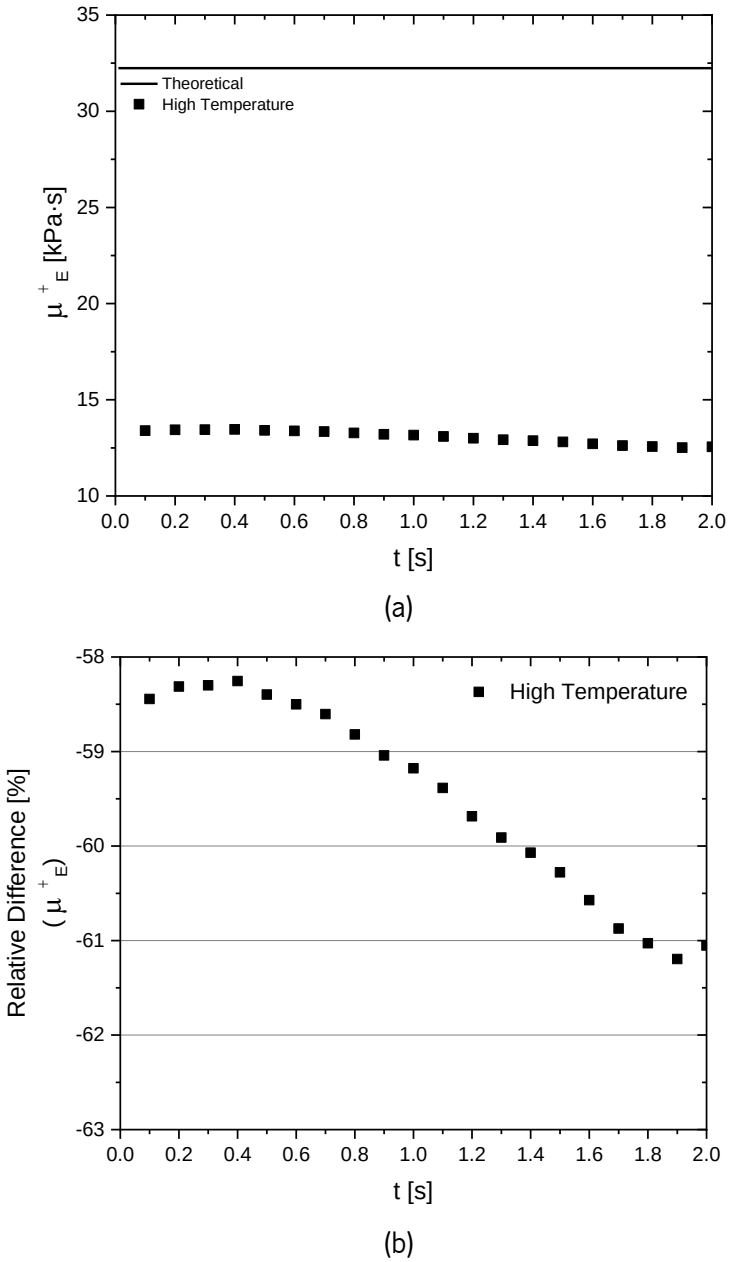

Figure 3.13: Results of the higher temperature case study: (a) extensional viscosity, (b) relative difference between theoretical and numerical extensional viscosities

As can be seen in Figure 3.13, the trend of the extensional viscosity evolution and its error is the same as the one observed for the sample dimensions errors cases studies, in which the numerical extensional viscosity is higher at the beginning of the calculation due to inertia effects. Consequently, the error is lower in that period. However, it should be noted that the magnitude of the errors is now much larger than the ones obtained on the dimensions error studies, which emphasizes the relevance of the temperature control in extensional rheometry tests.

3.5. Conclusions

The present work dealt with the numerical modeling of the uniaxial extensional rheometry tests performed with the Sentmanat Extensional Rheometer (SER) platform, using the OpenFOAM computational library, and aimed at establishing a modeling framework for these rheometry tests, which should provide additional insights on the relevance of the test parameters and potential error sources, to guide the work of interested experimentalists.

The initial phase of the studies aimed to define an appropriate modeling setup for the extensional rheometry tests. For that purpose, different geometries, boundary conditions, and modeling setups were tested. The selected combination of the system geometry and boundary conditions was the one that did not promote errors in the numerical results, such as the air penetration between the polymeric sample and the drum surface. Moreover, when the interface capturing approach was based on the algebraic Volume-of-Fluid (VOF) approach, some instabilities were observed on the predicted interface, which were absent when the geometric (isoAdvector) approach was employed. Consequently, the latter was selected to perform the modeling studies. The definition of the modeling setup also comprised the selection of the appropriate mesh refinement and the conclusion that the gravity can be neglected without affecting the numerical results. The numerical calculations were successfully performed with an Eulerian-based approach.

The second part of the study aimed to evaluate the effect of some common experimental errors, namely the sample dimensions, width and thickness, and the test temperature. The results obtained allowed concluding that the errors on the sample dimensions have similar effects on the predicted extensional viscosity, being approximately proportional to the induced errors, which, in the work, were ±10% and ±20%, respectively, for the thickness and width. On the other hand, a similar error order of magnitude on the test temperature (+8%) induced a huge difference in the predicted extensional viscosity (60%), which emphasizes the relevance of having an accurate control on this test parameter.

The results obtained also showed that inertia, which is present in practice, plays a relevant role in the results obtained since the extensional viscosity predicted at the initial phase of the test is always higher than that at the end. This happens because at the initial phase of the test the torque applied to the drum surface is used both to deform and accelerate the polymer sample, while in the theoretical test assumptions only the sample deformation is considered. This phenomenon and the role of inertia in the extensional tests should be studied in more detail in future work. Moreover, the identified modeling setup should be employed to study more complex rheology materials, following viscoelastic constitutive models.

References

[1] J.J. Sheng, Polymer Viscoelastic Behavior and Its Effect on Field Facilities and Operations, in: Mod. Chem. Enhanc. Oil Recover., 1st ed., Elsevier, Modern Chemical Enhanced Oil Recovery Theory and Practice James J. Sheng, Ph. D. AMSTERDAM, 2011: pp. 207–238. https://doi.org/10.1016/b978-1-85617-745-0.00006-1.

[2] F.A. Morrison, understanding rheology, Oxford university press, New York, NY, USA, 2001; ISBN: 0-19-514166-0.

[3] C.W. Macosko, Rheology: Principles, Measurements, and Applications, Wiley: New York, NY, USA;, 1994; ISBN: 978-0-471-18575-8.

[4] A. V. Shenoy, Extensional flow properties, in: Rheol. Fill. Polym. Syst., Springer Netherlands, 1999: pp. 395–415. https://doi.org/10.1007/978-94-015-9213-0_9.

[5] J.M. Dealy, R.G. Larson, J.M. Dealy, R.G. Larson, Structure and Rheology of Molten Polymers, 2006. https://doi.org/10.3139/9783446412811.fm.

[6] H.J. Karam, J.C. Bellinger, Tensile Creep of Polystyrene at Elevated Temperatures. Part I., Trans. Soc. Rheol. 8 (1964) 61–72. https://doi.org/10.1122/1.548969.

[7] G. V. Vinogradov, A.I. Leonov, A.N. Prokunin, On uniaxial extension of an elasto-viscous cylinder, Rheol. Acta. 8 (1969) 482–490. https://doi.org/10.1007/BF01976233.

[8] R.L. Ballman, Extensional flow of polystyrene melt, Rheol. Acta. 4 (1965) 137–140. https://doi.org/10.1007/BF01984710.

[9] A. Ziabicki, K. Kedzierska, Studies on the orientation phenomena by fiber formation from polymer melts. IV. Effect of molecular structure on orientation. Polyethylene and polystyrene, J. Appl. Polym. Sci. 6 (1962) 361–367. https://doi.org/10.1002/app.1962.070062114.

[10] R. Takserman-Krozer, A. Ziabicki, Behavior of polymer solutions in a velocity field with parallel gradient. I. Orientation of rigid ellipsoids in a dilute solution, J. Polym. Sci. Part A Gen. Pap. 1 (1963) 491–506. https://doi.org/10.1002/pol.1963.100010143.

[11] F.H. Müller, C. Engelter, Zur Spannungsabhängigkeit des Fließens Polymerer, Kolloid-Zeitschrift Zeitschrift Für Polym. 186 (1962) 36–41. https://doi.org/10.1007/BF01797951.

[12] F.T. Trouton, On the Coefficient of Viscous Traction and Its Relation to that of Viscosity, Proc. R.

Soc. A Math. Phys. Eng. Sci. 77 (1906) 426–440. https://doi.org/10.1098/rspa.1906.0038.

[13] E. Jenckel, K. Ueberreiter, Über Polystyrolgläser verschiedener Kettenlänge, Zeitschrift Für Phys. Chemie. 182A (2017) 361–383. https://doi.org/10.1515/zpch-1938-18240.

[14] E.N. da C. Andrade, B. Chalmers, The Resistivity of Polycrystalline Wires in Relation to Plastic Deformation, and the Mechanism of Plastic Flow, Proc. R. Soc. A Math. Phys. Eng. Sci. 138 (1932) 348–374. https://doi.org/10.1098/rspa.1932.0189.

[15] F.N. Cogswell, The rheology of polymer melts under tension, Plast. Polym. 36 (1968) 109–111.

[16] H. Münstedt, New Universal Extensional Rheometer for Polymer Melts. Measurements on a Polystyrene Sample, J. Rheol. (N. Y. N. Y). 23 (1979) 421–436. https://doi.org/10.1122/1.549544.

[17] T. Raible, A. Demarmels, J. Meissner, Stress and recovery maxima in LDPE melt elongation, Polym. Bull. 1 (1979) 397–402. https://doi.org/10.1007/BF00284409.

[18] J. Meissner, Development of a Universal Extensional Rheometer for the Uniaxial Extension of Polymer Melts., Trans Soc Rheol. 16 (1972) 405–420. https://doi.org/10.1122/1.549258.

[19] J. Meissner, J. Hostettler, A new elongational rheometer for polymer melts and other highly viscoelastic liquids, Rheol. Acta. 33 (1994) 1–21. https://doi.org/10.1007/BF00453459.

[20] G.H. Mckinley, T. Sridhar, FILAMENT-STRETCHING RHEOMETRY OF COMPLEX FLUIDS, Annu. Rev. Fluid Mech. 34 (2002) 375–415. https://doi.org/https://doi.org/10.1146/annurev.fluid.34.083001.125207.

[21] M.L. Sentmanat, Miniature universal testing platform: From extensional melt rheology to solid-state deformation behavior, Rheol. Acta. 43 (2004) 657–669. https://doi.org/10.1007/s00397-004-0405-4.

[22] M. Sentmanat, B.N. Wang, G.H. McKinley, Measuring the transient extensional rheology of polyethylene melts using the SER universal testing platform, J. Rheol. (N. Y. N. Y). 49 (2005) 585–606. https://doi.org/10.1122/1.1896956.

[23] R. Pivokonsky, M. Zatloukal, P. Filip, On the predictive/fitting capabilities of the advanced differential constitutive equations for branched LDPE melts, J. Nonnewton. Fluid Mech. 135 (2006) 58–67. https://doi.org/10.1016/j.jnnfm.2006.01.001.

[24] E. Mitsoulis, S.G. Hatzikiriakos, Rolling of bread dough: Experiments and simulations, Food Bioprod. Process. 87 (2009) 124–138. https://doi.org/10.1016/j.fbp.2008.07.001.

[25] J. Aho, V.H. Rolón-Garrido, S. Syrjälä, M.H. Wagner, Measurement technique and data analysis of extensional viscosity for polymer melts by Sentmanat extensional rheometer (SER), Rheol. Acta. 49 (2010) 359–370. https://doi.org/10.1007/s00397-010-0439-8.

[26] A. Oseli, B. Bizjan, E. Król, B. Širok, L. Slemenik Perše, Tensile properties of mineral fibers determined with Sentmanat extensional rheometer, Constr. Build. Mater. 253 (2020) 119215. https://doi.org/10.1016/J.CONBUILDMAT.2020.119215.

[27] E. Garofalo, L. Di Maio, P. Scarfato, A. Pietrosanto, A. Protopapa, L. Incarnato, Study on Improving the Processability and Properties of Mixed Polyolefin Post-Consumer Plastics for Piping Applications, Polym. 2021, Vol. 13, Page 71. 13 (2020) 71. https://doi.org/10.3390/POLYM13010071.

[28] A. Lyhne, H.K. Rasmussen, O. Hassager, Simulation of elastic rupture in extension of entangled monodisperse polymer melts, Phys. Rev. Lett. 102 (2009). https://doi.org/10.1103/PhysRevLett.102.138301.

[29] T.S.K. Ng, G.H. McKinley, M. Padmanabhan, Linear to non-linear rheology of wheat flour dough, Appl. Rheol. 16 (2006) 265–274. https://doi.org/10.1515/arh-2006-0019.

[30] P. Svrcinova, A. Kharlamov, P. Filip, On the measurement of elongational viscosity of polyethylene materials, Acta Tech. CSAV (Ceskoslovensk Akad. Ved). 54 (2009) 49–57.

[31] R. Pivokonsky, M. Zatloukal, P. Filip, C. Tzoganakis, Rheological characterization and modeling of linear and branched metallocene polypropylenes prepared by reactive processing, J. Nonnewton. Fluid Mech. 156 (2009) 1–6. https://doi.org/10.1016/j.jnnfm.2008.06.001.

[32] O. Delgadillo-Velázquez, S.G. Hatzikiriakos, M. Sentmanat, Thermorheological properties of LLDPE/LDPE blends, Rheol. Acta. 47 (2008) 19–31. https://doi.org/10.1007/s00397-007-0193-8.

[33] Y. Wang, S.-Q. Wang, From elastic deformation to terminal flow of a monodisperse entangled melt in uniaxial extension, J. Rheol. (N. Y. N. Y). 52 (2008) 1275–1290. https://doi.org/10.1122/1.2995858.

[34] E. Garofalo, G.M. Russo, P. Scarfato, L. Incarnato, Nanostructural modifications of polyamide/MMT hybrids under isothermal and nonisothermal elongational flow, J. Polym. Sci. Part B Polym. Phys. 47 (2009) 981–993. https://doi.org/10.1002/polb.21706.

[35] E.B. Muliawan, S.G. Hatzikiriakos, Rheology of mozzarella cheese, Int. Dairy J. 17 (2007) 1063–1072. https://doi.org/10.1016/j.idairyj.2007.01.003.

[36] B. Li, W. Yu, X. Cao, Q. Chen, Horizontal extensional rheometry (HER) for low viscosity polymer melts, J. Rheol. (N. Y. N. Y). 64 (2020) 177–190. https://doi.org/10.1122/1.5134532.

[37] M.I. Kolte, H.K. Rasmussen, O. Hassager, Transient filament stretching rheometer, Rheol. Acta. 36 (1997) 285–302. https://doi.org/10.1007/bf00366670.

[38] R. Sizaire, V. Legat, Finite element simulation of a filament stretching extensional rheometer, J. Nonnewton. Fluid Mech. 71 (1997) 89–107. https://doi.org/10.1016/S0377-0257(97)00013-X.

[39] M.F. Webster, H. Matallah, K.S. Sujatha, M.J. Banaai, Numerical modelling of step-strain for stretched filaments, J. Nonnewton. Fluid Mech. 151 (2008) 38–58. https://doi.org/10.1016/j.jnnfm.2008.02.002.

[40] V. Tirtaatmadja, T. Sridhar, A filament stretching device for measurement of extensional viscosity, J. Rheol. (N. Y. N. Y). 37 (1993) 1081–1102. https://doi.org/10.1122/1.550372.

[41] K. Yu, J.M.R. Marín, H.K. Rasmussen, O. Hassager, 3D modeling of dual wind-up extensional rheometers, J. Nonnewton. Fluid Mech. 165 (2010) 14–23. https://doi.org/10.1016/j.jnnfm.2009.08.006.

[42] O. Hassager, J.M.R. Marin, K. Yu, H.K. Rasmussen, Polymeric liquids in extension: Fluid mechanics or rheometry?, Rheol. Acta. 49 (2010) 543–554. https://doi.org/10.1007/s00397-010-0444-y.

[43] E. OpenFOAM, Standard solvers, (2021). https://www.openfoam.com/documentation/user-guide/a-reference/a.1-standard-solvers (accessed November 8, 2021).

[44] J. Roenby, H. Bredmose, H. Jasak, A Computational Method for Sharp Interface Advection, (2016). https://doi.org/10.1098/rsos.160405.

[45] L. Gamet, M. Scala, J. Roenby, H. Scheufler, J. Lou Pierson, Validation of volume-of-fluid

OpenFOAM® isoAdvector solvers using single bubble benchmarks, Comput. Fluids. 213 (2020) 104722. https://doi.org/10.1016/J.COMPFLUID.2020.104722.

[46] H. Jasak, Error Analysis and Estimation for the Finite Volume Method with Applications to Fluid Flows, Ph.D. Thesis, Imperial College, 1996.

[47] J.H. Ferziger, M. Peric, Computational Methods for Fluid Dynamics, 3rd Editio, Springer, Berlin, Heidelberg, Berlin, Heidelberg, New York, Barcelona, Hong Kong, London, Milan, Paris, Tokyo, 2002. https://doi.org/https://doi.org/10.1007/978-3-642-56026-2.

[48] C.W. Hirt, B.D. Nichols, Volume of fluid (VOF) method for the dynamics of free boundaries, J. Comput. Phys. 39 (1981) 201–225. https://doi.org/10.1016/0021-9991(81)90145-5.

[49] R. Comminal, Numerical simulation of viscoelastic free - surface flows using a streamfunction / log - conformation formulation and the volume - of - fluid method, Ph.D. Thesis, Technical University of Denmark, 2015.

[50] OpenFOAMWiki, BlockMesh - OpenFOAMWiki, (2021). https://openfoamwiki.net/index.php/BlockMesh (accessed November 8, 2021).

[51] J. Ahrens, B. Geveci, C. Law, Title: ParaView: An End-User Tool for Large Data Visualization ParaView: An End-User Tool for Large Data Visualization, 2005. www.paraview.org. (accessed November 8, 2021).

CHAPTER 4

USING COMPUTATIONAL MODELING TO STUDY EXTENSIONAL RHEOMETRY TESTS FOR VISCOELASTIC FLUIDS

This chapter was adapted from:
M Aali, W Galuppo, OS Carneiro, JM Nóbrega, Using computational modelling to study extensional rheometry tests for viscoelastic fluids, manuscript in preparation, 2022.

Abstract

In the present work, the effect of two critical sources of error namely: (i) sample dimensions and (ii) test temperature, which often occur in uniaxial extensional rheometry tests, are investigated. For this purpose, a computational framework is developed to model uniaxial extensional rheometry tests through the Sentmanat Extensional Rheometer (SER) platform, when a viscoelastic fluid is employed. A new numerical code based on an Eulerian algorithm is devised to capture a sharper polymer-air interface using the geometric Volume-of-Fluid approach (isoAdvector algorithm), in the OpenFOAM computational library. Moreover, a new code is developed to compute the forces and torques acting on any desired surface of the domain, for multimode viscoelastic fluids. The results obtained for extensional viscosity show that an error of 8% resulted in a deviation of 180% and 80% at the lower and higher temperatures, respectively. While the errors of ±10% and ±20%, for the thickness and width (sample dimensions), resulted in a deviation of ±10% and ±20%, respectively, for the thickness and width at predicted extensional viscosity. According to the results obtained, this is concluded that the accuracy of the extensional viscosity is considerably sensitive to the test temperature error when compared to the sample dimensions error.

Keywords: extensional rheometry, Sentmanat Extensional Rheometer (SER), computational modeling, viscoelastic fluid, isoAdvector, Eulerian, OpenFOAM.

4.1. Introduction

As noted in Chapter1, polymers and their processing techniques are very important since they are utilized in a variety of industrial fields [1]. As a result, the study of the rheological properties of polymers is critical for gaining a full understanding of their complex behavior. Comprehensive knowledge in this area enables achieving high production rates as well as high-quality products [2]. According to the importance of the rheological characterization of polymeric materials, a huge number of studies have been carried out on this subject. However, further research is needed to explore unknown aspects of the rheological behavior of the polymer melts [3]. Again, as stated in Chapter 1, extensional flows are dominant in some important processing techniques such as thermoforming, blow molding, film blowing, and fiber spinning. However, these types of flow have not been well investigated. The investigation in the extensional flow started in 1906 [4], and this type of flow became a well-known topic in the late 1960s [5–11]. As mentioned in Chapter 2, nowadays, several platforms are available for uniaxial extensional flow measurement purposes [12–19]. Converging flow lines and complex experimental methodologies (e.g. achieving steady-state processing conditions) are the main challenges in the extensional flow characterization, particularly, uniaxial one.

Sentmanat Extensional Rheometer (SER) platform [18,20] is one of the newest developed platforms among several alternatives for performing extensional rheometry tests. The SER is used as an add-on device on a rotational rheometer. Several types of measurements such as uniaxial extensional rheometry tests and peeling, etc. [18,20] can be performed using the SER. The working principle of the SER was explained in Chapter 3. The simple usage of SER, when compared to other concepts proposed before, is its main advantage [18,20]. This led to its dissemination in industry and academia [21–37]. The majority of the studies using SER were of experimental nature, and only a few numerical works are available [32,38–40].

The extensional rheometry tests are challenging to perform [41]. For instance, Aho et al. [42] and Svrcinova [34] indicated that the accuracy of the results obtained in these tests is essentially sensitive to the test conditions, such as test temperature, sample mounting procedure, and the sample dimensions used in the test [34,42]. They [34,42] employed two methods to identify the effect of the sample mounting procedure on the extensional viscosity data. For this propose, as the first method, the extensional viscosity data when the sample was mounted onto the drum with clamp were compared to the theoretical one, and a systematic difference was observed. As the second method, they mounted samples without the clamp, and compared the extensional viscosity obtained with this method to the

theoretical one, which was found that the difference was reduced remarkably [34,42]. Afterwards, Aho et al. [42] compared the experimental data (without and with preheating) with the theoretical one. This allowed finding that the experimental data obtained with preheating was in better agreement with the theoretical assumptions [42].

As already referred to, the numerical modeling approaches are robust tools, which can provide useful insights that are not easily achievable on experimental tests. Moreover, these approaches can provide useful predictions, allowing to reduce the trial-and-error iterations in experimental tests, and increasing the accuracy of the measurements performed.

Lyhne et al. [32] numerically modeled the necking phenomenon in the SER using a Lagrangian modeling approach. They employed varied Hencky strains in order to identify the causes of the necking phenomenon. It was found that inhomogeneous stress distributions were the main motivation of the necking of the polymer sample at the contact point with the drum. Yu et al. [38] modeled the extensional rheometry test in 3D and studied the effect of the rectangular sample thickness (T_0) and width (W_0), for a fixed length (L_0), on the generation of the pure uniaxial extensional flow. The results obtained allowed to conclude that for $T_0/L_0 \leq 0.04$ and $W_0/L_0 \leq 0.5$, there is a pure uniaxial flow, as desired. For the values above, the flow deviates from the desired test conditions (pure uniaxial extensional flow condition). The effects of the cylindrical sample initial diameter on the accuracy of the uniaxial extensional flow were investigated by Yu et al. [40] in another work. It was found that the sample with a higher diameter (> 0.5 mm) caused a higher deviation in the numerical data. For instance, an initial diameter of 1 mm leads to more than 10% deviation from the expected Hencky strain due to the non-pure uniaxial extensional flow condition. The deviation was found to reduce linearly with the initial diameter value. Hassager et al. [39] also studied the 3D numerical necking phenomenon during the uniaxial extensional tests using the SER. The results obtained allowed to conclude that the actual deformation process verified in the SER depends on the sample initial dimensions and rheology [39]. The largest deviation from uniaxial deformation tends to occur for samples with a large initial width to thickness ratio (W_0/L_0), and for materials models that predict a small or no second normal stress difference in shear [39]. Furthermore, it was found that the sample incomplete relaxed condition was the main reason for the necking.

Despite the significance of the impacts of the sample dimensions and test temperature error on the accuracy of the results obtained in the uniaxial extensional rheometry tests through the SER, there is a gap in the investigations carried out to assess the effects of them when a viscoelastic fluid is employed.

The motivation of this work is to help experimentalists be aware of the magnitude of the errors, caused by each sources of error when a realistic material (viscoelastic fluid) is employed. For this purpose, in this work, the study of the previous chapter is extended, and the main objective is to investigate the effect of common sources of errors (sample dimensions and test temperature) on the accuracy of the extensional rheometry tests, when a viscoelastic fluid constitutive model is considered.

For the above purposes, a new solver is developed in the framework of OpenFOAM computational library [43], using geometric VOF approach (isoAdvector algorithm) [44,45], for capturing a sharper polymer-air interface. Moreover, a new code must be devised to compute forces/torques in desired regions of the domain, for multimode viscoelastic fluids.

The present chapter is organized as follows. The numerical modeling, and case studies are addressed in Section 4.2. The results obtained, and corresponding discussion, are presented in Section 4.3. The main conclusions of this chapter and the final remarks are provided in Section 4.4.

4.2. Case Study

All the required information in terms of the rheological characterization of the material used, and the corresponding fitting and the SER platform, including operating principle, geometry, appropriate equations for calculating force, area, and extensional viscosity was already provided in Chapter 2 and 3, respectively. This section consists of two subsections, namely: (i) numerical modeling including solver and code developments, and (ii) case studies.

4.2.1. Numerical Modeling

All the information related to the newly developed solver and the code for computing the forces and torques is addressed in this section.

4.2.1.1. Computational Modeling Solver

Aimed to model the uniaxial extensional rheometry tests using the SER platform, a novel solver denominated rheoInterIsoFoam was developed through the OpenFOAM computational library. Apart from the interface capturing approach, the developed solver followed essentially the same calculation techniques and used the same constitutive models as originally implemented for the rheoInterFoam solver available in the rheoTool [46,47] toolbox.

Originally, the rheoInterFoam solver uses the algebraic Volume-of-Fluid (VOF) approach [48] for capturing the interface. This approach is simpler to implement, efficient in terms of the calculation time, and the

most prominent variation of the interface capturing approaches [48,49]. The newly developed solver (rheoInterIsoFoam) uses the geometric VOF approach (isoAdvector algorithm) [44,45]. The geometric VOF approach enables to predict a sharper interface when compared to the algebraic one [44,45], and this was the main reason to develop the rheoInterIsoFoam solver.

4.2.1.1.1. Algebraic VOF vs Geometric VOF Approach

The algebraic and geometric VOF approach use a marker function that represents the phase fraction of the fluids in each computational cell [45,48]. OpenFOAM uses for the VOF formulation a scalar fraction function named α as a location marker function varying from 0 to 1 for a two-phase flow, thus a unit value of α phase fraction corresponds to a cell full of one fluid phase (polymer), while a cell with α value of zero indicates a full of the other fluid phase (air) [48]. Cells with α value between zero and one are the ones where the interface is located.

The only exception that the isoAdvector algorithm [44,45] implemented in the rheoInterIsoFoam is that it uses the iso-surfaces concept and solves additional equations to compute the interface [44,45]. Indeed, the isoAdvector algorithm computes the location of each phase in addition to the definition of the amount of each phase in cells [44,45], while the algebraic VOF approach does not consider the location of the phases [48,49], and just defines the amount of each phase in cells [48,49]. As a result, the predicted interface using the geometric algorithm is much sharper when compared to the algebraic counterpart [44,45].

isoAdvector algorithm follows the following steps to predict the interface:

First, the interface is geometrically reconstructed through a sub-grid reconstruction step, then the interface is advected within the time step (the advection-step). The reconstruction-step is done using iso-surfaces concept inside each cell where the interface ($0<\alpha<1$) is located. For this purpose, the cell volume fractions must be interpolated to the cell vertices. The inversed cell center-cell vertex distances are used to calculate the value. Following that, and for each cell, the iso-face is determined at a value of α, and two sub-volumes are formed that are proportional to the volume fraction of that cell. The isoface motion is then calculated within the time-step, in the advance-step, utilizing the velocity data of the surrounding cells, resulting in motion evaluation in a sub-time step. The face-interface intersection line is generated by the intersection of the isoface with the faces of the cell, and it is used to determine the volume conveyed via the face, from which the new distribution of the domain is obtained.

The required information about the principle of both algebraic and geometric VOF approaches is presented above. To obtain more insights about the solvers and their governing equation, the work of Pimenta and Alves [46,47], and Roenby et al. [44,45] are advised.

4.2.1.2. Loads Utility

Forces code (function object) is one of the plenty useful utilities available in the framework of the OpenFOAM computational library, which is used to compute the forces and torque data in any desired surfaces and porous regions. The available code is just valid for inelastic fluid models. Equations (4.1) and (4.2) are used to compute the normal pressure ($\underline{F}_p$) and viscous ($\underline{F}_v$) force vectors, respectively, for inelastic fluid models (Newtonian and generalized Newtonian), and Equation (4.3) is used to compute the moment.

$$\underline{F}_p = \sum_i \underline{S}_{f,i} \bullet P_i \tag{4.1}$$

$$\underline{F}_v = \sum_i \underline{S}_{f,i} \bullet (\underline{\underline{\tau}}_{dev}) \tag{4.2}$$

where the subscript i is representative of each boundary face, $\underline{S}_f$ the face area vector, P is the pressure, and $\underline{\underline{\tau}}_{dev}$ is the deviatoric stress tensor for an inelastic fluid.

$$\underline{T} = \underline{M}_d \times \underline{F}_v \tag{4.3}$$

where $\underline{M}_d$ is the distance vector to the origin of the domain, $\underline{F}_v$ is the viscus force vector.

In the newly developed force code, Equations (4.2) was adapted based on the available stress tensor fields in incompressible viscoelastic fluid models, as expressed in Equations (4.4).

$$\underline{F}_v = \sum_i \underline{S}_{f,i} \bullet (\underline{\underline{\tau}}_{MF,i} - P_i \underline{\underline{I}}) \tag{4.4}$$

where $\underline{\underline{\tau}}_{MF,i}$ is the combination of the polymeric and solvent multiphase stress tensor in each cell, $\underline{\underline{I}}$ is the identity tensor.

Like the incompressible inelastic fluids case, Equation (4.3) was employed to compute the torque for incompressible viscoelastic fluids. However, the computed forces obtained in Equation (4.4) and was used to compute the torque.

4.2.2. Case Studies

This section introduces the case studies addressed in the present work and consists of the following subsections: (i) modeling setup, such as system geometry/computational domain (3D), initial and boundary conditions, (ii) mesh sensitivity analysis, and (iii) studies performed (sample dimensions and test temperature variations).

4.2.2.1. Modeling Setup

The same geometry (**G2**), and methodology used in the previous chapter (Section 3.3) are employed in this work. Again, only half of the system geometry was used in the computational model due to symmetry reasons, which allowed for a significant reduction in calculation time, without impacting the correctness of the results.

The following were the initial conditions used in this work: null values for velocity, pressure, stress, and α . Moreover, for the α field, a value of 1 was imposed at the polymeric sample cells, and a zero value was set for the remaining (air region).

The boundary conditions employed for the computational domain (see Figure 3.2) were the following: for the velocity field, a rotating wall boundary condition was imposed at the Drum, where the z-axis was the rotation axis. The angular velocity of 0.987 rad·s^{-1} (corresponding to a 0.8 s^{-1} constant Hencky strain rate) was applied; moreover, a null normal gradient boundary condition was used at the Wall, Right, Bottom, Front and Back patches, and a slip boundary condition was imposed on the Sample. Concerning the pressure field, a null normal gradient was used at all the patches, except the Right, on which a null pressure was imposed. Concerning the stress field, a null normal gradient was used at all the patches. Regarding the α field, a null normal gradient boundary condition was used on all the patches. Symmetry plane boundary condition was imposed at patch symmetry for the velocity, pressure, and stress fields.

4.2.2.2. Mesh Sensitivity Analysis

The mesh sensitivity analysis carried out to select the most appropriate mesh refinement level to be used in the subsequent studies. In this work, the number of cells of the computational meshes tested is as

follows: M0-273,000 cells; M1-780,000 cells; M2-1,856,400 cells; and M3-4,440,800 cells. All the meshes are depicted in Figure 4.1. The mesh refinement was mainly carried out in the sample section (close to the drum surface), where the region of interest is located, and higher gradients are expected. All computational meshes were generated using the blockMesh utility [50] available in OpenFOAM.

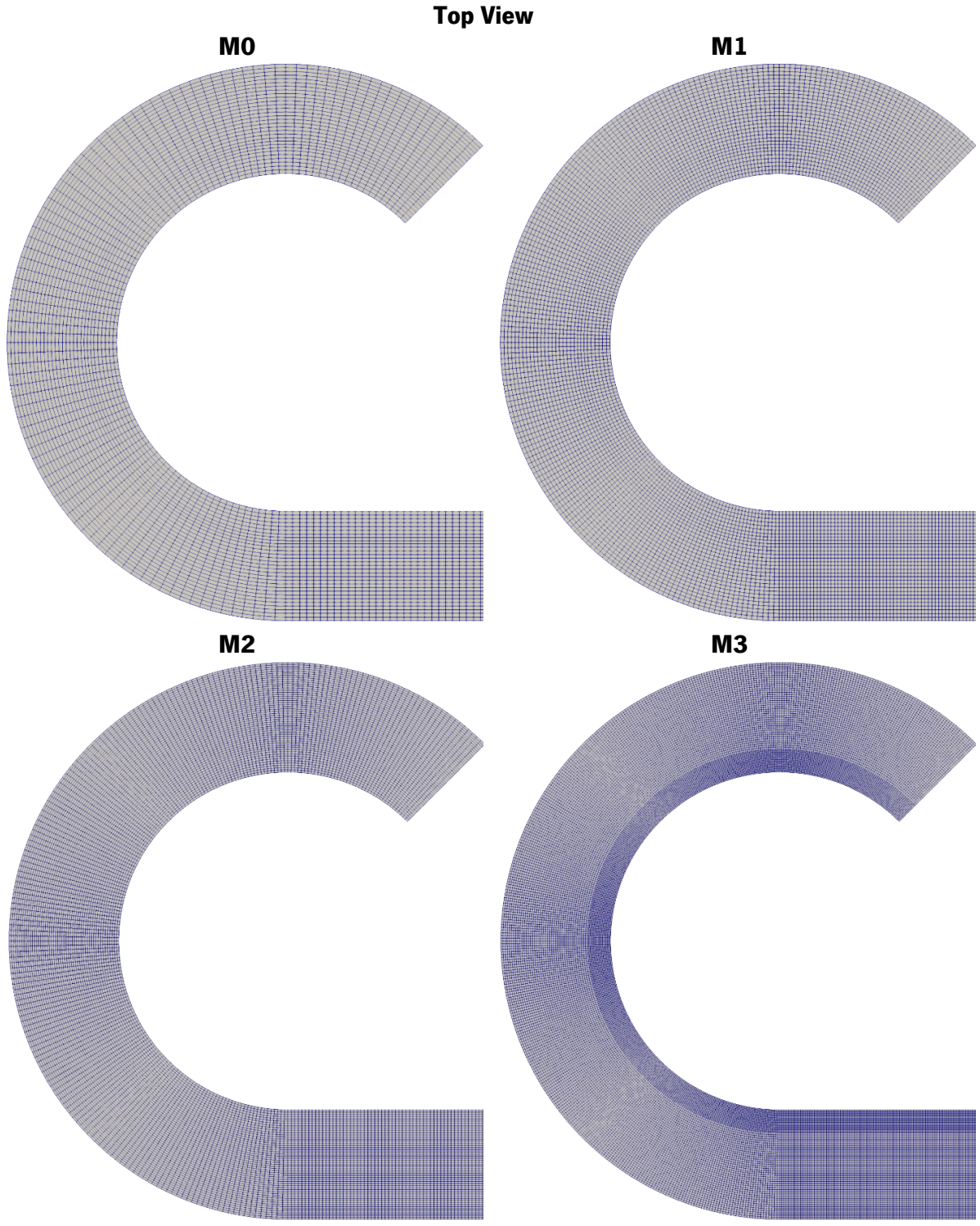

Figure 4.1: Schematic representation of the different meshes used

In order to identify the appropriate level of mesh refinement, the numerical values of the extensional viscosities obtained with the various meshes were compared to the corresponding theoretical values, as illustrated in Figure 4.2(a). The data of the theoretical approach were obtained from the fitting of the uniaxial extensional rheometry data (see Figure 2.4). As addressed in the case study section, the developed force utility was used to compute the numerical torque on the drum surface. Then, the computed torque was used to calculate the numerical extensional viscosity by using Equation (3.7).

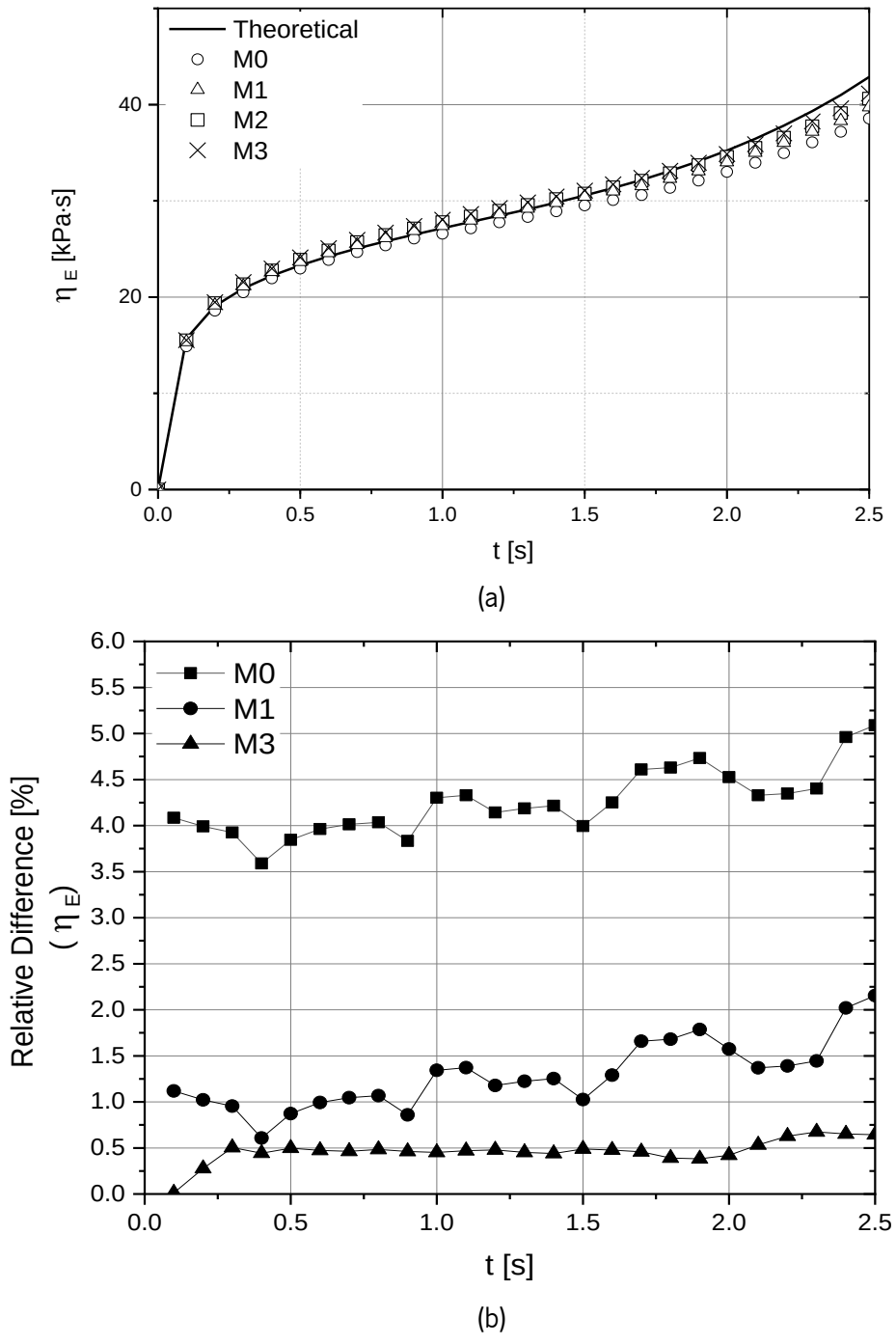

Figure 4.2: Mesh sensitivity analysis. comparison of the numerical and theoretical results for (a) extensional viscosity, and (b) relative differences of different meshes compared with M2

As depicted in Figure 4.2(b), the predictions of the uniaxial extensional viscosity are considerably different from M2 in comparison to M0, while the difference visible between the results obtained with M1, and M3 is very small.

According to the results obtained in the mesh sensitivity analysis, all the subsequent numerical runs were made using M2. For this level of mesh refinement, the calculation time was approximately 6 days and 21 hours, using 192 cores. In these studies, a gravitational acceleration equal to 9.81 $m \cdot s^{-2}$ was imposed in the negative z direction, and surface tension equal to 0.025 $N \cdot m^{-1}$ was also used in order to replicate the real process conditions.

4.2.2.3. Studies Performed

In order to identify the effect of sources of error on the accuracy of the extensional viscosity data, the errors were induced by ourselves on the referred variables in the same manner as explained in Chapter 3, then numerical calculation was performed, and the erroneous predicted extensional viscosities were compared with the theoretical ones.

4.2.2.3.1. Sample Dimensions

As mentioned in Chapter 3, sample dimensions are a common source of experimental error in extensional rheometry tests. The same methodology illustrated in Chapter 3 was followed here to induce the error on the sample dimensions, and variations of ±20% and ±10% on the width and the thickness, respectively, as listed in Table 3.1. It should be noted that the sample dimensions used in the present work are in the range recommended by Yu's [38] work, to avoid altering the nature of the test from pure uniaxial extensional flow to any other type of extensional flow (planar and/or combination of uniaxial and planar extensional flow).

4.2.2.3.2. Test Temperature

The test temperature is another essential and relevant subject that affects the accuracy of data obtained in the uniaxial extensional rheometry tests. In order to eliminate this type of error in the experimental tests, some particular techniques are used, such as allowing the system's temperature to stabilize for a few hours [42]. The importance of this issue is highlighted in experimental works by Aho et al. [42] and Svrcinova [34], which assessed the effects of errors on the test temperature. However, although the effect of test temperature error on the uniaxial extensional data is assessed for an inelastic fluid in Chapter 3, still the effect of this source of error is not clear for a viscoelastic fluid employed.

In this work, a temperature error of approximately 8% was considered, ranging from the reference temperature, 250 °C, to 230 °C and 270 °C. Since the solver used is isothermal, the appropriate rheological characterization data corresponding to the higher and lower temperatures, as listed in Tables 4.1 and 4.2, were used in the numerical modeling to impose the desired conditions in terms of the test temperature. To determine the required parameter, shear flow and oscillatory tests were performed at 230 °C and 270 °C. Then the experimental data were fitted in the same manner as presented in Section 2.2.2. The uniaxial extensional rheometry tests were not performed at the higher and lower temperatures, thus, the same α (mobility factor in Giesekus model) values corresponding to 250 °C were used.

Table 4.1: Relaxation spectrum, and mobility factor for the polymer melt at 230 °C

Mode	G (Pa)	λ (s)	η_k (Pa.s)	α
1	800000	0.002	1600	0.1
2	250000	0.02	5000	0.6
3	50000	0.13	6500	0.001
4	8000	0.75	6000	0.007
5	1000	4.50	4500	0.0008

Table 4.2: Relaxation spectrum, and mobility factor for the polymer melt at 270 °C

Mode	G (Pa)	λ (s)	η_k (Pa.s)	α
1	400000	0.0008	320	0.1
2	100000	0.0055	550	0.6
3	50000	0.001	50	0.001
4	15000	0.025	375	0.007
5	1000	0.2	200	0.0008

4.3. Results and Discussion

In this section, the effect of sample dimensions and test temperature error sources were investigated. As mentioned in Chapter 3, the theoretical cross-sectional area evolution (see Equation (3.6)), and theoretical Hencky strain rate were used in those calculations. The only variable that was different from the theoretical one was the torque (or numerical normal force) which was numerically computed and used to calculate the extensional viscosity (see Equation (3.7)).

4.3.1. Sample Dimensions Error

The numerical extensional viscosity obtained from case studies with higher and lower thicknesses and widths will be compared to the theoretical one. Figure 4.3 depicts the initial and final geometries of the samples used in this work, where the changes in sample width and thickness are clearly visible. These

results showed that the necking phenomenon, often reported in the literature [32,39], was not observed in the tested case studies.

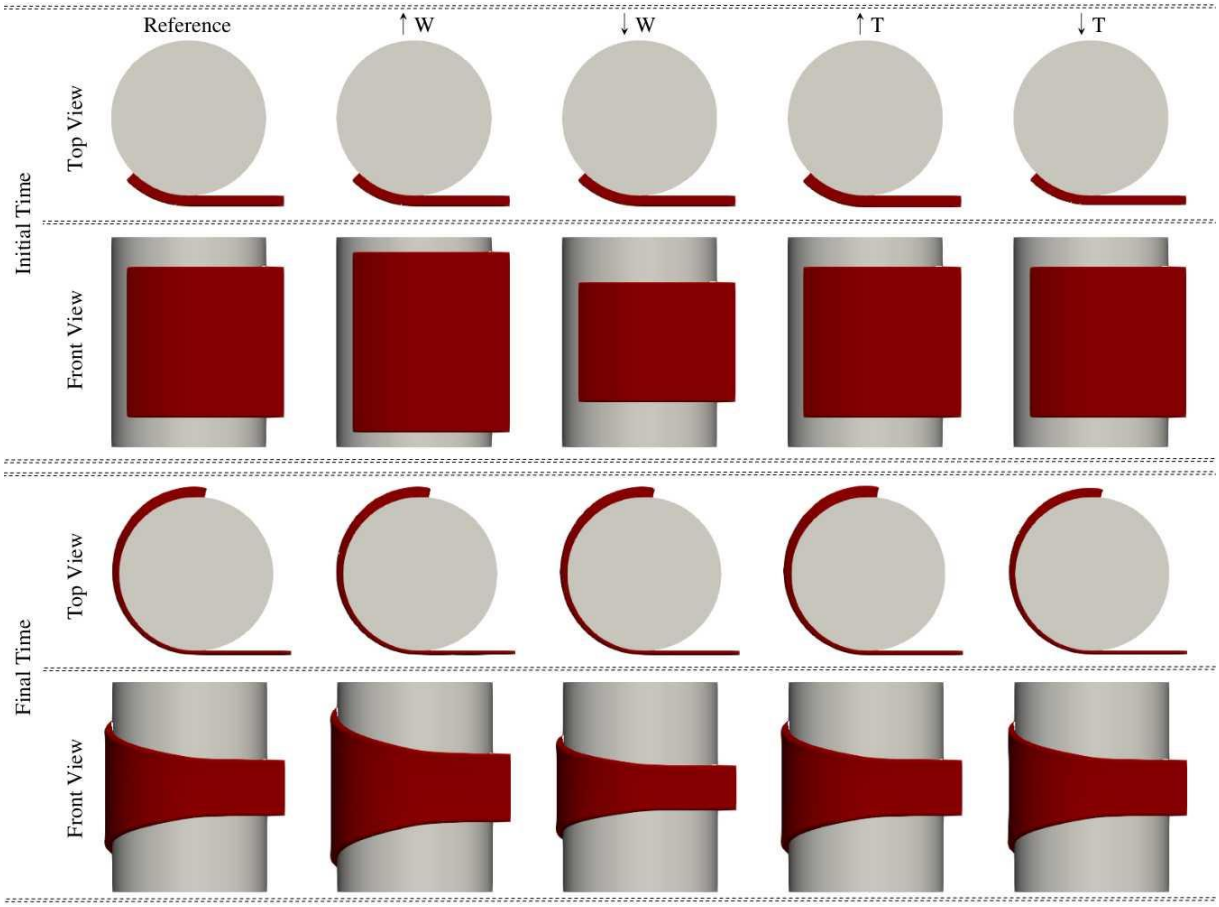

Figure 4.3: Schematic representation of the numerical results of the sample dimensions errors case studies compared to the reference one, at the initial and final times

As depicted in Figure 4.4(a), the trends of the extensional viscosity are the same for all the case studies and follow the trend of the theoretical one. Moreover, the visible difference between the numerical predictions and the theoretical one, is promoted by the induced error. Figure 4.4(b) shows the relative difference between the numerical and theoretical extensional viscosities. The trends observed in terms of the relative difference (higher difference at the beginning and lower difference at the end of modeling) are the same as those occurred for the inelastic fluid addressed in Chapter 3, and that occurred due to the sample inertia effect. The reason for the observed behavior of sample inertia is already explained in Chapter 3.

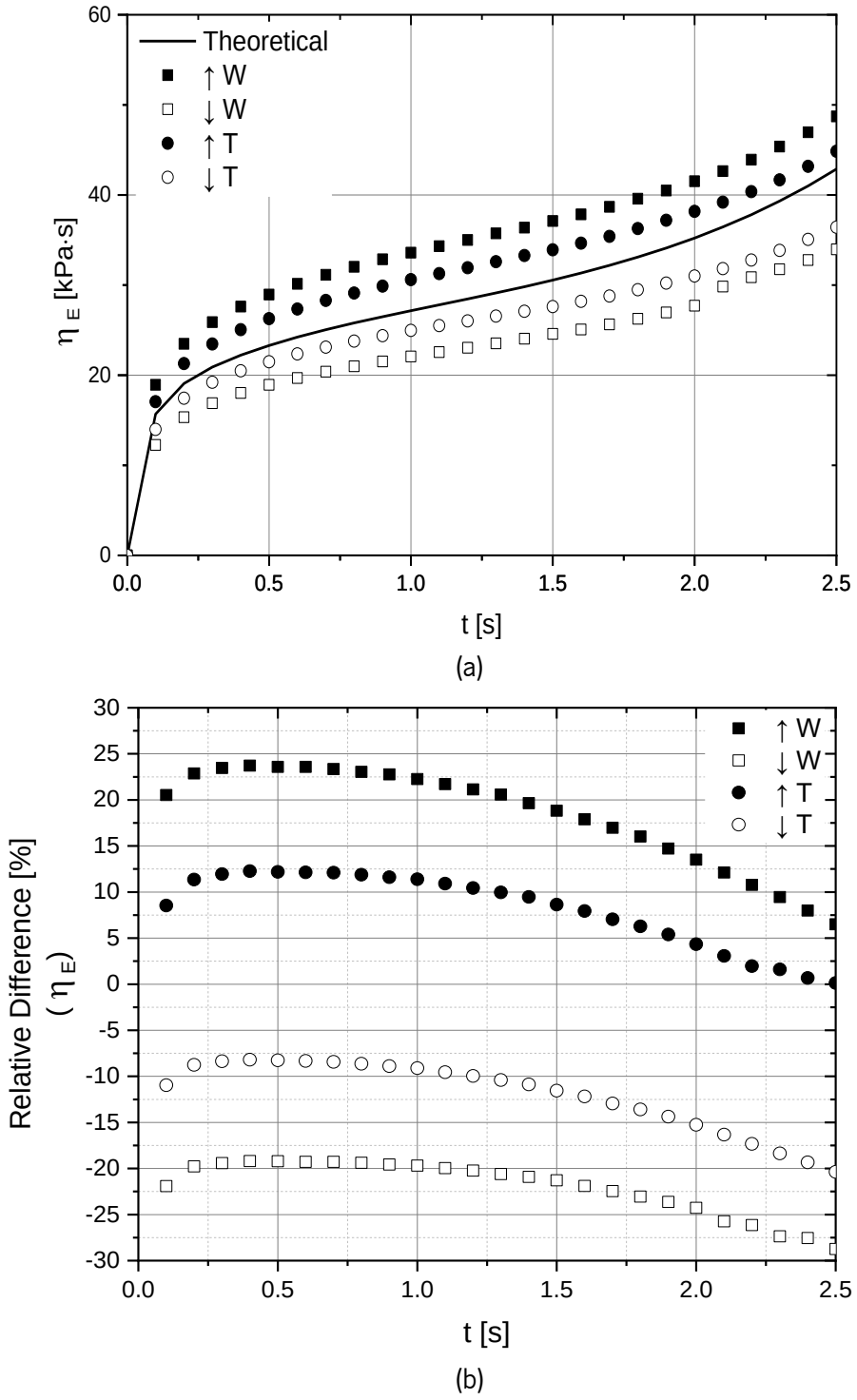

Figure 4.4: Results for the sample dimensions errors case studies: (a) extensional viscosity, (b) relative difference between numerical and theoretical viscosities

Concerning the difference observed in between the numerical and theoretical case studies, as mentioned in Section 3.4.1, the sample demonstrated stronger resistance to deformation owing to its higher cross-sectional area in the ↑W and ↑T cases and, therefore, the rheometer had to apply a higher torque to attain the stated Hencky strain rate, and the opposite behavior occurred in smaller samples (↓W and ↓T). It should be referred to that when width and thickness variations are promoted, the magnitude of

the errors obtained in the extensional viscosity was similar to the induced errors, 10% for thickness and 20% for width.

According to the results obtained for the low Hencky strain, it seems that the nature of the model employed (viscoelastic or inelastic) does not affect the errors caused by the sample dimensions, and the error pronounced by the sample dimensions in the viscoelastic fluid was in the same range as those observed for the inelastic fluid (see Figure 3.12).

4.3.2. Test Temperature Error

As can be seen in Figure 4.5, the trend of the extensional viscosity evolution is not the same as the one observed for the sample dimensions errors case studies. The numerical extensional viscosity, and the obtained relative difference, are increased over time in both cases corresponding to higher and lower test temperatures. The relative difference observed in the lower temperature case is significantly deviated (110%~180%) in comparison to the higher temperature one (80%~90%).

Furthermore, it should be noted that the magnitude of the errors in these types of sources of error is much larger than the ones resulting from sample dimensions errors. This emphasizes the relevance of the temperature impact in extensional rheometry tests.

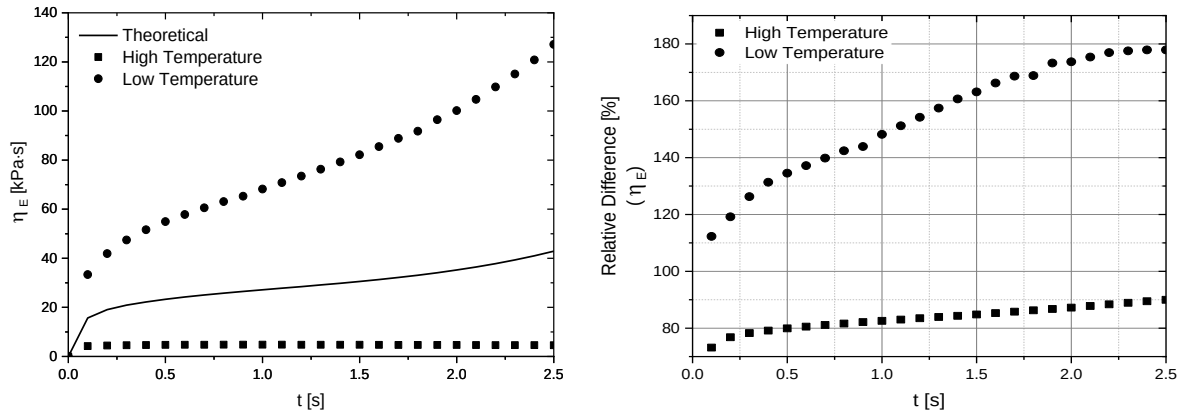

Figure 4.5: Results of the higher and lower temperature case studies: (a) extensional viscosity, (b) relative difference between theoretical and numerical extensional viscosities

According to the results obtained from the test temperature case studies, this can be concluded that the effects of the test temperature on the extensional viscosity data was significant when viscoelastic fluids employed due to the material viscoelasticity.

4.4. Conclusions

In the present work, a computational modeling framework was established aimed at modeling the extensional rheometry tests performed with the Sentmanat Extensional Rheometer (SER) platform for viscoelastic fluids.

A new solver was developed in the framework of the OpenFOAM computational library based on an Eulerian algorithm, where the isoAdvector approach (geometric VOF) was employed, to capture a sharper polymer-air interface. The modeling setup was defined after selecting an appropriate level of mesh refinement and applied initial and boundary conditions. The sample weight (gravity) and surface tension were considered in all case studies. The extensional rheometry tests were appropriately modeled numerically, and a shaper polymer-air interface was predicted.

A new code was devised aimed at computing forces and torques in any desired region of the domain for incompressible viscoelastic fluid models. The effect of the common experimental errors, namely, sample dimensions and test temperature in the uniaxial extensional rheometry tests, was investigated. According to numerical modeling predictions, the necking phenomenon was not observed during the test for all the case studies.

In terms of the sample dimensions error, it was concluded that the deviation of the extensional viscosity data was approximately of the same order of magnitude of the induced error, 10% and 20% respectively, for the thickness and width. The results obtained allowed us to conclude that in terms of the test temperature error, the deviation of extensional viscosity data promoted by this type of error was huge, since a 8% error induced on the lower and higher test temperatures promoted an approximately 180% and 80% deviation, respectively.

The largest deviation verified on the extensional viscosity data was promoted by the test temperature error. According to the results, it can be inferred that the extensional viscosity is more sensitive to test temperature error, than to the sample dimensions error. It is important to notice that the magnitude of the error promoted by the sample dimensions in viscoelastic fluids was similar to the ones obtained with the inelastic fluid (Chapter 3). Based on the results obtained for low Hencky strain and at the beginning of the non-linear region, it seems that the nature of the employed constitutive model (viscoelastic or inelastic) did not affect the errors caused by the sample dimensions. However, the modeling time should be extended to cover a wider range of non-linear model behavior, and the identified modeling setup should be employed to investigate non-uniform samples, inertia effect, and other constitutive models.

References

[1] C. Hopmann, W. Michaeli, Extrusion Dies for Plastics and Rubber, 3th Editio, Hanser Publishers, Munich, 2003.

[2] C. Rauwendaal, Polymer Extrusion, 5th ed., Hanser Publishers, Munich, 2012.

[3] J.J. Sheng, Polymer Viscoelastic Behavior and Its Effect on Field Facilities and Operations, in: Mod. Chem. Enhanc. Oil Recover., 1st ed., Elsevier, Modern Chemical Enhanced Oil Recovery Theory and Practice. AMSTERDAM, 2011: pp. 207–238. https://doi.org/10.1016/b978-1-85617-745-0.00006-1.

[4] F.T. Trouton, On the Coefficient of Viscous Traction and Its Relation to that of Viscosity, Proc. R. Soc. A Math. Phys. Eng. Sci. 77 (1906) 426–440. https://doi.org/10.1098/rspa.1906.0038.

[5] E. Jenckel, K. Ueberreiter, Über Polystyrolgläser verschiedener Kettenlänge, Zeitschrift Für Phys. Chemie. 182A (2017) 361–383. https://doi.org/10.1515/zpch-1938-18240.

[6] E.N. da C. Andrade, B. Chalmers, The Resistivity of Polycrystalline Wires in Relation to Plastic Deformation, and the Mechanism of Plastic Flow, Proc. R. Soc. A Math. Phys. Eng. Sci. 138 (1932) 348–374. https://doi.org/10.1098/rspa.1932.0189.

[7] H.J. Karam, J.C. Bellinger, Tensile Creep of Polystyrene at Elevated Temperatures. Part I., Trans. Soc. Rheol. 8 (1964) 61–72. https://doi.org/10.1122/1.548969.

[8] G. V. Vinogradov, A.I. Leonov, A.N. Prokunin, On uniaxial extension of an elasto-viscous cylinder, Rheol. Acta. 8 (1969) 482–490. https://doi.org/10.1007/BF01976233.

[9] R.L. Ballman, Extensional flow of polystyrene melt, Rheol. Acta. 4 (1965) 137–140. https://doi.org/10.1007/BF01984710.

[10] A. Ziabicki, K. Kedzierska, Studies on the orientation phenomena by fiber formation from polymer melts. IV. Effect of molecular structure on orientation. Polyethylene and polystyrene, J. Appl. Polym. Sci. 6 (1962) 361–367. https://doi.org/10.1002/app.1962.070062114.

[11] F.H. Müller, C. Engelter, Zur Spannungsabhängigkeit des Fließens Polymerer, Kolloid-Zeitschrift Zeitschrift Für Polym. 186 (1962) 36–41. https://doi.org/10.1007/BF01797951.

[12] F.N. Cogswell, The rheology of polymer melts under tension, Plast. Polym. 36 (1968) 109–111.

[13] H. Münstedt, New Universal Extensional Rheometer for Polymer Melts. Measurements on a Polystyrene Sample, J. Rheol. (N. Y. N. Y). 23 (1979) 421–436. https://doi.org/10.1122/1.549544.

[14] T. Raible, A. Demarmels, J. Meissner, Stress and recovery maxima in LDPE melt elongation, Polym. Bull. 1 (1979) 397–402. https://doi.org/10.1007/BF00284409.

[15] J. Meissner, Development of a Universal Extensional Rheometer for the Uniaxial Extension of Polymer Melts., Trans Soc Rheol. 16 (1972) 405–420. https://doi.org/10.1122/1.549258.

[16] J. Meissner, J. Hostettler, A new elongational rheometer for polymer melts and other highly viscoelastic liquids, Rheol. Acta. 33 (1994) 1–21. https://doi.org/10.1007/BF00453459.

[17] G.H. McKinley, T. Sridhar, F ILAMENT -S TRETCHING R HEOMETRY OF C OMPLEX F LUIDS , Annu. Rev. Fluid Mech. 34 (2002) 375–415. https://doi.org/10.1146/annurev.fluid.34.083001.125207.

[18] M.L. Sentmanat, Miniature universal testing platform: From extensional melt rheology to solid-state deformation behavior, Rheol. Acta. 43 (2004) 657–669. https://doi.org/10.1007/s00397-004-0405-4.

[19] B. Li, W. Yu, X. Cao, Q. Chen, Horizontal extensional rheometry (HER) for low viscosity polymer melts, J. Rheol. (N. Y. N. Y). 64 (2020) 177–190. https://doi.org/10.1122/1.5134532.

[20] M. Sentmanat, B.N. Wang, G.H. McKinley, Measuring the transient extensional rheology of polyethylene melts using the SER universal testing platform, J. Rheol. (N. Y. N. Y). 49 (2005) 585–606. https://doi.org/10.1122/1.1896956.

[21] M. Aali, C. Fernandes, O.S. Carneiro, J.M. Nóbrega, Using Computational Modelling to Study Extensional Rheometry Tests for Inelastic Fluids, Fluids. 6 (2021) 464. https://doi.org/10.3390/FLUIDS6120464.

[22] M. Aali, O.S. Carneiro, J.M. Nóbrega, Profile extrusion die design: A comparative study between elastic and inelastic fluids, Polym. Eng. Sci. 62 (2022) 497–509. https://doi.org/10.1002/PEN.25862.

[23] Y. Wang, S.-Q. Wang, From elastic deformation to terminal flow of a monodisperse entangled melt in uniaxial extension, J. Rheol. (N. Y. N. Y). 52 (2008) 1275–1290.

https://doi.org/10.1122/1.2995858.

[24] E. Garofalo, G.M. Russo, P. Scarfato, L. Incarnato, Nanostructural modifications of polyamide/MMT hybrids under isothermal and nonisothermal elongational flow, J. Polym. Sci. Part B Polym. Phys. 47 (2009) 981–993. https://doi.org/10.1002/polb.21706.

[25] E.B. Muliawan, S.G. Hatzikiriakos, Rheology of mozzarella cheese, Int. Dairy J. 17 (2007) 1063–1072. https://doi.org/10.1016/j.idairyj.2007.01.003.

[26] E. Mitsoulis, S.G. Hatzikiriakos, Rolling of bread dough: Experiments and simulations, Food Bioprod. Process. 87 (2009) 124–138. https://doi.org/10.1016/j.fbp.2008.07.001.

[27] J. Aho, V.H. Rolón-Garrido, S. Syrjälä, M.H. Wagner, Measurement technique and data analysis of extensional viscosity for polymer melts by Sentmanat extensional rheometer (SER), Rheol. Acta. 49 (2010) 359–370. https://doi.org/10.1007/s00397-010-0439-8.

[28] A. Oseli, B. Bizjan, E. Król, B. Širok, L. Slemenik Perše, Tensile properties of mineral fibers determined with Sentmanat extensional rheometer, Constr. Build. Mater. 253 (2020) 119215. https://doi.org/10.1016/J.CONBUILDMAT.2020.119215.

[29] E. Garofalo, L. Di Maio, P. Scarfato, A. Pietrosanto, A. Protopapa, L. Incarnato, Study on Improving the Processability and Properties of Mixed Polyolefin Post-Consumer Plastics for Piping Applications, Polym. 2021, Vol. 13, Page 71. 13 (2020) 71. https://doi.org/10.3390/POLYM13010071.

[30] M. Sentmanat, B.N. Wang, G.H. McKinley, Measuring the transient extensional rheology of polyethylene melts using the SER universal testing platform, J. Rheol. (N. Y. N. Y). 49 (2005) 585–606. https://doi.org/10.1122/1.1896956.

[31] R. Pivokonsky, M. Zatloukal, P. Filip, On the predictive/fitting capabilities of the advanced differential constitutive equations for branched LDPE melts, J. Nonnewton. Fluid Mech. 135 (2006) 58–67. https://doi.org/10.1016/j.jnnfm.2006.01.001.

[32] A. Lyhne, H.K. Rasmussen, O. Hassager, Simulation of elastic rupture in extension of entangled monodisperse polymer melts, Phys. Rev. Lett. 102 (2009). https://doi.org/10.1103/PhysRevLett.102.138301.

[33] T.S.K. Ng, G.H. McKinley, M. Padmanabhan, Linear to non-linear rheology of wheat flour dough,

Appl. Rheol. 16 (2006) 265–274. https://doi.org/10.1515/arh-2006-0019.

[34] P. Svrcinova, A. Kharlamov, P. Filip, On the measurement of elongational viscosity of polyethylene materials, Acta Tech. CSAV (Ceskoslovensk Akad. Ved). 54 (2009) 49–57.

[35] R. Pivokonsky, M. Zatloukal, P. Filip, On the predictive/fitting capabilities of the advanced differential constitutive equations for linear polyethylene melts, J. Nonnewton. Fluid Mech. 150 (2008) 56–64. https://doi.org/10.1016/j.jnnfm.2007.10.005.

[36] R. Pivokonsky, M. Zatloukal, P. Filip, C. Tzoganakis, Rheological characterization and modeling of linear and branched metallocene polypropylenes prepared by reactive processing, J. Nonnewton. Fluid Mech. 156 (2009) 1–6. https://doi.org/10.1016/j.jnnfm.2008.06.001.

[37] O. Delgadillo-Velázquez, S.G. Hatzikiriakos, M. Sentmanat, Thermorheological properties of LLDPE/LDPE blends, Rheol. Acta. 47 (2008) 19–31. https://doi.org/10.1007/s00397-007-0193-8.

[38] K. Yu, J.M.R. Marín, H.K. Rasmussen, O. Hassager, 3D modeling of dual wind-up extensional rheometers, J. Nonnewton. Fluid Mech. 165 (2010) 14–23. https://doi.org/10.1016/j.jnnfm.2009.08.006.

[39] O. Hassager, J.M.R. Marin, K. Yu, H.K. Rasmussen, Polymeric liquids in extension: Fluid mechanics or rheometry?, Rheol. Acta. 49 (2010) 543–554. https://doi.org/10.1007/s00397-010-0444-y.

[40] K. Yu, H.K. Rasmussen, J.M.R. Marín, O. Hassager, The dynamics of cylindrical samples in dual wind-up extensional rheometers, J. Rheol. (N. Y. N. Y). 55 (2011) 571. https://doi.org/10.1122/1.3568816.

[41] F.A. Morrison, understanding rheology, Oxford university press, New York, 2001.

[42] J. Aho, V.H. Rolón-Garrido, S. Syrjälä, M.H. Wagner, Measurement technique and data analysis of extensional viscosity for polymer melts by Sentmanat extensional rheometer (SER), Rheol. Acta. 49 (2010) 359–370. https://doi.org/10.1007/s00397-010-0439-8.

[43] H. Jasak, Error Analysis and Estimation for the Finite Volume Method with Applications to Fluid Flows, Ph.D. Thesis, Imperial College, 1996.

[44] J. Roenby, H. Bredmose, H. Jasak, A Computational Method for Sharp Interface Advection,

(2016). https://doi.org/10.1098/rsos.160405.

[45] L. Gamet, M. Scala, J. Roenby, H. Scheufler, J. Lou Pierson, Validation of volume-of-fluid OpenFOAM® isoAdvector solvers using single bubble benchmarks, Comput. Fluids. 213 (2020) 104722. https://doi.org/10.1016/J.COMPFLUID.2020.104722.

[46] F. Pimenta, M.A. Alves, rheoTool, https://github.com/fppimenta/rheoTool, (n.d.).

[47] F. Pimenta, M.A. Alves, Stabilization of an open-source finite-volume solver for viscoelastic fluid flows, J. Nonnewton. Fluid Mech. 239 (2017) 85–104. https://doi.org/10.1016/J.JNNFM.2016.12.002.

[48] C.W. Hirt, B.D. Nichols, Volume of fluid (VOF) method for the dynamics of free boundaries, J. Comput. Phys. 39 (1981) 201–225. https://doi.org/10.1016/0021-9991(81)90145-5.

[49] R. Comminal, Numerical simulation of viscoelastic free - surface flows using a streamfunction / log - conformation formulation and the volume - of - fluid method, Ph.D. Thesis, Technical University of Denmark, 2015.

[50] OpenFOAMWiki, BlockMesh - OpenFOAMWiki, (2021). https://openfoamwiki.net/index.php/BlockMesh (accessed November 8, 2021).

CHAPTER 5

CONCLUSIONS AND FUTURE WORK

5.1. Conclusions

The present thesis focuses on an important subject that contributes to the thermoplastics profile extrusion die design and polymer rheological characterization, particularly to uniaxial extensional rheometry. The knowledge resulting from the work can be useful to the rheologists and experimentalists, in what concerns the effects of the employed constitutive model in the confined flow modeling, occurring in complex profile extrusion dies. Moreover, on the side of materials characterization, the effects of some error sources on the uniaxial extensional rheometry tests accuracy were quantified, for the Sentmanat Extensional Rheometer (SER) platform. The material employed in the present thesis was an extrusion grade of polycarbonate (Trirex 3027U(M1)), used by the partner extrusion company, Soprefa SA, to produce a swimming pool cover profile.

In **Chapter 2**, the effects on the total pressure drop and flow distribution at the flow channel outlet of the melt viscoelasticity, when compared to the inelastic fluid case, in confined flow, were investigated. To assure a proper comparison of the results, a methodology was established to determine the parameters of the inelastic constitutive model based on the viscoelastic counterpart. In the analysis two extrusion dies, one representative of a realistic profile extrusion die (pool cover profile) and a simple one for a rectangular profile were studied. The investigation started with the simple extrusion die, which allowed performing a detailed study aiming at identifying the effect of the most relevant process parameters (flow rate and convergence angle) on the flow distribution obtained at the flow channel outlet, and the total pressure drop. Then, the study was extended to a (realistic) complex profile extrusion die. The results obtained allowed to conclude that the effect of the convergence angle was not significant on neither the flow distribution nor the pressure drop, both with viscoelastic and inelastic fluids. Furthermore, the velocity profile evolved quickly, along the parallel zone, for both fluid models. It was also verified that, in terms of pressure drop (pressure gradient along the parallel zone of the extrusion die), the typical length (L) over thickness (t) ratio used in industrial practice ($L/t = 10$) was too short for the achievement of fully developed flow conditions, when the viscoelastic model was employed. In this case, a much longer parallel zone was required ($L/t > 60$). As a result, the pressure drop obtained from the viscoelastic fluid model was relatively lower (~20%) than the one predicted with the inelastic fluid model. While in terms of velocity distribution, the predictions obtained with the viscoelastic fluid model were in the most extreme elemental sections around 20% different from the ones obtained with the inelastic fluid counterpart. The simulations performed with the inelastic constitutive model required a shorter computational time (each run took about 1 hour in an one core calculation), and thus promote a

faster design stage, when compared to the viscoelastic constitutive model (where each run took circa 7 days, resorting to a parallelized calculation with 20 cores). However, due to its more realistic nature, the predictions of the viscoelastic constitutive model are potentially more accurate than those obtained with the inelastic constitutive model. However, it can be stated that the number of experimental trial-and-error iterations required to design dies using viscoelastic constitutive models is expected to be less than that corresponding to the use of inelastic constitutive models. Consequently, the best option concerning the modeling approach to employ requires additional studies, to confirm if the benefits obtained with the expected improved precision provided by the viscoelastic constitutive models surpass the additional calculation time required.

In the second part of the work, the effects of typical sources of error, namely sample dimensions and test temperature, on the accuracy of the uniaxial extensional rheometry data using the SER platform, when inelastic and viscoelastic constitutive models were employed, were investigated, respectively, in **Chapter 3** and **Chapter 4**. For this purpose, a computational modeling setup was developed in the framework of the OpenFOAM computational library, which allowed modeling of the envisaged extensional rheometry tests. It was demonstrated that employing an appropriate computational domain (case geometry) and adequate initial and boundary conditions were crucial for the accuracy of the numerical modeling results obtained. In fact, the initially proposed domain and boundary conditions caused an error of 25% on the numerical predictions, and it was reduced to 4% after employing appropriate computational domain geometry, mesh and boundary conditions. Afterwards, a methodology was proposed to replicate the extensional viscosity calculation used in the SER platform, where the extensional viscosity was calculated based on the forces/torques acting on the region of interest (drum surface). For this purpose, a new code was developed to compute forces and torque for multimode viscoelastic fluids in any desired region of the domain. Furthermore, a new solver was developed in the framework of OpenFOAM computational library to calculate multiphase flows of viscoelastic fluids using the geometric Volume-of-Fluid (isoAdvector algorithm) interface capturing approach. The developed solver was able to predict a much sharper polymer-air interface, when compared to the previously available solver, which used the algebraic Volume-of-Fluid (VOF) approach. The results obtained allowed to conclude that the sample weight (isoAdvector algorithm) and surface tension did not affect the results for both types of fluids. Also, the necking phenomenon, commonly reported in the literature, was not observed in all studies performed. Regardless of the nature of the fluid employed (viscoelastic or inelastic), the errors induced on the sample dimensions, ±10% and ±20% for the thickness and width, respectively, promoted approximately the same deviation on the predicted extensional viscosity. In terms of test temperature error, an induced error of

8% resulted in a deviation of 60% in the extensional viscosity prediction for the inelastic fluid at the higher temperature, and of approximately 180% and 80% for the viscoelastic fluid at the lower and higher temperatures, respectively. These effects show that the sensitivity of the results obtained for the extensional viscosity is higher when the viscoelastic fluid model is employed. These results can be justified by the high sensitivity of the viscoelastic fluids to temperature variations when compared to the inelastic ones. In what concerns the temperature induced errors, the numerical predictions of the extensional viscosity were more sensitive to the test temperature than to the sample dimensions variations, for both types of fluids. Finally, according to the results obtained in both viscoelastic and inelastic fluid models, the sample inertia also affects the evolution of the calculated extensional viscosity, since the predicted values at the initial phase of the test were always higher than those observed at the end, reducing over time. This occurred because at the initial phase of the test, the torque applied to the drum surface must promote both deformation and acceleration of the polymeric sample, while in the theoretical test assumptions only the sample deformation is considered.

5.2. Future work

According to the results and knowledge obtained in the frame of the present thesis, the following topics can be considered for future work:

- Perform experimental tests using the complex profile extrusion die (swimming pool cover), and compare the experimental pressure drop and flow distribution with the corresponding numerical predictions [30] obtained for both viscoelastic and inelastic constitutive models, targeted at determining which constitutive model predictions (viscoelastic or inelastic) are closest to the reality data (experimental data).
- As reported by Hassager et al. [105] and Yu et al. [112], some test conditions such as samples with higher width, and/or thickness, and low and/or high Hencky strain rate, can promote a deviation from non-pure extensional flow, which is undesirable. Therefore, it would be useful to employ a methodology like the one proposed in those works [105] to properly understand the dominant flow condition in the SER for a wider range of conditions.
- Extend the investigation of errors in the accuracy of the extensional rheometry tests, by considering the following conditions:
    - Slip of the polymer sample at the drum surface, which might take place in the test. For this purpose, different boundary conditions, such as partial slip should be applied at the drum surface, and the corresponding effects should be quantified.
    - Non-uniform sample geometry in terms of thickness, width, and/or shape (non-rectangular samples).
    - Longer simulated time, in order to reach the state where the material non-linearity affects the result. For this purpose, the computational domain employed in the present work should be modified.

References

[1] J.M. Nóbrega, O.S. Carneiro, F.T. Pinho, P.J. Oliveira, Flow balancing in extrusion dies for thermoplastic profiles, Part III: Experimental assessment, Int. Polym. Process. 19 (2004) 225–235. https://doi.org/10.3139/217.1825.

[2] O. Hassager, J.M.R. Marin, K. Yu, H.K. Rasmussen, Polymeric liquids in extension: Fluid mechanics or rheometry?, Rheol. Acta. 49 (2010) 543–554. https://doi.org/10.1007/s00397-010-0444-y.

[3] K. Yu, J.M.R. Marín, H.K. Rasmussen, O. Hassager, 3D modeling of dual wind-up extensional rheometers, J. Nonnewton. Fluid Mech. 165 (2010) 14–23. https://doi.org/10.1016/j.jnnfm.2009.08.006.